Technical University of Denmark

DTU

Dynamic Influences of Wind Power on The Power System

Rosas, Pedro Andrè Carvalho; Nielsen, Arne Hejde; Sørensen, Poul Ejnar; Bindner, Henrik W.

Publication date:
2004

Document Version
Publisher's PDF, also known as Version of record

Link back to DTU Orbit

DTU Library
Technical Information Center of Denmark

Pedro Rosas

DYNAMIC INFLUENCES OF WIND POWER ON THE POWER SYSTEM

PhD thesis

Section of Electric Power Engineering

Ørsted·DTU

March 2003

DYNAMIC INFLUENCES OF WIND POWER ON THE POWER SYSTEM

By

Pedro Rosas

Thesis submitted to Ørsted Institute, Section of Electric Power Engineering

Technical University of Denmark

In partial fulfilment of the requirements for the degree of Doctor of Philosophy

Ørsted Institute, Risø National Laboratory & Brazilian Wind Energy Centre

Denmark, March 2003

Pedro André Carvalho Rosas
Risø National Laboratory, Wind Energy Department
&
Ørsted Institute – Section of Electric Power Engineering,
Technical University of Denmark

Abstract

The thesis first presents the basics influences of wind power on the power system stability and quality by pointing out the main power quality issues of wind power in a small-scale case and following, the expected large-scale problems are introduced. Secondly, a dynamic wind turbine model that supports power quality assessment of wind turbines is presented. Thirdly, an aggregate wind farm model that support power quality and stability analysis from large wind farms is presented. The aggregate wind farm model includes the smoothing of the relative power fluctuation from a wind farm compared to a single wind turbine. Finally, applications of the aggregate wind farm model to the power systems are presented. The power quality and stability characteristics influenced by large-scale wind power are illustrated with three cases.

In this thesis, special emphasis has been given to appropriate models to represent the wind acting on wind farms. The wind speed model to a single wind turbine includes turbulence and tower shadow effects from the wind and the rotational sampling turbulence due to the rotation of the blades. In a park scale, the wind speed model to the wind farm includes the spatial coherence between different wind turbines. Here the wind speed model is applied to a constant rotational speed wind turbine/farm, but the model is suitable to variable speed wind turbine/farm as well.

The cases presented here illustrate the influences of the wind power on the power system quality and stability. The flicker and frequency deviations are the main power quality parameters presented. The power system stability concentrates on the voltage stability and on the power system oscillations.

From the cases studied, voltage and the frequency variations were smaller than expected from the large-scale wind power integration due to the low spatial correlation of the wind speed. The voltage quality analysed in a Brazilian power system and in the Nordel power system from connecting large amount of wind power showed very small voltage variations. The frequency variations analysed from the Nordel showed also small variations in the frequency but it also showed that the wind turbines excites the power system in the electromechanical modes.

Concerning the stability analysis, the study cases showed that large-scale wind power modifies the voltage stability of the power system and can cause power oscillations. It is showed here that the reactive power from the wind farms is the key factor on the voltage stability problem. During continuous operation, the distributed wind power variations did not give any problems to the power system stability concerning the power oscillations.

DYNAMIC INFLUENCES OF WIND POWER ON THE POWER SYSTEM

Pedro André Carvalho Rosas
Risø National Laboratory, Wind Energy Department
&
Ørsted Institute – Section of Electric Power Engineering,
Technical University of Denmark

Resumé

Først i afhandlingen introduceres de vigtigste elkvalitetsproblemstillinger, elsystemets stabilitet og elkvalitet, i relation til vindkraft, når vindmøller tilsluttes i mindre og stor skala. Efterfølgende præsenteres en dynamisk vindmøllemodel, der er specielt egnet til analyse af elkvalitet fra en vindmølle. Herefter introduceres en aggregeret vindmølleparkmodel til brug ved analyse af elkvalitet og netstabilitet fra store vindmølleparker. Den aggregerede vindmølleparkmodel indeholder den udglatning af de relative effekfluktuationer fra en vindmøllepark sammenlignet med en enkelt vindmølle. Endelig præsenteres nogle anvendelser af den aggregerede vindmølleparkmodel i forskellige cases.

I afhandlingen er der lagt specielt vægt på at opstille relevante og anvendelige modeller af vinden i en vindmøllepark. Modellen for vindhastigheden for enkelt vindmølle inkluderer turbulens og tårnskygge herunder især roterende sampling af turbulensen som fremkommer pga. vingernes rotation. I park-skala modellen er der taget hensyn til den rummelige koherens mellem de forskellige vindmøller. Vindhastighedsmodellen er i afhandlingen anvendt på vindmøller med konstant omløbstal, men den kan også umiddelbart anvendes på møller med variabelt omløbstal.

De cases, der præsenteres, illustrerer indflydelsen af vindmølleparker på elsystemets stabilitet og på elkvaliteten. Flicker og frekvensafvigelser er de vigtigste elkvalitetsparameter, der benyttes til vurderingen af indflydelsen. Stabiliteten af elsystemet vurderes vha. spændingsstabilitet og effekt- og frekvenssvingninger.

Resultaterne fra de forskellige cases viser at spændings- og frekvensvariationerne er mindre end man kunne forvente på grund af den lille rumlige korrelation af vindhastighederne ved de forskellige vindmøller. Undersøgelsen af spændingskvaliteten i den brasilianske case og og i Nordel-casen viser at der kan forventes små spændingsvariationer selv når der tilsluttes meget vindkraft. Undersøgelsen af frekvensvariationerne i Nordel-casen viser også kun små variationer i frekvensen, men den viser også at der kan være tilfælde, hvor vindmøllerne anslår elektromekaniske egensvingninger i elsystemet.

Med hensyn til stabilitets analyserne viser de forskellige cases at stor-skala integration af vindkraft kan ændre grænsen for spændingstabilitet og kan forårsage effektfluktuationer. Det fremgår endvidere af analyserne at den reaktive effekt der forbruges i parkerne spiller en nøglerolle med hensyn til spændingstabiliteten. Effektfluktuationerne under normal drift af vindmølleparkerne i Nordel-systemet i de undersøgte tilfælde viser at vindfluktuationerne ikke giver anledning til noget problem med stabiliteten af elsystemet.

Acknowledgment

Table of Contents

List of Figures

List of Tables

Chapter 1

1   Introduction

Wind energy is said to be one of the most prominent sources of electrical energy in years to come. The increasing concerns to environmental issues demand the search for more sustainable electrical sources. Wind turbines along with solar energy and fuel cells are possible solutions for the environmental-friendly energy production. In this report, the focus is on the wind power as it is said to hit large integration in the near future. This technology has already reached a penetration level in some areas, which raises some technical problems concerning grid integration.

Wind power has to overcome some technical as well as economical barriers if it should produce a substantial part of the electricity. In this report, some of the technical aspects are treated, particularly those regarding the power system quality and stability.

1.1 Motivation

It is possible to state that the significant impact of wind power started in the beginning of 80s very much related to the mid 70s oil crises. During the period, a simple and robust wind turbine concept emerged and became very popular pulling the wind power industry. The simple and robust concept includes a three bladed wind turbine rotor, a gearbox, an induction machine directly connected to the grid and a control system.

It was cheap and very robust but the power quality was poor and, in some cases, it influenced the voltage level on the grid. During the 80s, most of wind power installations were limited to few hundreds kilowatts to the existing distribution grids. The size of those installations did not threaten the overall power system stability and the voltage quality assessment was simple (when connected to the conventional power system). In this thesis, the wind power installations to small isolated networks are not included. During the period, the analysis concentrated on development of the wind turbine technology and investigation of the dynamic behaviour of the wind turbines.

The 90's represented an important break through; new concepts emerged because of a demand for more efficient power production and to comply with power quality requirements. During the 90s, the wind turbines (and farms) grew in size and ratio from the few hundreds kilowatts to the megawatt size. The increased rated power of the wind farms to areas with good wind resources leads to concerns on: *"to which extent the wind power interferes to the power system?"* Most of the decade has been dedicated to voltage quality analysis of wind power and to economics of the power systems including wind power.

In the late 90s, with the wind farms rating hundreds megawatts, the concerns start to focus on the transient voltage stability of the power system. The studies focus on the dynamic behaviour of the induction machines during disturbances, where the dynamic effects of the turbulence were neglected. During the same period an International Electrotechnical Commission (IEC) task force issued a standard procedure: the IEC 61400-21[1] to fill-in the lack of technical standards on assessment of power quality from wind turbines.

Nowadays, some power systems start to face problems of integrating thousands megawatts of wind power, which are decentralised spread over large extensions. At this

moment, the problems of planning, operation and control of the power systems with large wind power become very important [2]. On these problems, the main challenges are classified in long-term planning, operation and energy management systems, and power system performance.

The long term planning focuses on several topics, such as the adjustment of agreements between transmission system operators to cope with the stochastic nature of the wind power, this also includes economical and financial issues. Another important aspect included in this topic relates the distribution system reliability with wind power.

The operation and energy management systems focus on the forecast of the wind power and its relation to trade agreements. It also includes the security analysis and the reserve of power to ensure reliable operation of the entire power system.

The last topic, the power system performance, focuses on the control of voltage and frequency, power quality issues, and on the dynamic behaviour of the wind power sources. This report focuses on the dynamic behaviour of the wind power resources to an extensive area and its influences on the power quality and voltage stability issues.

1.2 Literature Review

Integration of wind power into the power system has been studied by many authors before but most of them focused on different characteristics and issues of the power system. Wind power influences several power system characteristics from economic dispatch to stability and quality issues.

Wan and Brian in [3] pointed out main factors to utility integration of solar and wind power where studies from late 1970s until 1980s provided a starting point and general classification of the most relevant power system aspects. One of the main aims was to define technical limits to intermittent power integration. One of the conclusions was that there were no clear limits on wind power integrations and that penetration limits from many studies were economic rather than technical limits. It also clearly concluded that the spatial distribution of the wind must be taken into account and wind speed data are needed.

A project report (ALTENER) in [2] aimed to establish insight and to orient works in the integration of renewable power in the European Network. It characterized the impacts of large amount of renewable energy on European conventional utility practice (not only operation but the institutional aspects also). This latter report related potential problems on the power exchange agreements, stability of the network and power quality. Some of the conclusions are that dynamic studies of the power system characteristics are required in large-scale renewable energy penetration and the stochastic nature of the wind speed is relevant to the power system control and quality.

A more recent report by Nielsen et all in [4] reviews the technical options and constrains of integration of distributed power generation. One of the focuses was on a new power system structure to deal with the imbalance on consumption and production from the stochastic nature of the wind power. Similar work was presented by Jørn et all in [5] where the focus were on the trading/economic aspects from operation of large–scale wind power in the Danish power system.

On the dynamic subject, several works have been done on the analysis of power quality and on the transient stability from wind turbines to the power systems.

Tande et all in [6] developed an extensive analysis of the potential impacts of wind turbines on the power quality, where the work focused on the small scale integration. Similarly, Sørensen in [7] and Larsson in [8] characterized the moderns wind turbines and classified the most relevant characteristics that supported the IEC 61400-21[1]. Tande in [9] explained how to assess the voltage quality from wind turbines using wind turbine characteristics. All works have focused on the power quality of wind turbines.

Akhmatov et all in [10], Brunt et all in [11] and Wiik et all in [12] presented transient stability analysis of the power system with large amount of wind power. On those works, the transient voltage collapse was investigated as well as the wind turbines behaviour during short circuits.

On modelling wind turbines/farms, some textbooks present the wind turbine characteristics. Freris in [13] and Hau in [14] both detailed the wind energy conversion systems presenting a general overview of the wind turbine and Heier in [15] addressed specifically the integration of wind power where much effort was given on the characterization of the wind turbine/farms components.

Wilkie et all in [16] presented simple models to wind turbines and argued that the contributions of wind turbines components must be modelled into the overall simulation but the total accuracy was not essential to obtain an adequate representation. Estanqueiro in [17] and Petru in [18] presented wind turbine models that could be used to power quality studies.

Sørensen et all in [19] and Estanqueiro et all in [20] showed that the assessment of power quality from wind farms depends on appropriate representation of the wind speed. In wind farms, the turbulence spatial correlation must be included.

Giebel in [21] showed that the spatial distribution of the wind turbines gives benefits in long term because it reduces the power variations from the wind energy. Beyer et all in [22] showed that the spatial correlation of the wind speed influences the power production of wind farms. From both works, the power variations from wind farms can be reduced significantly particularly in large scale applications. However, none of them analysed the results to the dynamics of the power systems.

The dynamic power system analyses have been extensively investigated. Kundur et all in [23] and Anderson and Fouad in [24] present dynamic models to the power system components and means to analyse the stability of it. Some of the analyses include the simulations of the entire power system under normal operation and faults. The Power System Engineering Committee of the IEEE in [25] resume several works on power system analysis specifically on modal analyses for system dynamic performance that can identify the possible problems on normal operation of the power system, however the modal analysis must be complemented with dynamic simulations.

Dynamic simulations of very large power systems are very expensive. Lei et all in [26] and Eliasson in [42] present dynamic reduction of large power systems for stability studies aggregating machines with similar (coherent) dynamic characteristics. With the reduced model, the overall dynamic analyses are time feasible. Aggregate dynamic models are used to simulate integration of wind power to the dynamic operation of the power system in this thesis.

Voltage stability has been pointed out as another problem to large integration of wind power because wind farms demand reactive power. Taylor in [27] and Custem in [28]

presented an extensive explanation of the voltage stability problem and means of copying with it. In addition, the Power System Stability Subcommittee of the IEEE in [29] and Cañizares in [30] suggest several tools to analyse the voltage stability, one of them is the loadability curves to characterize the maximum load that can be installed before the voltage collapses. The loadability curves are used in this thesis in connection with the wind power.

1.3 Wind Power Basics

The wind turbines are composed of an aerodynamic rotor, a mechanical transmission system, an electrical generator, a control system (including a soft-starter device), limited reactive power compensation and a step-up transformer. The conventional wind turbine is even at the present time, the most common type of wind turbine installed. Figure 1.1 presents the basic components of a conventional wind turbine.
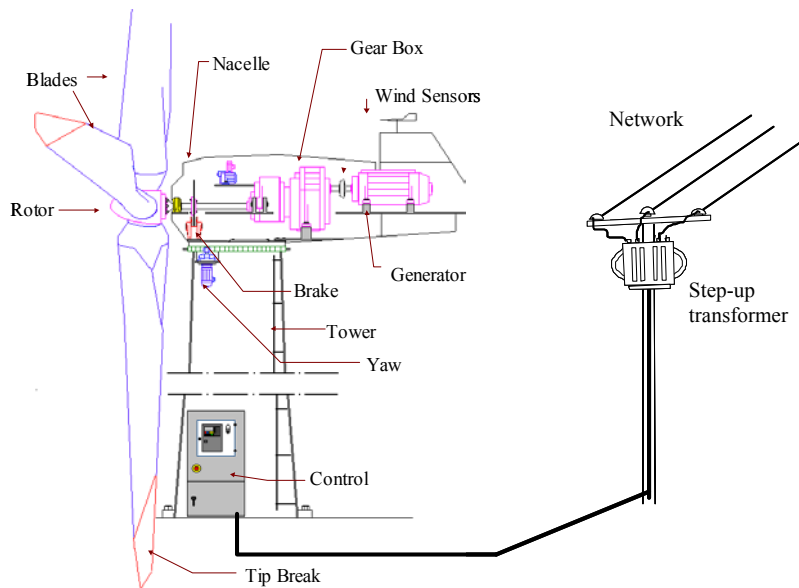
Figure 1.1 Basic components of a wind turbine unity.

The conventional wind turbine is connected directly to the grid and the generator is "synchronized" to the network. This technology has been named "fixed" rotational speed wind turbine because the induction generator allows small mechanical speed variations.

The main power system problems from this wind turbine technology come from the lack of control on the active and reactive powers. The active and reactive power control is very important to keep the frequency and voltage stable within limits. Lack of reactive power can lead to voltage problems and no control in the active power can cause frequency deviations.

This report focuses on this wind turbine technology influences on the power system voltage stability and on the power system quality. Because of lacking controls on active and reactive power, this wind turbine technology is considered the poorest power quality when harmonics problems are not concerned.

In addition, this report focus on the large-scale integration hence a substantial part of this report is dedicated to model the power fluctuations from large groups of wind turbines. The power produced from a large number of wind turbines will vary relatively less than the power produced from a single wind turbine due to the cancellation effect from the poor

spatial correlation of the wind acting on each wind turbine. Figure 1.2 illustrates the power "smoothing" effect when increasing the number of wind turbines.
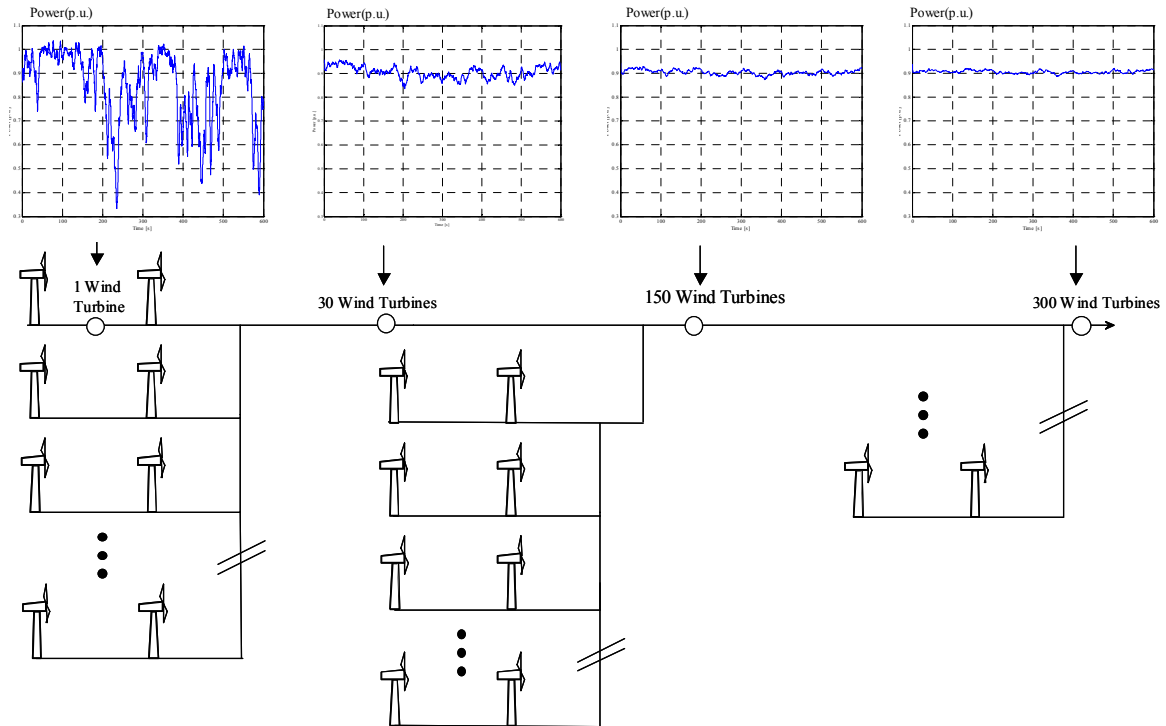
Figure 1.2 Power smoothing effect from wind farms.

The power variation from wind turbines is very complex and demand special techniques to cope with the spatial distribution of the wind turbines than a simple scale up from a single wind turbine.

In addition to the problems of dynamic power fluctuations, another important issue investigated in this report is the voltage stability from connecting large amount of wind power.

The voltage stability in the power system can be classified in slow dynamic and transient. The slow dynamic is related to slow increase in load in the power system and deals with the reactive and active power supply. Once the wind turbines have limited reactive power compensation and usually demands reactive power from the power system, here its influences of the reactive power demand and the active power injection are investigated.

Transient voltage stability problems have also been related to large integration of wind turbines. The transient voltage stability deals with the voltage stability after the power system being subjected to large disturbances, normally short circuits. Here transient stability is not studied.

1.4 Thesis Outline

Chapter 2 addresses the main problems of the power system that are related to the wind turbines. It starts introducing the main power quality characteristics of the wind turbines and proceeds to present the main problems from integrating single wind turbines in the power system are presented. After having presented the power system interactions with

wind turbines, the possible problems to large integration of wind turbines in to the power system, based on a scale up from a single wind turbine, are discussed.

Chapter 3 presents the main characteristics of the wind acting on the rotor of wind turbines. The wind is classified in two main components, and the most relevant characteristics of each part are described. In the final section, a suitable wind speed model to assess the power quality from wind turbines is presented.

Chapter 4 presents the main components from wind turbines. It starts dividing the wind turbine in aeroelastic and electrical components. The aeroelastic components present the relevant characteristics and models to the wind turbine aerodynamic rotor and drive train. In this thesis, the dynamic wind turbine model is implemented in SIMPOW/ABB[1], where available dynamic models to the electrical components are used. The dynamic wind turbine model however can be directly applied to other simulation tools. In the last part of the chapter, the wind turbine model to power quality assessment is presented and compared against measurements.

Chapter 5 presents the turbulence coherence effects on the wind farm production. The main characteristics of coherence and its influences on the dynamic wind farm power production are presented. Chapter 5 also presents an Aggregate Wind Farm (AWF) model that can be used to power quality assessment of wind farms and to dynamic stability analysis of power systems with large number of wind turbines. The AWF model is a single equivalent wind turbine that replaces several wind turbines in the wind farm. The wind speed to the AWF takes into account the wind farm layout and the spatial coherence.

Chapter 6 presents some illustration cases of the voltage stability analysis and power quality from large integration of wind turbines. First, the large wind farms impacts on the voltage stability to a part of a power system are illustrated. In the second part, the connection of large amount of wind power to a Brazilian network is presented in terms of voltage stability and quality. Finally, the integration of more than 4GW of wind power to the Nordic Power System illustrates application of the aggregate wind farm.

---

[1] SIMPOW® is a dedicated digital simulation tool to power system dynamic analysis developed by ABB©, www.abb.se

Chapter 2

2   Wind Power Integration

Large integration of wind power can lead to problems on the voltage control or on the stability of the power systems as mentioned in chapter 1. Chapter 2 presents the main impacts from wind power on the power system with emphasis on the voltage stability and power quality.

The power quality and stability problems, and means of coping with them, are not new to the power system engineers. However, those problems related to wind power are not well described when it comes to large-scale integration.

Here the main problems to the voltage stability and to the power quality related to large-scale integration of wind power are presented. The problem is introduced by pointing out the relevant power quality characteristics of a small wind farm (or a single wind turbine) and after it is scaled up to represent the large-scale case.

First, the scales of integration are defined as follow:

- *Small-scale wind power integration* – the wind power installed is relatively small compared to the conventional power system. The wind energy counts for small part of the total energy production in the power system (i.e. up to few percents e.g. 2%). In small-scale integration, the power system is assumed to have enough spinning reserve of active power and the frequency is kept constant therefore only voltage problems are concerned.

- *Large-scale wind power integration* – the wind power installed sizes the conventional power stations. The wind power counts for large part of the total energy production in the power system (e.g. above 10%). The large-scale integration can cause power quality or stability problems and, in some particular cases, the frequency ca be affected by the wind turbines. Hence, the voltage and frequency problems are concerned.

2.1   Small-Scale Integration of Wind Power

In this case, the power system is considered strong and the main problems from connecting wind farms come from the voltage control. The wind farm is composed by several wind turbines. Each wind turbine has as basic electrical components: an induction generator, local reactive power compensation and a step-up transformer. The wind farm limit is defined by the Point of Common Coupling (PCC), additionally the wind farm may use an integration transformer to connect to a higher voltage level e.g. transmission systems.

Figure 2.1 presents the relevant electrical components of a conventional wind farm. In this thesis, the focus is on the direct connected wind turbines type (so called "fixed" rotor speed). On those types of wind turbines, the active power that comes from the wind is transferred to the power system without storage devices.
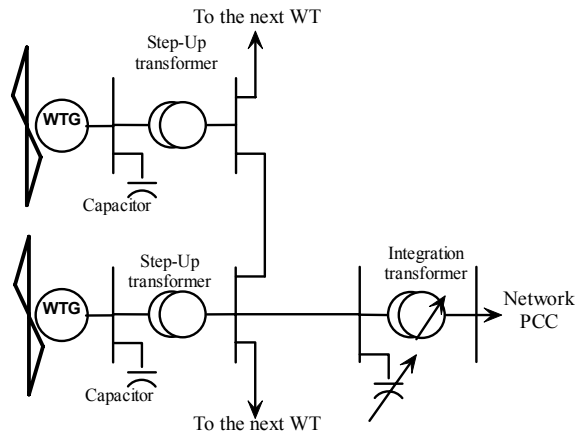
Figure 2.1 Basic components of a wind farm.

Induction (or asynchronous) machines applied as generators demand reactive power from the network (chapter 4), which is partially compensated with shunt capacitor banks. In special configurations, special reactive power compensation is demanded and installed at the PCC (e.g. variable reactive power compensation). In special installations, the voltage level/variations at the PCC can demand a variable tap change transformer.

Wind farms have very little control of the active power due to the stochastic behaviour of the wind, in addition, the voltage control on this type of wind turbine can be done only by changing the amount of reactive power compensation (shunt capacitors installed). The lack of control on the active and reactive powers can disturb the voltage on the PCC.

The disturbances on the voltage from wind turbines are classified in different time scales. The classification presented as follow is in agreement with IEC 61400-21 [1]:

- Steady-state – does not include dynamics (very slow dynamics representing periods above 10 minutes to hours);

- Dynamic – include the dynamics in the time frame from milliseconds to 10 minutes;

- Harmonics – includes voltage variations in high frequency (e.g. above 50Hz to Europe and 60Hz to US and Brazil, periods less than 20 milliseconds) due to the electronic equipments installed in the wind turbines (this last part is not related to the wind speed).

Here, the harmonics are not an important issue because this report focus on the direct connected wind turbine type that does not emit harmonics components on current, therefore it is not included in the following subsections.

2.1.1 Steady – state operation

The steady-state operational analysis assures that the:

- The currents will not exceed thermal limits nor will the protections act during extreme powers;

- The voltage levels will not exceed limits.

In near future, wind turbines can be certified to power quality [1]. From these certifications, a set of data will help to verify the steady-state operation of the wind turbines and wind farms. Table 2.1 presents the main steady-state parameters to wind turbines certified to power quality [1].

Table 2.1 Main steady state parameters defined in IEC 61400-21 [1].

Parameters
Rated active power
Rated reactive power
Rated apparent power
Rated current of the wind turbine at rated voltage
Rated voltage of the wind turbine
Maximum permitted power set-up in the controller
Maximum measured power in 60 seconds average period
Maximum recorded power in 0,2 seconds average period
Reactive power demand/supply as function of the active power
Reactive power measured or estimated to the P_{mc}
Reactive power measured or estimated to the P_{60}
Reactive power measured or estimated to the $P_{0,2}$

Based on the parameters specified on Table 2.1 and with the electrical characteristics of the network it is possible to determine the impacts on the voltage quality as well as the maximum currents on the cables and transformers.

The impacts on the voltage quality to the different conditions as expressed in Table 2.1 can be computed with help of a load flow program or by simple equations. Following, simple equations to determine the voltage levels are introduced. Figure 2.2 presents the electrical representation of the wind turbine and the power system, where the reference node and the equivalent impedance represent the entire power system at the wind turbine terminals.
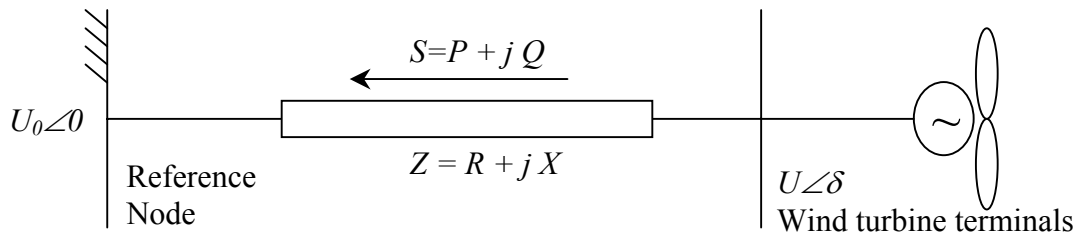
Figure 2.2 Single line equivalent for a wind turbine connection.

P and Q are the active and reactive powers respectively from the wind turbine, there are no load or shunt elements installed at the wind turbine terminals. The voltage at the wind turbine terminals (U) can be determined as follow:

$$U = U_0 + \Delta U \qquad (2.1)$$

where, U_0 is the voltage at the reference node, U is the voltage at the wind turbine terminals and ΔU can be computed as:

$$\Delta U = \frac{(PR + QX)}{U_0} + \frac{(PX - QR) \cdot j}{U_0}$$ (2.2)

where, R and X are the resistance and reactance inductive characteristics of the electrical network respectively. The voltage can increase or decrease depending on the amount of the reactive and active power flux and on the network characteristics. Using Equation (2.2) it is possible to compute the voltage levels and compare to preset limits imposed by the local network operator.

However, in most cases, it is important to detail the network and include the loads installed and to use a load flow program to compute the voltage and currents on the relevant nodes and lines respectively.

2.1.2 Dynamic Operation

The wind turbines dynamically produce power that varies in a broad range of frequencies and amplitudes. These continuous variations of active and reactive powers from the wind farm cause dynamic voltage variations. The dynamic voltage variations from the wind turbines during operation are quantified by flicker and step change [1].

The flicker emissions during continuous and switching operations and the voltage step change are the voltage quality indicators influenced from small number of wind turbines connected to the grid. The flicker emission is computed from flicker coefficients measured from wind turbines during the power quality data sheet.

The flicker emission is a measure of the human perception of the bulb light variation consequent of the voltage low frequency variation. The value is computed to short term (10 minutes) and long term (120 minutes). The flicker emission includes voltage variations in frequencies up to 25 Hertz that are weighted with an eye perception function according to [32] and its posterior amendments [33] and [34].

Figure 2.3 presents the voltage fluctuations as a function of frequency that will represent a unity of short-term flicker perceptivity (P_{st}) to two different conditions: sinusoidal voltage fluctuations and rectangular voltage fluctuations based on [34].
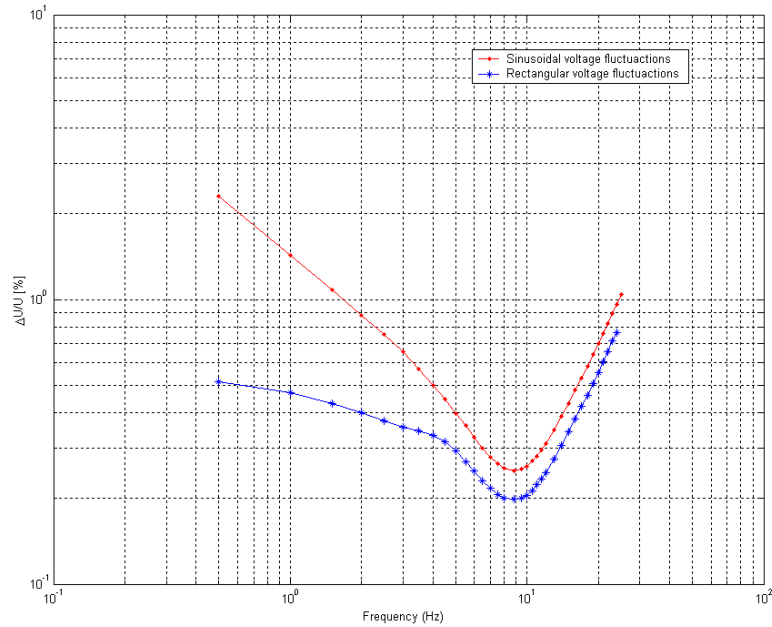
Figure 2.3 Voltage fluctuations corresponding to flicker emission unity [34].

From Figure 2.3, the maximum flicker perception comes from around 8Hz where the voltage fluctuations must be reduced in order to respect the flicker limits. The limits on Figure 2.3 considers that voltage variations leads to light intensity variations in light bulbs.

In order evaluate the flicker contribution from wind turbines, Figure 2.4 presents the Power Spectral Distribution (PSD) of the power produced from a three bladed wind turbine (225kW).
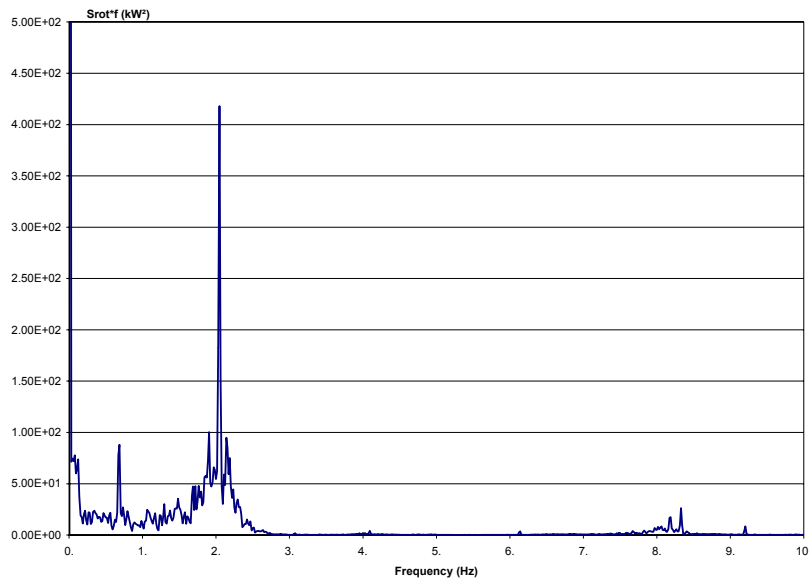
Figure 2.4 Measured power spectra of the electrical power from a 225kW pitch regulated wind turbine.

The PSD in Figure 2.4 includes contributions from deterministic and stochastic parts. The fundamental frequency of rotation (1p – one time the rotational speed of the rotor) is approximately 0.7Hz, at this frequency there is a small contribution related to some asymmetry in the rotor. At the frequency of 2.1Hz (3p – three times the rotational speed of the rotor) there is a large contribution to the power variation. The 3p effect is related to

rotational turbulence and the blades passing the tower in a three-bladed rotor type of wind turbines. In the frequency of 8.4Hz, corresponding to 12p, a small amount of energy is also presented that has been related to the flexible aeroelastic part of the wind turbine in addition to the induction generator [66]. PSD of power measurements from different three-bladed wind turbines show similar pattern, i.e. the power variations reduce significantly above the frequency of 3p. Although one could expect high power variations in a broad frequency range, a three bladed rotor cancels the multiples harmonics different from the 3np and in addition, the dynamic components of the wind turbines damp the high frequency power oscillations.

The power variations are consequence of the wind field on the rotor area and the wind turbine dynamics. The turbulence and tower shadow influence the wind field on the rotor area and the three blades crossing the wind field transfer the power variations to the main shaft. The power on the main shaft will dynamically interact with the wind turbine components, e.g. drive train torsional moments, and finally the generator will convert the power to the network.

Figure 2.3 and Figure 2.4 indicate that the main flicker contributions from wind turbines comes from the 3p power variations. The power variation in very low frequency below 0.7 Hz is caused by the simple turbulence acting on the rotor area but has small influence on the flicker. The high-energy content on 3p frequency comes from the effect of the blades rotating on the turbulent field added together to the tower shadow. These effects will be more detailed in chapters to come where each component of the power fluctuation from a wind turbine is explained and models presented to simulate them.

The flicker defined in the previous paragraphs is related to the continuous operation of the wind turbines. In addition, wind turbines also generate flicker due to switching operation and start-up. The flicker during continuous operation is caused by the power fluctuation from the turbulence added to the wind turbine dynamics. The flicker due to switching operations is caused by start-up or switching of generators of wind turbines because the high in-rush currents cause voltage dips. Associated to the flicker emissions during switching operations, the voltage dip is relevant because the voltage will drop instantaneously due to the in-rush current.

This report focus on the analysis of the continuous operation of wind turbines, therefore it is restricted to the flicker emission during continuous operation. The flicker and voltage dips from switching operations are not treated in this report.

The flicker emission in short term and long term can be estimated from the power quality tests [1]. The power quality tests of wind turbines express a flicker coefficient for each wind turbine for different network phase angle condition and different annual mean wind speeds for a wind farm. The short-term flicker emission (P_{st}) and the long-term flicker emission (P_{lt}) to a wind farm can be estimated according to [1]:

$$ P_{st} = P_{lt} = \frac{1}{S_k} \sqrt{\sum_{i=1}^{N_{wt}} \left(c_i\left(\psi_k, v_a\right) \cdot S_{n,i}\right)^2} \qquad (2.3) $$

where S_k is the short circuit capacity, c_i is the flicker coefficient of wind turbine i to specific network impedance phase angle (ψ_k) and annual average wind speed v_a from the site, $S_{n,i}$ is the rated power of wind turbine i and N_{wt} is the number of wind turbines in the wind farm.

The P_{st} and P_{lt} are assumed the same because it is assumed that the mean wind speed and turbulence will be maintained in 10 minutes average as well as in 120 minutes.

Equation (2.3) takes into account the "cancellation" effects, which comes from the wind dynamics in the wind farm that is not correlated, so the flicker is not a linear sum of all flicker produced from each wind turbine. Because the 3p is the main flicker contribution and these relatively high frequencies are approximately uncorrelated this is a reasonable assumption.

2.2 Large-Scale Integration of Wind Energy

As introduced before, here the large-scale integration problems are based on the small-scale ones. The large-scale integration means a relatively high wind power compared to the local power system. The large integration can occur in two main conditions:

- Large wind farms connected to the transmission system or;

- Several small wind farms connected to the distribution systems in one area of the power system.

In either condition, the power quality and system stability assessment become more complex and depending on the sizes, they demand special investigations of voltage and frequency variations.

In the small-scale integration, the frequency was assumed constant. With high wind power capacity installed, the large active power variations can interact with the frequency controllers in the conventional power stations, so frequency variations can happens. In addition, large reactive power demanded by the wind farms can reduce the reactive power supply, hence the voltage stability limits can be reduced and must be analysed too.

There are several issues arising from large-scale wind power integration, but here the focus is on the voltage stability and the dynamic power oscillations during normal operation of the power system. In order to introduce the maim issues of the power system and wind turbines, Figure 2.5 presents a simple single line with the basic structure of the power system, where it is possible to distinguish the main system components.
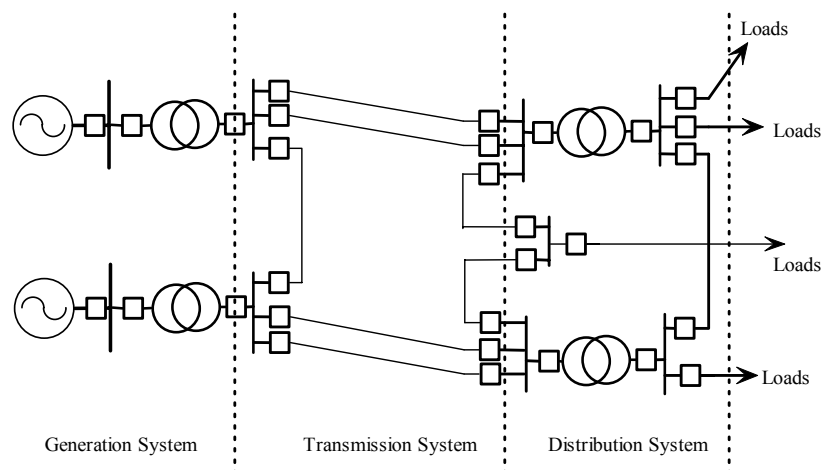
Figure 2.5 Basic Power System Structure.

The generation system is mainly composed by synchronous machines that are usually large. The transmission system is composed by transmission lines that extend for large

distances and interconnect different generation units. The transmission lines demand special consideration in controlling the voltage at the terminals due to reactive power flow (in AC type lines). Distribution systems delivery power to the loads where the voltage level is lower. The distribution lines require special attention to control the voltage at the loads.

The power system must supply a reliable and quality electrical power to the loads. In order to achieve reliability, the power system must have reserves and controllers that can deliver the power when it is demanded, task mainly supplied by conventional generators and controllers installed throughout the power system. On the other hand, active controllers compensate the voltage and frequency variations keeping the power quality within limits.

The power system *quality and stability* depends mainly on the *power system controllability* [23], assuming that the power is available. Figure 2.6 presents a simple equivalent of the entire power system including the main controllers where only conventional equipments are included.
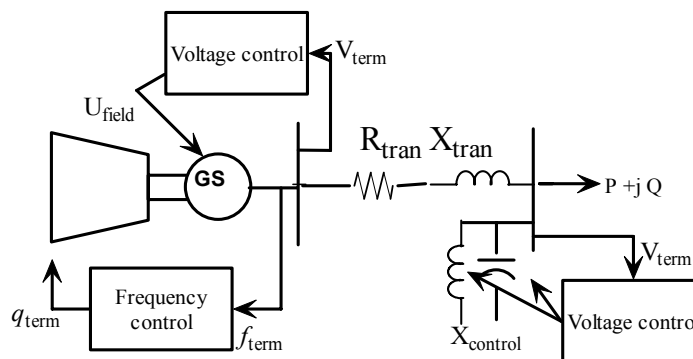
Figure 2.6 Single line equivalent of a Power System.

In Figure 2.6, the apparent power supplied to the load ($P+jQ$) flows through the transmission and distribution system from the generators (GS). The power flux results in voltage variations compensated near to the loads with decentralized voltage controllers – by adding or reducing reactive power – and in the generation stations with voltage controllers that change the excitation level of the synchronous machines. Variations on the active power result in frequency deviation that speed governors act to keep the balance on consumption and production increasing or reducing the prime-mover power. The voltage controllers are mainly related to the reactive power while the frequency controllers to the active power ([23] and [27]).

Wind turbines are a special kind of generators, which has none or little voltage and frequency control capabilities and they supply an intermittent power. In addition, wind turbines in general use asynchronous generators that demand reactive power from the network to its excitation. The reactive power demanded to the wind farms is partially compensated by capacitor banks and the network supplies the rest of the reactive power.

The active power produced from wind farms varies all the time and leads to continuous power flux variations. On the generation stations, it leads to continuous action of the frequency controllers to keep the balance on production and consumption (and the frequency constant).

2.2.1   Voltage Stability Problem

A definition to the voltage stability phenomenon has not been widely accepted yet. Nevertheless, several task forces have worked on basic definitions of voltage stability. For instance, the IEEE Task Force Report in [29] defines the voltage stability in terms of the ability of maintain voltage so that when load is increased, load power will increase hence voltage and power are controlled.

Although voltage stability definition is not widely accepted, the voltage collapse is well recognized. Here, the voltage collapse occurs if after an increase in load or power injection, the voltages are below acceptable levels followed by a progressive and uncontrollable decline in voltage [29].

The voltage stable operation means that the voltages near to loads are identical or close to the pre-disturbance values [27], where disturbances may be a simple load increase or a variation in power from a wind farm.

The voltage collapse in general results from an incident of voltage instability. The voltage instability phenomenon is defined here as having crossed the maximum deliverable power limit, the mechanism of load power restoration becomes unstable, reducing instead of increasing the power consumed [29]. The voltage instability event can grow to voltage collapse leading to entire or a large part of the power system with very low voltage profile.

Here, in order to illustrate the voltage collapse, a simple formula based on the load flow calculations is introduced. Figure 2.7 presents a single line diagram used to define simple analytical equations to voltage stability (please note that the shunt elements are not included).
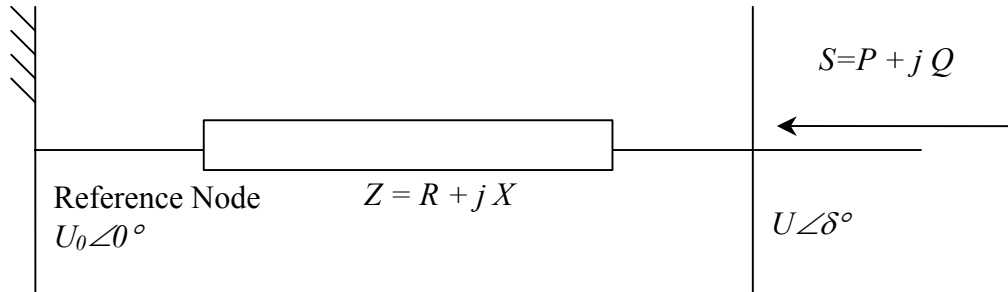
Figure 2.7 Simplified transmission line equivalent diagram.

above, U_0 is the infinite node voltage, Z is the impedance characteristic to the specific node (also called short circuit impedance). The voltage difference between the two nodes can be defined as:

$$U - U_0 = Z \cdot \frac{S^*}{U^*}$$

(2.4)

Assuming U_0 real and rewriting Equation (2.4) as:

$$U \cdot U^* = U_0 \cdot U^* + Z \cdot S^*$$
$$U_R^2 + U_I^2 = U_0 \cdot (U_R - jU_I) + (R + jX) \cdot (P - jQ)$$

(2.5)

and remembering that $U^* = U_R - jU_I$. In addition, a function H is defined as $H = ZS^* = H_R + jH_I$. Isolating the imaginary part of the voltage (U_I) as:

$$U_I = \frac{(PX - QR)}{U_0} = \frac{H_I}{U_0} \qquad (2.6)$$

and inserting in Equation (2.5):

$$U_R^2 + \left(\frac{(PX - QR)}{U_0}\right)^2 - U_0 \cdot U_R - (RP + XQ) = 0$$

$$U_R^2 + \left(\frac{H_I}{U_0}\right)^2 - U_0 \cdot U_R - H_R = 0 \qquad (2.7)$$

The real part of the voltage in the node can be defined as:

$$U_R = \frac{1}{2}\left[U_0 \pm \sqrt{U_0^2 - 4\left(\left(\frac{H_I}{U_0}\right)^2 - H_R\right)}\right] \qquad (2.8)$$

For the sake of simplicity, it is assumed that the infinite node voltage $U_0 = 1$ p.u., then Equation (2.8) becomes very simple as:

$$U_R = \left[\frac{1}{2} \pm \sqrt{\frac{1}{4} - \left(H_I^2 - H_R\right)}\right] \qquad (2.9)$$

Adding the real part of the voltage in Equation (2.9) and the imaginary in Equation (2.6) results in the voltage at the node as follow:

$$U = \left[\frac{1}{2} \pm \sqrt{\frac{1}{4} - \left(H_I^2 - H_R\right)}\right] + jH_I \qquad (2.10)$$

Now it is possible to state that:

- If $H_R - H_I^2 < -1/4$ – there is no physical solution.
- If $H_R - H_I^2 = -1/4$ – both solutions coalesce and the point of voltage collapse is reached.
- If $H_R - H_I^2 > -1/4$ – the solution is double: one physical and one spurious (unstable).

The voltage stability is complex and, even to a very simple case, includes the load, network characteristics, and the voltage at the sending node.

Using the diagram in Figure 2.7, it is possible to illustrate the maximum power transferred to a specific node as a relation of the voltage at that node (Figure 2.8) to different load factor conditions.
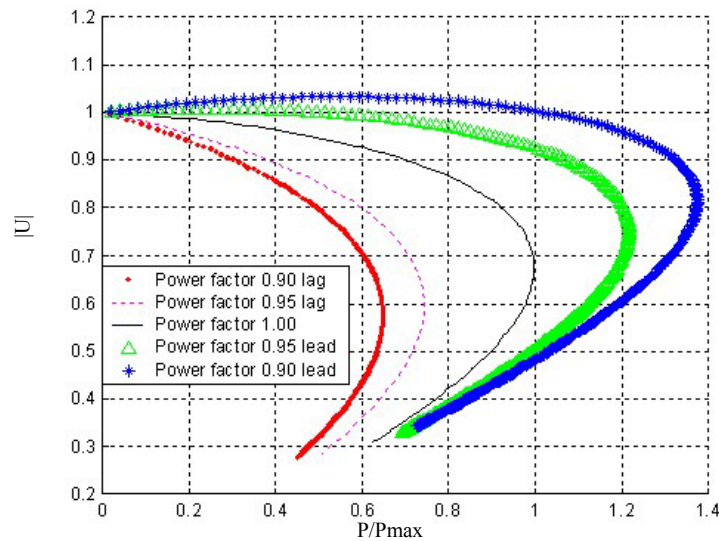
Figure 2.8 Power transfer to a node as function of the voltage (*"nose curve"*).

Figure 2.8 is a simple illustration of the relation between the power transmitted to a node and its voltage. This curve is the Voltage vs. Power characteristic of the node also called "*nose-curve*". Using Figure 2.8, the voltage stability limit is characterised by the vertical tangent at the *nose point* that is in fact the maximum power transmitted to the node in agreement with definitions above.

When transferring the problem to the complex power system, the relevant factors that lead to voltage instability are: the transmission lines and power transfer strength of the power system; generator reactive power/voltage control limits [35]; load characteristics [36]; characteristic of reactive power compensation; and the action of voltage control devices such as under load tap transformers [37].

The dispersed voltage controllers acting on the distribution grid also influence the voltage stability. Distribution grids uses under load tap changer transformer, which under voltage instability events, tends to increase the problem by increasing the current flow in order to re-establish the set voltage level.

In addition, the characteristics of the reactive power compensation devices with the voltage contribute to the voltage instability. Usually, shunt capacitor banks compensate the reactive power in the power system. The reactive power supplied from shunt capacitors is related to the squared of the voltage. Hence, when started a voltage decline it will reduce the local reactive power production stressing even further the transmission lines and reducing further the voltage level. Similarly, the loads response to voltage changes influences the voltage stability.

Finally, large number of wind farms on power systems (high penetration) demands reactive power and in addition some synchronous generators (generation stations) are shut down in order to achieve cheaper energy production. Under this condition, the excessive demand for reactive power can be a problem.

2.2.1.1 Analysis of Voltage Stability

The analysis of voltage stability for a given power system involves examination of several aspects, e.g. distance to voltage collapse, mechanisms that lead to voltage collapse

among others [27]. The voltage stability problem has been discussed in a large number of papers and always analysed by means of expensive and complicated models. A comprehensive reference list can be found in [28].

The voltage stability here includes periods from 15 minutes to hours, being a dynamic problem rather than static [29]. However, as the dynamics involved in the voltage stability problem are very slow, the voltage instability is analysed by static models.

The load flow problem is very closely associated with voltage stability analysis [27]. The load flow programs determine the operational characteristics of the power system based on the load schedule and voltage reference in the generation units.

In load flow problems, the Jacobian (Newton-Raphson algorithm) represents a linear relation between the power and voltage at a specific operational point. When the voltage collapses, the maximum power transferred was reached and the Jacobian becomes singular. At that point, there is no solution to the load flow problem and that is the maximum transmissible load. The use of the Jacobian properties has been pointed by several authors where modal analysis and voltage collapse proximity indicators have been proposed [29].

Here, the voltage stability is defined in terms *loadability curves* to a specific node before voltage collapses [28]. The loadability curves are similar to the "nose-curve" in Figure 2.8, however, the lower part (unstable part) of the curve is not simulated here. The load to a specific node of the power system is stressed until the Jacobian matrix becomes singular and, at that point, the maximum load is defined.

The loadability curves are computed using a loadability computation tool based on a load flow program using Newton-Raphson algorithm, which was implemented in Matlab as part of this project.

The loadability curve indicates the maximum load increase in the power system under specific conditions. Here, the loadability curve is also used to define the maximum wind power to the power system. The wind power to a node is increased until the maximum power transfer is reached. The loadability curves are similar to the injection of wind power but the power to the node is injected instead of a drained.

2.2.2   Frequency Control Problem

The power system has a nominal frequency for which all generators are synchronized. In a synchronized system, the power is naturally shared between different generators based on the rate of the rating of the generators or as defined by the system operators.

The frequency control in 10 minutes can be classified in primary and secondary [38]. The primary control is fast control actions to keep the instantaneous balance between production and consumption. Secondary control is slow control actions to re-establish nominal system frequency and scheduled power interchanges. This thesis focuses on the primary control of frequency because it is the controller acting instantaneously to avoid frequency deviations related to stochastic variations from wind turbines.

The primary frequency control is done by speed governors, which automatically adjust the prime movers driving the generator to keep the balance on consumption and generation. The speed governor acts based on speed deviation where, "*(...) most automatic controls use high gain negative feedback, which, by its active nature, can cause oscillations to grow in amplitude with time.*"[39].

Originally, the interconnected generators were fairly close to one another, and oscillations were at frequencies of the order of 1 to 2Hz ([23] and [24]). Dampers windings on the generators were used to prevent the oscillations to grow. Increasing the demands for reliability makes the rapid automatic voltage controllers that are used to prevent the generator loosing synchronism following a system fault. This fast action tends to reduce the damping of the system oscillations hence special Power System Stabilizers – PSS – were designed to damp those oscillations [39]. The power system is very complex and specific components can interact with other causing oscillations.

From an operating point of view, oscillations are acceptable as long as they decay. Oscillations are a characteristic of the power system, which are initiated by the normal small changes in the system load and, in this report, from wind farms power variations. The wind farm power produced can be viewed as a continuous negative load variation that demands the speed governors to act all the time to keep the balance on the system.

The power oscillations can be sustained due to the controller natural characteristic. Although the oscillations are not expected to increase in time, the sustained variations can become a problem.

2.2.2.1 *Analysis of Power System Oscillations*

The power system oscillations analysis may be done by modal analysis complemented by dynamic simulations ([23], [24], [25] [39] [40] and [41]). The modal analysis uses a linear representation to the entire power system being suitable to analyse small disturbances in the power system (it is also called small signal stability analysis of the power system). The modal analysis however must be used with caution because it does not include the non-linear behaviour of equipments on the electrical power system. Hence, it is also important to include dynamic simulations to analyse the power system oscillations during normal operation.

The modal analysis has been recognized as one of the most reliable tools to analyse power systems ([23] and [25]). With the modal analysis it is possible to define the eigenvalues of the power system hence it is possible to identify the electromechanical oscillation modes.

The power system can be described by equations that include: all electromechanical characteristics, the network equations and the controllers. These equations can be linearised on an operational point. Where, the linear model put on the form of a set of first order differential equations with constant coefficients (state equations) have the form:

$$[\dot{x}] = [A] \cdot [x] + [B] \cdot [u]$$
$$[y] = [c] \cdot [x] + [d] \cdot [u]$$

(2.11)

where, x is a vector of the dynamic state variables, A is the state matrix, B is the input matrix, y is the output (or measured) variables, c is the output coefficient matrix and d is a matrix of coefficients describing the direct connection between the input and output variables: the vector u.

The eigenvalues of A represents the roots of the state equations defined as the values of s that satisfies:

$$\det[A - s_i I] = 0 \tag{2.12}$$

where each solution s_i defines a time function $e^{(s_i\ t)}$ that satisfies the state equations [25]. The function is called a mode of oscillation of the system.

If all eigenvalues have a negative real part all modes decay with time and the system is said to be stable. If one eigenvalue has a positive real part, the corresponding mode will grow exponentially in time being unstable.

The modal analysis characterizes the modes of oscillation of the power system and the less damped oscillation modes, i.e. the modes that the respective eigenvalues are close to the positive plane. Hence, the possible problems in the frequency control in the power system are characterized.

However, the modal analysis must be accompanied with dynamic simulations in order to include the non-linear characteristic of the power system [39]. Hence, dynamic models to large-scale wind power must be applied to the power system dynamic simulations to analyse the interactions between the wind power and frequency controllers during normal operation of the power system, in addition to the modal analysis.

Dynamic simulations including the entire power systems are very expensive. In order to analyse the main characteristics of the power system, dynamic reduced models are used as pointed in [26] and [42]. The dynamic reduction is an aggregation of machines and loads with similar dynamic performance that reduces the number of equations to describe the power system and does not lose important information [26]. In this thesis, dynamic reduced models are used to analyse the power system performance with wind power.

2.3 Remarks on Wind Energy Integration

The integration problems caused by wind power have been discussed in this chapter. The problems were classified in small-scale and large-scale integration. Table 2.2 presents the main integrations problems from wind power [20].

Table 2.2 Main power system influences from the wind energy integration

Integration scale		Problems	Causes
Large Scale	Small Scale	Steady state voltage rise	Wind speed variation
		Over-current	Peaks of wind speed
		Protection error action	Peaks of wind speed
		Flicker emission during continuous operation	Dynamic operation of wind turbines
		Flicker emission during switching operations	Switching/start up operation of generators
		Voltage drop	In rush current due to switching operations of generators
		Harmonics	Power electronic converters
	Power system Oscillations		Inability of the power system controllers to cope with the power variations from the wind farm and loads
	Voltage stability		Reactive power limitations and excessive reactive power demand from the power system

The small-scale wind power integration into power system is well investigated and there are plenty of tools available to analyse its interaction. The problems from connecting

small numbers of wind turbines to the power system are related to the voltage quality and thermal capacity of the lines and cables.

The large-scale integration of wind farms, however, it is not properly investigated yet and it is very complex. The large-scale problems include all problems from the small-scale and in addition problems of voltage stability and power system quality. The voltage stability problem is related to the limitation of power transfer. The extensive use of capacitors banks to compensate reactive power can result in larger problems in event of islanding e.g. self-excitation of the induction generators.

Large disturbances such as short circuits in sites with large amount of wind turbines can result in voltage transient instability due to the reduced capacity in transferring reactive power and the huge demand from the induction generators as well as transformers after the fault is removed.

The power system quality can deviate from limits. The voltage quality deviates because of the power flux in the network, and in large-scale integration, the frequency can deviate from its limits as well.

The main conclusions are:

- Small-scale integration of wind energy deals mainly with voltage quality and reliability;

- Large integration of wind turbines includes the small-scale problems and overall stability problems;

- The analysis of large-scale integration demands suitable models to represent wind power;

- Network characteristics play an important role on the power system stability and quality;

- Wind turbines power characteristics play also another important role in the overall power system stability and quality

In order to investigate the wind power influences on the power system quality and stability it is imperative the use of appropriate models to represent the wind farm and the power system. The wind turbine models must have the following characteristics:

- Dynamics models for the wind speed acting on each wind turbine;

- The spatial wind coherence in large-scale;

- Detailed model to the wind turbine dynamics;

- Proper representation of the power flux of the wind turbine generator;

- Time feasible in order to analyse large power system.

Moreover, the power system models must have the following characteristics:

- Include proper models to the electrical components;

- Include models to the loads;

- Be flexible to allow the implementation of wind turbine/farm models and interact with other simulation tools;

- Input/output capabilities in order to analyse the data;

- Allow the implementation of large power systems;

- In large integration, represent properly the electro-mechanical modes in the power system.

Chapter 3

3   Wind Speed Model

Wind turbines produce a complex and continuously fluctuating power. A large part of the complexity resides on the input: the wind. The main source of power variation on conventional wind turbines is the wind speed variation.

The wind is complex and the blades crossing the wind field modify the power fluctuations. The main objective of this chapter is to present a dynamic wind model for power quality assessment of a three bladed up-wind horizontal axis wind turbine type. The wind speed model includes the turbulence and tower shadow in the rotor area.

Figure 3.1 illustrates an example of the wind field acting on the rotor area of a wind turbine (borrowed from [43]).
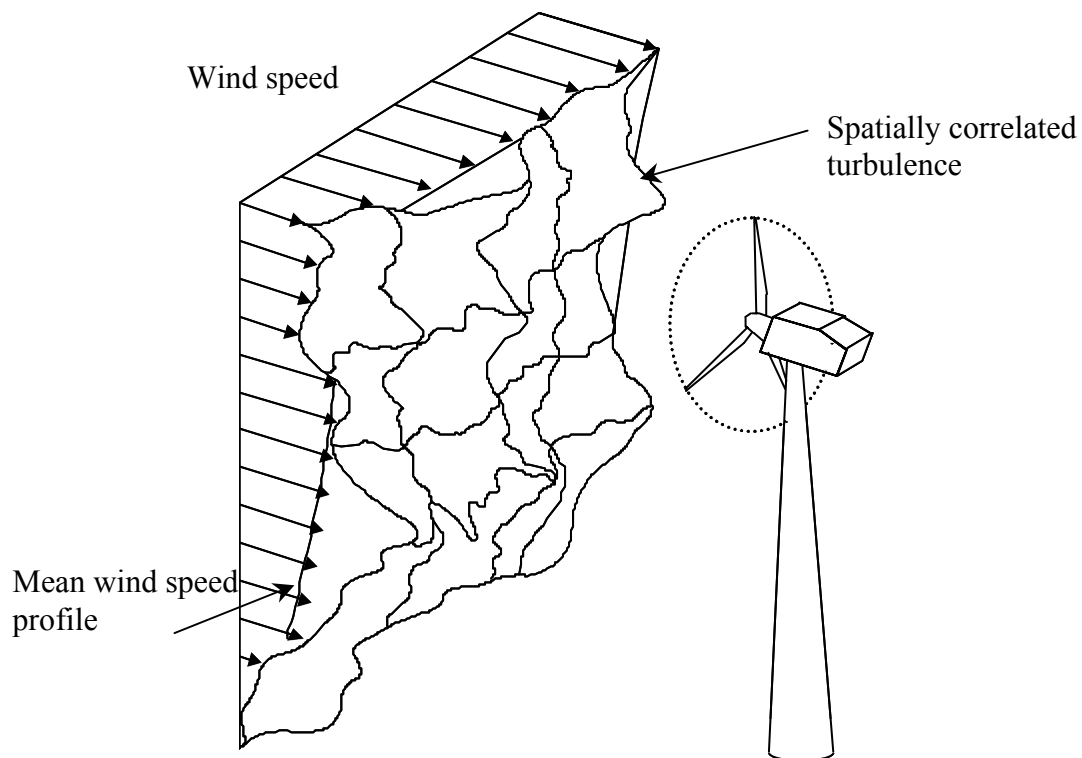
Figure 3.1 Illustration of the wind on the rotor area of a wind turbine [43].

The wind is classified in two main parts: the first part represents a mean wind speed profile over the rotor area, here defined as deterministic; and the second part is turbulence on top of the deterministic (see Figure 3.1), here assumed as stochastic.

The deterministic part of the wind over the rotor area is assumed "*constant*" in 10 minutes period and the wind variations are the time variant part that has a stochastic behaviour. This assumption is valid only in periods up to few minutes because above this there is a slow wind variation in the mean wind speed due to continuous change in the atmosphere.

Returning to Figure 3.1, the wind acting on each rotating blade section is different from the wind in a stationary reference frame. The blades pass through different wind

speeds in each revolution. The process of passing several times through this wind speed field results in power variations at n times the rotational speed revolution of the rotor called np's.

Figure 3.2 presents a measured time series of active power produced from a 500kWstall regulated, three-bladed wind turbine type (direct connected to the grid). Figure 3.2 also shows the power variations classified in fast and slow where the mean value is removed.
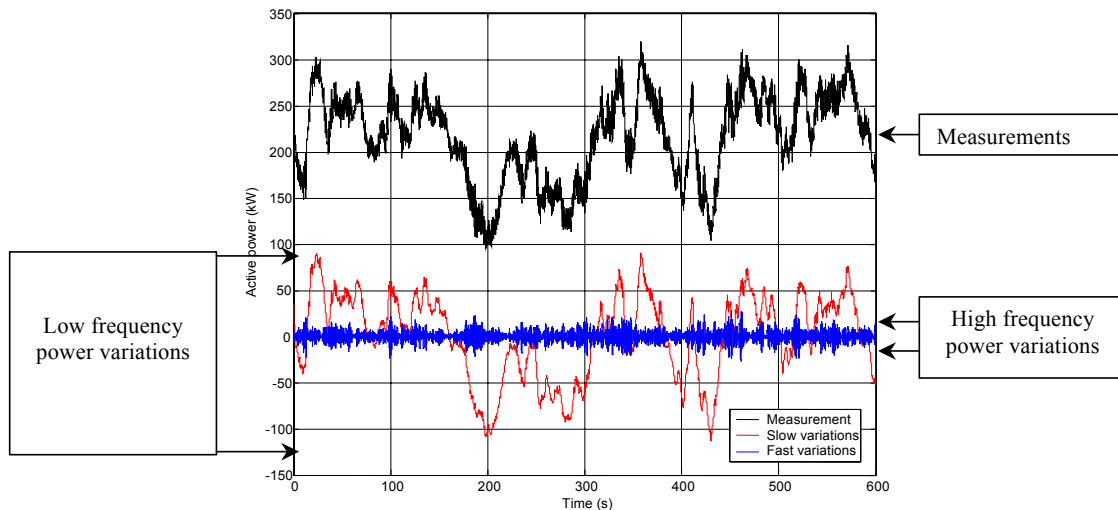
Figure 3.2 Power produced by a 500kW stall regulated wind turbine.

In Figure 3.2 the active power measured from a three bladed wind turbine vary in a broad frequency range. It is possible to decompose the measurements in slow and fast power variations where the slow power variation includes frequencies up to 0.5Hz and the fast power variation includes all frequencies above 0.5Hz.

The low frequency power variations are the largest variations and they are related to turbulence on the rotor area as it has been recorded in anemometers. In this particular case, the slow power variations are within +80kW and–110kW, which is the main responsible for high standard deviation of power produced from wind turbines.

The high frequency power variations are much smaller, in this case within ±10kW. The high frequency power variations cannot be directly related to the turbulence but to the dynamics of the wind turbine including the blade rotation in the wind field. The relatively high frequency power variation has been related as one of the main responsible for the flicker problems [60] as introduced in chapter 2.

This chapter presents the general main *wind-related* power output variations from wind turbines. The aim is to reproduce the mechanical torque using an equivalent wind speed model to the entire rotor. The *Equivalent Wind Speed (EWS)* model simulates the wind by an equivalent time series that when applied to a specific aerodynamic model reproduces the aerodynamic torque from a wind turbine, which applied to a drive train/generator model simulates the electrical power from a real wind turbine (Figure 3.3). The dynamics of the wind turbines are explained in chapter 4 where the wind turbine components are introduced.
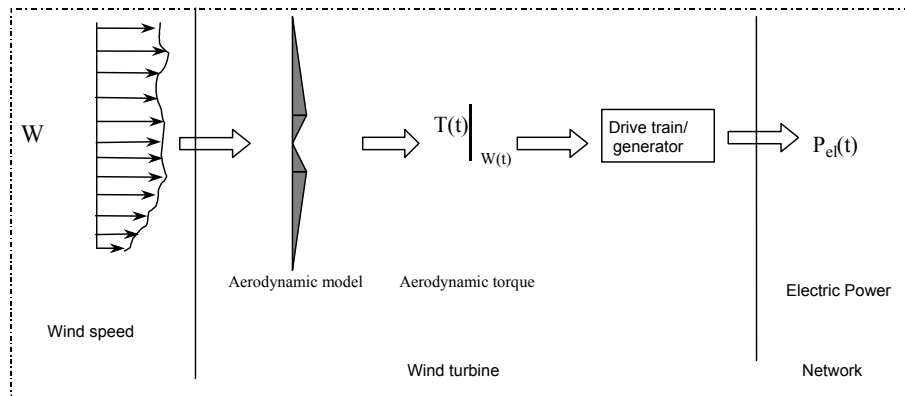
Figure 3.3 General overview of wind turbine models.

In Figure 3.3, W is the wind speed over the rotor area, T is the aerodynamic torque and P_{el} is the electrical power transferred to the utility network.

3.1 Model Description

Measurements of turbulence in a stationary reference frame show that the amplitudes of the wind speed variation reduce with the frequency. Above a few Hertz, the wind speed variations are insignificant [44]. However, the rotation of the blades causes variations in the effective wind acting on each blade section on n times the rotor speed frequencies.

Figure 3.4 presents the Power Spectral Density (PSD) of the wind measured on a rotating blade section [45]. The wind speed variation on multiples frequencies of the rotor (that in this case is 0.5 Hz) is clear.
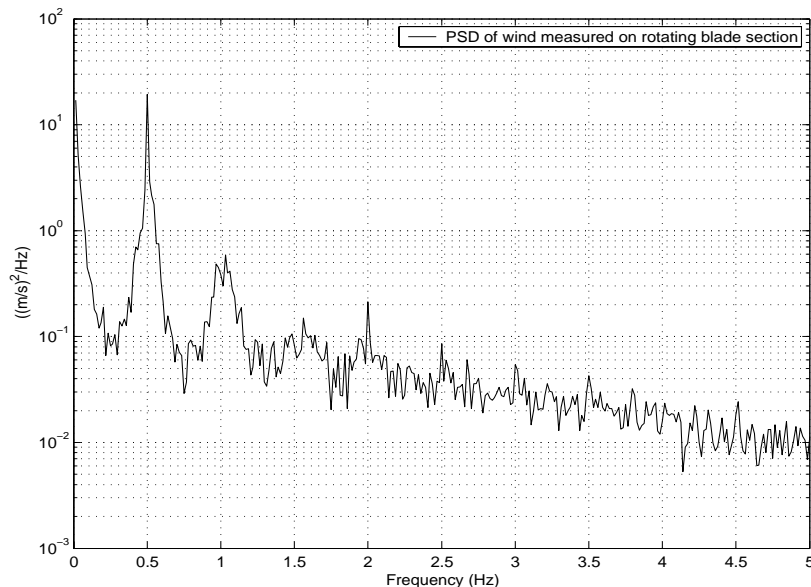
Figure 3.4 Wind speed measured on a section of a rotating blade [45].

The PSD (in Figure 3.4) shows that each blade section of the wind turbine experiences high wind speed variations on the rotational speed of the rotor. In the low frequency range from 0 to 1.5Hz are the main wind variations. Above that frequency, the wind speed variations are very reduced mostly because of the dynamics of turbulence.

The measurements were done on a single section of a rotating blade, hence when adding up the wind effects on the remaining others two blades in a symmetrical three-bladed rotor of a wind turbine, all the frequencies different from 3 times the rotor speed (3np) are cancelled. The cancellation effect is expected due to the symmetric position of the three-bladed rotor and has been supported by power measured from wind turbines. Figure 3.5 presents the PSD of the measured electrical power from a three bladed wind turbine, 500kW, stall regulated and operating with in constant speed.
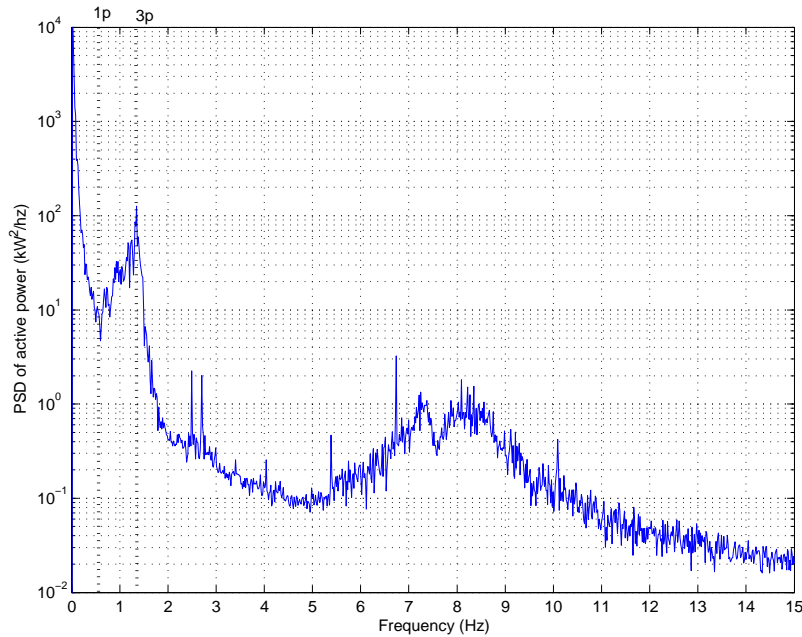
Figure 3.5 PSD of measured electrical power output of a 500kW stall regulated wind turbine.

The PSD in Figure 3.5 correspond to the measured time series of power presented in Figure 3.2. The fundamental frequency (1p) is approximately 0.4Hz (indicated in the figure). At this frequency, a small contribution is present that is related to some asymmetry in the rotor. At the frequency of 0.8Hz (2p), a small power variation is presented that is also related to some asymmetry on the rotor. The torsional drive-train mode (dynamic from the wind turbine) is around 1.08Hz that gives a small power variation. The most relevant power variation is at 3p frequency (1.2Hz), which is relevant to the power quality analysis hence it is retained in the dynamic wind model. At the frequency range from 6 to 11Hz, a small amount of energy is presented, which is related to a complex mode of the wind turbine. The complex mode is related to a dynamic interaction between the electrical generator and the flexible wind turbine, it is not related to the wind turbulence.

In this chapter, only the wind-induced power variations that are relevant to power quality are treated hence the dynamics of the wind turbine is not included in this chapter but explained in chapter 4. Considering the measured PSD of power produced from wind turbines and the measured wind speed on a rotating blade, the main wind related power variations are from the 0 and 3 times the revolution of the rotor.

The wind speed model represents the power variations from the wind in the frequency range of interest as a time domain model. It generates 10 minutes period time series. The 10 minutes period was selected for several reasons, first of all the 10 minutes period avoid most of the cyclical variations related to meteorological phenomena (e.g. diurnal variations related to periods of hours). Second, the period matches the time frame of the primary

frequency controllers from power systems, which its performance with large amount of wind power is one of the aims of this report. Moreover, the voltage quality assessment (e.g. statistics and flicker) in [46] as well as wind turbines characteristics, e.g. power curve, are based on 10 minutes measurements

In 10 minutes period, the stochastic and deterministic parts can be combined to express the total wind at one position as:

$$W(x,y,z,t) = U(x,y,z) + g(x,y,z,t) \qquad (3.1)$$

where $W(x,y,z,t)$ is the total wind speed in position xyz at time t, $U(x,y,z)$ is the deterministic wind speed that is assumed time independent and $g(x,y,z,t)$ is the stochastic part that has mean value zero. Figure 3.6 presents the references axis and notation of the wind turbines. The origin of the coordinate system is the centre of the nacelle precisely at the height of the centre of the rotor, so the *z-axis* is negative in the direction to ground.
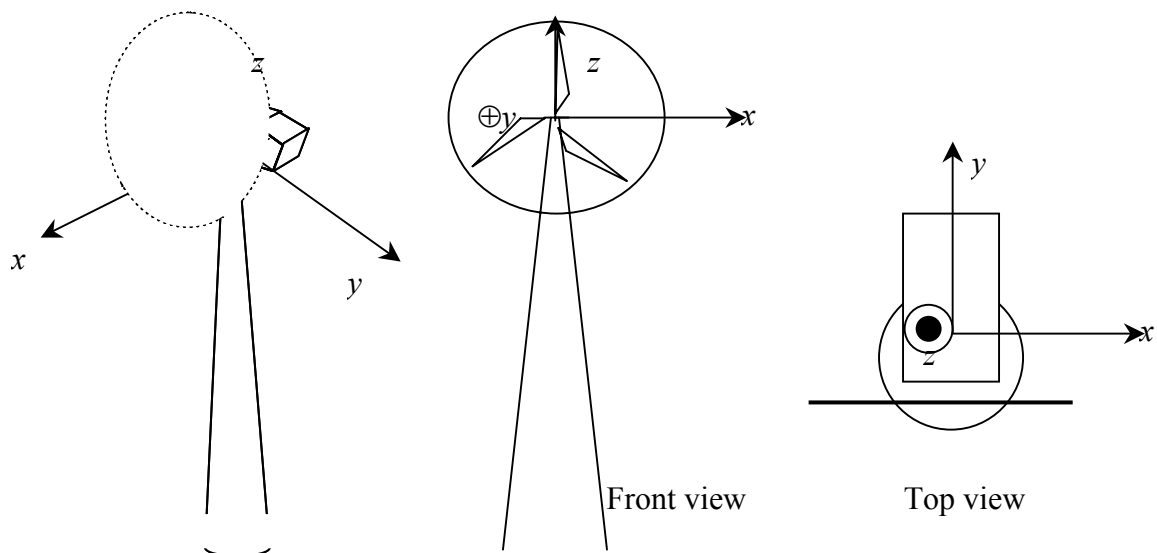
Figure 3.6 Reference axis used in the wind turbine.

3.1.1 Equivalent Wind Speed Model

The Equivalent Wind Speed (EWS) model is an equivalent for the entire rotor that takes into account the stochastic and deterministic wind speed actions on the rotor area. The EWS applied to an aerodynamic function simulates the real torque on the main shaft of wind turbines. Figure 3.7 illustrates the principle of the EWS.
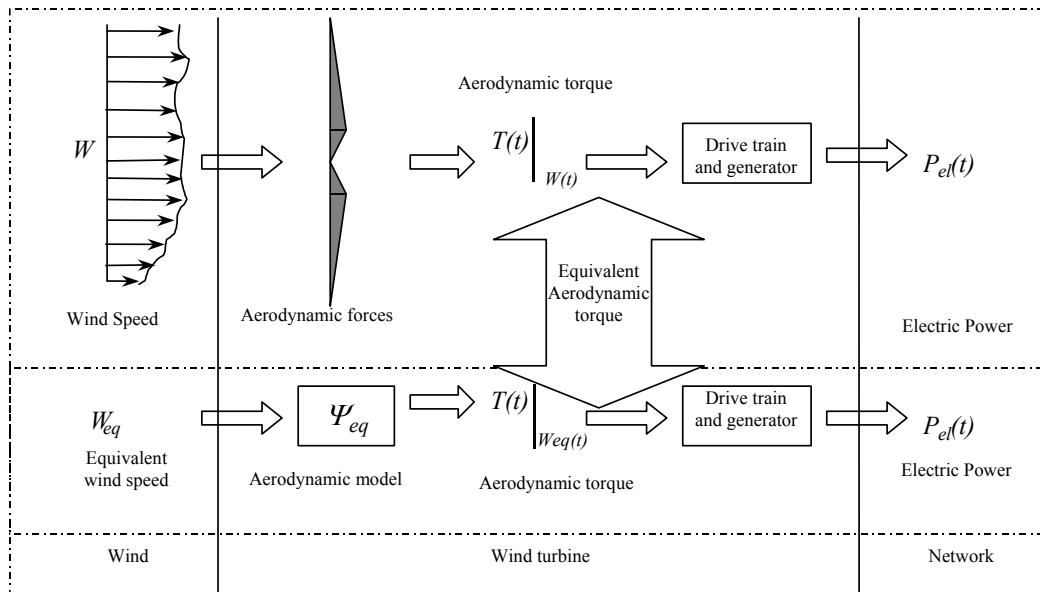
Figure 3.7 Equivalent Wind Speed Model principle.

The upper part of Figure 3.7 illustrates how the power is produced in a real wind turbine. The wind speed (*W*), which is different at each rotor position for each time, acts on the blades of the wind turbine. The aerodynamic blades convert the wind by complex aerodynamic effects on mechanical power on the mechanical shaft of the wind turbine (aerodynamic torque (*T*) times the rotor speed). The mechanical power is then converted into electrical power in the electrical generator. The lower part of Figure 3.7 illustrates the main idea of the EWS, which is to reproduce the same mechanical torque using a single equivalent wind speed time series applied to an aerodynamic model. Because the rotational speed depends on the electrical generator, it is assumed that the electrical power produced by the EWS is the same as the one produced in a real wind turbine.

3.1.2   Description of the Equivalent Wind Model

The wind acting on the rotor area of a wind turbine can be modelled in several ways. The objective of the model defines the type and details to be retained of the wind model. The EWS aims to simulate the electrical power output variations from a three-bladed wind turbine.

Usually the wind models assumes that the continuous wind field on the rotor area can be replaced by discrete time series of wind speeds in a grid of points on the rotor area. This process is very common and reliable, however, it generates many time series that are only used partly and generally, it consumes much simulation time [47].

Yet, in the grid wind model, an aerodynamic routine interpolates between the appropriate points of the wind grid to generate a continuous wind speed at a given section (radius) of the rotor blade. Based on the continuous wind speeds in a number of blade sections, an aerodynamic module calculates the aerodynamic torque on the main shaft. Finally, the aerodynamic torque enters a dynamic model of the drive train and electrical generator, which will output the electrical power.

The EWS replaces all wind time series on the rotor area and a relatively simple aerodynamic function supplies the aerodynamic torque. The main advantages of the

equivalent wind speed model are: fast computation and reduced memory requirements. The single equivalent wind speed model is also very suitable for simultaneous simulation of a large number of wind turbines making it possible to efficiently estimate the impact of a large wind farm on the power quality.

The Equations (3.2) to (3.4) below provide a more formal description of the aerodynamic model for a 3-bladed wind turbine shown in Figure 3.7. Applying blade element theory, an aerodynamic coefficient ($\Psi(r)$) on a given blade section r is calculated. $\Psi(r)$ and $W(t, r, \phi)$ are used to calculate the contribution from a single blade to the aerodynamic torque $M(t,\phi)$ according to Equation (3.2). It must be noticed that in the following equations polar coordinates is used: r, ϕ are the rotor position in polar coordinates where r is the radial position and ϕ is the angular position of the blade section.

$$M(t,\phi) = \int_{r_0}^{R} \Psi(r) \cdot W(t,r,\phi) dr \tag{3.2}$$

where R is the length of the blade, and r_0 is the inner radius, where the aerodynamic forces start to develop. The effect of all three blades are then added to give the total aerodynamic torque $T(t,\phi)$ using:

$$T(t,\phi) = \sum_{b=1}^{3} M(t,\phi_b) \tag{3.3}$$

For the summation in Equation (3.3), it can be assumed that the azimuth position ϕ_b of blade number b is given by:

$$\phi_b = \phi + \frac{2\pi}{3}(b-1),$$
$$b = 1,2,3 \tag{3.4}$$

The Equations (3.2) to (3.4) describe how the aerodynamic torque is generated physically. The equivalent wind speed is based on an expansion of the wind speed field in the azimuth angle (ϕ). A similar expansion was done by Madsen and Rasmussen [48] using real expansion coefficients. Using complex expansion coefficients, the expansion of the wind speed field formally becomes much simpler as given in Equation (3.5).

$$W(t,r,\phi) = \sum_{n=-\infty}^{\infty} \widetilde{W}_{\{n\}}(t,r)e^{jn\phi} \tag{3.5}$$

$\widetilde{W}_{\{n\}}(t,r)$ is the complex azimuth expansion coefficient. This azimuth expansion coefficient indicates the amplitude of the nth harmonic in the rotational speed [49]. Inserting (3.5) into (3.2) provides the expanded expression for $M(t,\phi)$ in:

$$M(t,\phi) = \sum_{n=-\infty}^{\infty} \widetilde{M}_{\{n\}}(t) \cdot e^{jn\phi} \tag{3.6}$$

the azimuth expansion coefficients $\widetilde{M}_{\{n\}}(t)$ are given in:

$$\widetilde{M}_{\{n\}}(t) = \int_{r_0}^{R} \Psi(r) \cdot \widetilde{W}_{\{n\}}(t,r)dr \qquad (3.7)$$

Inserting Equation (3.7) into Equation (3.3), and further using Equation (3.4) yields the azimuth expansion of the torque $T(t,\phi)$ according to:

$$T(t,\phi) = \sum_{n=-\infty}^{\infty} \widetilde{T}_{\{3n\}}(t) \cdot e^{j3n\phi} \qquad (3.8)$$

where the azimuth expansion coefficients of the torque $\widetilde{T}_{\{3n\}}(t)$ are given as:

$$\widetilde{T}_{\{3n\}}(t) = 3 \cdot \widetilde{M}_{\{3n\}}(t) \qquad (3.9)$$

From Equation (3.8), the summation of the contributions from the three blades remove harmonics which are not multiple of three. This effect will be complete if the rotor is symmetrical, which e.g. requires that the blades have the same tip pitch angle. Substantial first harmonics have been measured on wind turbines with unsymmetrical rotors typically due to pitch misalignment.

Now defining the equivalent wind speed $W_{eq}(t,\phi)$ according to:

$$W_{eq}(t,\phi) = \sum_{n=-\infty}^{\infty} \widetilde{W}_{eq\{3n\}}(t)e^{j3n\phi} \qquad (3.10)$$

with the weighted azimuth expansion coefficients $\widetilde{W}_{eq.\{3n\}}(t)$ given in:

$$\widetilde{W}_{eq.\{3n\}}(t) = \frac{\int_{r_0}^{R} \Psi(r) \cdot \widetilde{W}_{\{3n\}}(t,r)dr}{\int_{r_0}^{R} \Psi(r)dr} \qquad (3.11)$$

Finally, the equivalent torque $T_{eq}(t,\phi)$ is defined as:

$$T_{eq}(t,\phi) = \Psi_{eq} \cdot W_{eq}(t,\phi) \qquad (3.12)$$

with the equivalent aerodynamic influence coefficient Ψ_{eq} defined according to:

$$\Psi_{eq} = 3\int_{r_0}^{R} \Psi(r)dr \qquad (3.13)$$

Using the definitions in the Equations (3.10) to (3.13), it can be shown that the equivalent wind speed $W_{eq}(t,\phi)$ generates the same torque $T_{eq}(t,\phi)$ as the wind speed field $v(t,\phi)$, i.e. $T_{eq}(t,\phi) = T(t,\phi)$.

In principle, the aerodynamic load influence coefficient $\Psi(r)$ has to be determined individually based on the geometry and hence the distribution forces along the blade radius r. In the present model, it has been assumed that the contribution to the torque is proportional to the radius, i.e. $\Psi(r)=k \cdot r$ and r_0 is 10 % of the radius R. These assumptions are based on the physical aerodynamic performance of the blades that excluding the region in the beginning of the blade (root) and the region near to the tip presents the torque proportional to the radius, fact that has been observed in different blades and have been justified in [50].

The equivalent wind speed is the sum of the *deterministic* and *stochastic* components, i.e.

$$W_{eq}(t,\phi) = U_{eq,\det}(\phi) + g_{eq,sto}(t,\phi) \qquad (3.14)$$

The deterministic part, as explained before, is independent of the time. It will only influence the dynamics of the wind turbine, because the blades rotate.

In the following sections, the implementation of EWS model is presented after having introduced the main deterministic and stochastic components. The EWS implementation is based on Equation (3.10), however, the EWS only includes the 0p and the 3p harmonics components because they are the most relevant to power quality assessment, an assumption that is supported by measurements.

3.1.3   Deterministic Part of the Wind

3.1.3.1   Tower Shadow

Tower shadow along with mean wind speed are the most relevant deterministic effect on the electrical power output from three-bladed wind turbines. Horizontal axis wind turbines always have some form of tower support structure. The tower can be lattice or cylindrical. Usual, small wind turbines use lattice towers and large new wind turbines use cylindrical towers.

Towers are obstacles to the free wind that modifies the wind flow. The upstream flow is reduced in front the tower and increased laterally. Downstream the tower makes a wake effect that reduces the horizontal wind (Figure 3.8).

Here the model is limited to the effects on horizontal up-wind wind turbines type, hence the relevant effect is the upstream flow. Mathematically the wind field can be calculated by approximating the tower to a cylinder and assuming the existence of a two dimensional potential flow ([13], [61] and [51]). The flow is then decomposed in the longitudinal and lateral wind components, i.e. the wind in the y direction and x direction respectively.

The horizontal longitudinal (y-axis) is the most relevant to power variations because it turns to be the wind converted into active power. The wind far from the wind turbine is called the ambient wind speed (U_h) and it is not interfered by the tower. When the wind comes close to the tower, the tower deviates the wind as shown in Figure 3.8.

The potential flow for the wind is constant all places around the tower, and can be expressed as [51]:

$$\psi_{wind} = U_h \sin(\beta) \cdot \left(d_{ts} - \frac{a^2}{d_{ts}} \right) \qquad (3.15)$$

ψ_{wind} is the potential flow of the wind in polar coordinates where d_{ts} is the distance of the blade section to the tower centre and β is the angle between the blade section and the horizontal flux. Decomposing the wind in the rotor area in radial – U_{hr} – and tangential – U_{ht} – components as illustrated in Figure 3.8. The radial and tangential wind speed components can be derived from the potential flow as Equations (3.16) and (3.17) (from [51]):

$$U_{hr} = -\frac{1}{d_{ts}} \frac{\partial \psi_{wind}}{\partial \beta} = -U_h \left(1 - \frac{a^2}{d_{ts}^2} \right) \cos(\beta) \qquad (3.16)$$

$$U_{ht} = \frac{\partial \psi_{wind}}{\partial d} = U_h \left(1 + \frac{a^2}{d_{ts}^2} \right) \sin(\beta) \qquad (3.17)$$
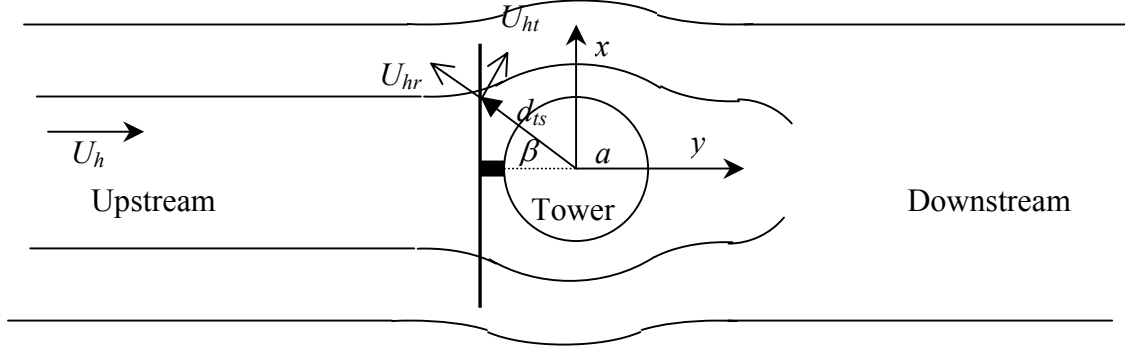
Figure 3.8 The tower shadow effects on the horizontal wind (top view).

Finally, the wind speed components presented in Equations (3.16) and (3.17) are converted to the *x-y* axis (longitudinal and lateral components) of the wind turbine.

$$U_{hx} = \begin{cases} U_h \left(\frac{a^2}{d_{ts}^2} \right) \sin(2 \cdot \beta) & \text{for } 0 \le \phi \le \pi \\ 0 & \text{for } \pi \le \phi \le 2\pi \end{cases} \qquad (3.18)$$

$$U_{hy} = \begin{cases} U_h \left(1 - \frac{a^2}{d_{ts}^2} \cos(2 \cdot \beta) \right) & \text{for } 0 \le \phi \le \pi \\ U_h & \text{for } \pi \le \phi \le 2\pi \end{cases} \qquad (3.19)$$

where ϕ is the rotor azimuth position angle, β is the angle between the blade section and the rotor axis and d_{ts} is the distance from the tower centre to the blade section expressed as (3.20).

$$d_{ts}^2 = x^2 + y^2 \qquad (3.20)$$

The tower is finite, thus the tower shadow will only influences the semi plane up to the tower height in terms of azimuth angles (ϕ) the tower influences the range from [0 π].

Figure 3.9 illustrates the tower shadow effect on the wind speed field in front of the rotor on an up-wind type rotor and a cylindrical tower.
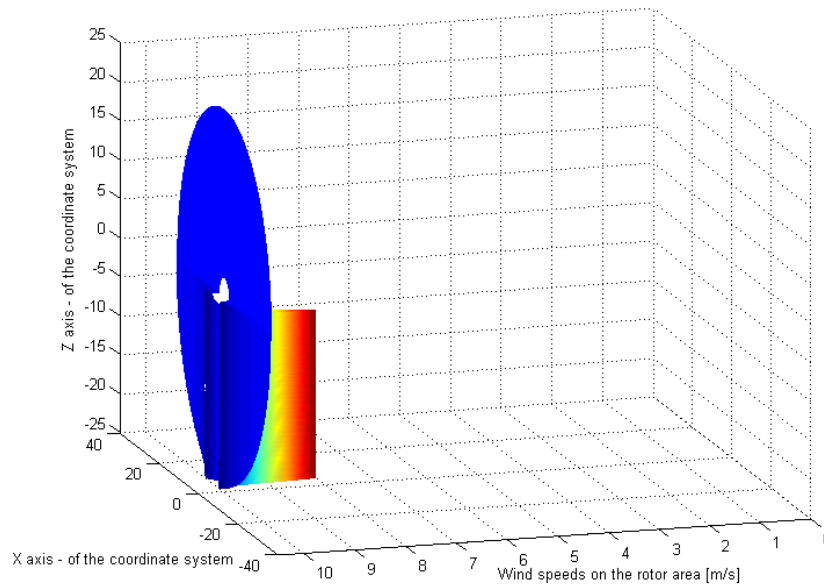
Figure 3.9 Wind speed field interference by the tower shadow.

In this particular case, the tower reduces 20% the wind speed in front of the tower and the tower influences only the lower semi plane. Above the tower, it has been assumed that the wind is not modified by the tower presence because only the horizontal component of the wind is modelled. Only the horizontal part of the wind was modelled in the first place because it is the most relevant to the aerodynamic process of generating lift hence converting the wind power into mechanical power.

Figure 3.10 illustrates the effects of tower shadow on the main shaft torque of three bladed wind turbines rotors.
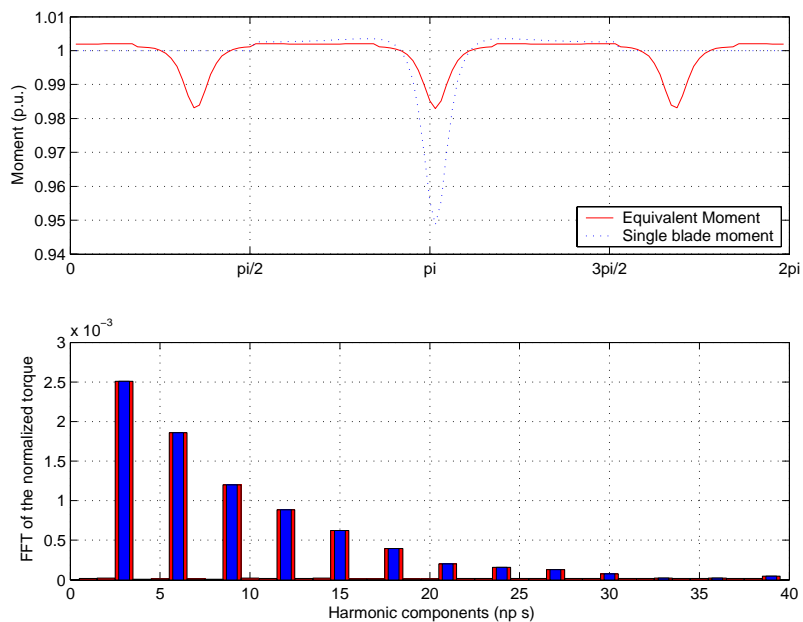
Figure 3.10 Normalised torque influenced by the tower shadow.

The upper part of Figure 3.10 presents the time series of normalised torque in a three bladed wind turbine rotor. The tower influences each one of the blades generating several harmonic components on the torque. The lower part of Figure 3.10 presents a Fourier transformation of the normalised moment influenced by tower shadow, which reveals that practically only the 3np components are presented in it. The wind turbine dynamics filter out the higher 3np frequency elements in Figure 3.10 in accordance to the PSD of the measured power output from wind turbines that shows small fluctuations in frequencies different from 3p (Figure 3.5)

3.1.3.2 Wind Shear

The friction between the ground and the moving air generates a vertical wind profile where the mean wind speed increases with the altitude. This process is called wind shear. The ground/wind friction influences the wind speed up to hundreds meters, acting on the rotor area of all commercial wind turbines [13].

The wind shear has a strong relation with the site. A smooth site, with small obstacles, e.g. sea with small waves, has a small wind speed variation with the height. On the other hand, the urban areas present a high wind speed variation with the height. That phenomenon is expected because in smooth areas the friction is much lower.

In general, the electrical power outputted from a three bladed wind turbine has very little influences from the wind shear because it is quite linear. However, the wind shear is very important to blade loads analyses but it is not transmitted to the electrical power.

The wind speed relation between two different heights can be expressed according to Equation (3.21) [13], derived from the Prandtl logarithm law model [52].

$$\frac{U(h+z_1)}{U(h+z_2)} = \frac{\ln\left(\frac{h+z_1}{z_0}\right)}{\ln\left(\frac{h+z_2}{z_0}\right)} \tag{3.21}$$

where z_1 and z_2 are the heights from the rotor centre (see Figure 3.6 for reference axis), h is the height of the centre of the rotor, U is the wind speed and z_0 is the roughness length that characterizes the terrain. The wind shear modifies only the vertical profile i.e. there is no influences on lateral space x-axis or to the wind speed related to the position of the wind turbine –y-axis.

The z_0 of a terrain is a measurement of the roughness, which can be determined in various ways, one very common is to make comparisons with sites for which z_0 has been determined from measurements and decide the most suitable one [13]. Typical values for various types of surfaces are given in Table 3.1 [53].

Table 3.1 Typical values of surface roughness length z_0 for various types of terrain [53].

Type of terrain	z_0 (m)
Smooth sea	$2.0 - 3.0 \times 10^{-4}$
Sand	$0.2 - 1.0 \times 10^{-3}$
Low grass	$1.0 - 4.0 \times 10^{-2}$
High grass	$0.4 - 1.0 \times 10^{-1}$
Forest	$0.1 - 1.0$
City	$1.0 - 4.0$

Using Equation (3.21), Figure 3.11 illustrates wind shears for different sites with an average wind speed of 10 m/s at 10 m height.
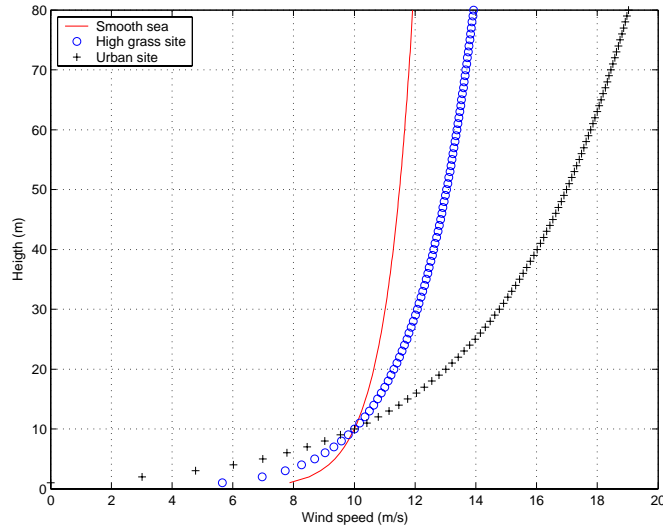
Figure 3.11 Wind shear for different sites (ground is reference for height).

The wind speed difference with the height depends mainly on the site. The wind turbine blades rotating on the wind sheared leads to cyclical loads on the mechanical torque. In smooth sites the effects are reduced leading to reduced power variations, on the other hand in sites with tall obstacles, the wind shear leads to higher wind speed variation hence higher cyclic torque variations. A wind turbine applied to wind field sheared (e.g. Figure 3.11) will suffer cyclic loads because when the blades rotate on the field, the height a blade section (point p in Figure 3.12) changes according to:

$$z_p = h - r \cdot \cos(\phi) \tag{3.22}$$

Hence, each blade section in position p is subjected to the wind speed U_p:

$$U_p(h - r\cos(\phi)) = U(h) \cdot \frac{\ln\left(\dfrac{h - r\cos(\phi)}{z_0}\right)}{\ln\left(\dfrac{h}{z_0}\right)} \tag{3.23}$$

where the variables are presented in Figure 3.12 as well as the reference axis used here.
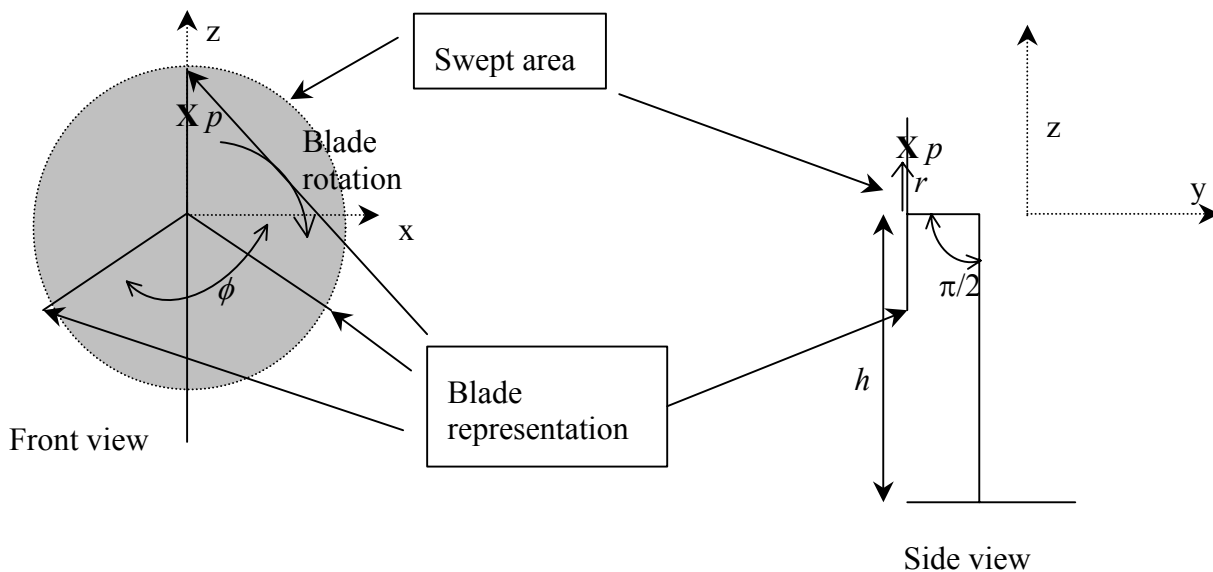
Figure 3.12 Reference axis and angles used in the wind turbine.

Where, ϕ is the angular position of a blade, p is a point in the rotating blade section distant r from the root and h is the height of the wind turbine.

Using Equation (3.23), Figure 3.13 illustrates the normalised mechanical torque of a three bladed wind turbine from the wind shear in a site with z_0=0.05 (the wind turbine is the same used to compute the tower shadow effects in Figure 3.10).
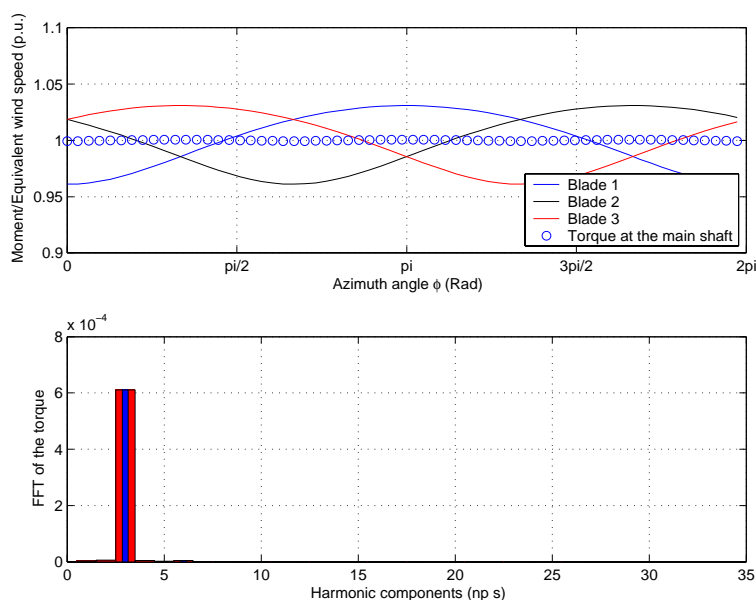
Figure 3.13. Normalised torque influenced by wind shear (site with a medium z_0).

The upper part in Figure 3.13 presents the normalised torque variations due to wind shear. The 120° displacements between the three blades cancel the symmetrical torque resulting in cancellation of torque contributions in frequencies that are different from 3np. The FFT of the resulting torque presented in the lower part of Figure 3.13 shows that in

symmetrical rotors the total torque on the main shaft presents mostly 3p frequency variations. The variation in the 3p frequency is very small.

The effects from the tower shadow were much more relevant (the FFT in 3p was around 2.5×10^{-3}) compared to the effects from wind shear (6×10^{-4}). The wind shear effect is very important in mechanical and fatigue analysis of blade loads but to the power quality, it is neglected. Currently, the deterministic part of the EWS model only includes the tower shadow and the mean wind speed as it is presented in the following section.

3.1.4 Implementation of the Deterministic Component

The deterministic part represents only the tower shadow effect, in particular the interference from tubular towers in up wind turbines type. The implemented deterministic model is illustrated as block diagrams in Figure 3.14, where *"detr3rd"* is the amplitude from the contribution of the 3rd harmonic calculated based in the geometric parameters of the wind turbine, *"um"* is the mean wind speed specified and *"Wsdet"* is the output deterministic wind time series [54].
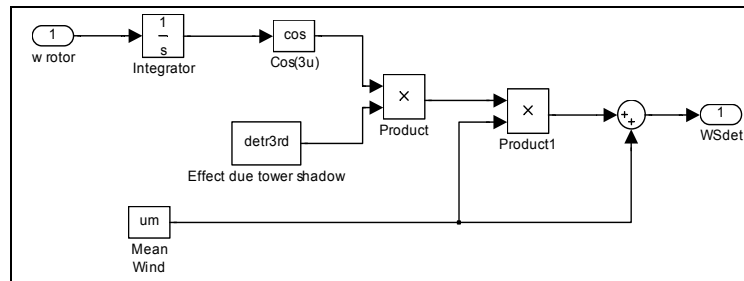
Figure 3.14 Implementation of the deterministic model in Simulink/MATLAB.

The implementation in Figure 3.14 first generates the rotor position ϕ as the integral of the rotor speed, which is a feedback from the wind turbine model. The remaining implementation in principle corresponds to Equation (3.10). However, Equation (3.10) is based on complex numbers and for the implementation only the mean value and the third harmonics are included. In addition, only the *cos* part of the third harmonic is included because the tower shadow is symmetric, so the imaginary part of the third harmonic expansion coefficient is zero.

3.1.5 Stochastic Part – Turbulence

The stochastic part of the wind, in this thesis called turbulence, is the time variant part of the wind acting on the rotor area. Turbulence is the wind speed variations in a broad range from seconds to minutes. The variations have naturally a random behaviour but the air dynamics creates a main pattern on the wind speed variations. Low frequency variations have large amplitudes and higher frequency variations have lower amplitudes. Recording the definition in Equation (3.1), the turbulence can be measured in terms of its variance:

$$\sigma^2 = \mathrm{E}\left[(W - \mathrm{E}[W])^2 \right] \tag{3.24}$$

where $E[\ ]$ is the mean expectation operator, and W is the wind speed. The turbulence is also expressed in terms of standard deviation divided by the average wind speed ($U_0 = E[W]$) – so named turbulence intensity – I_u, defined as:

$$I_u = \frac{\sigma}{U_0} \tag{3.25}$$

3.1.5.1 Power Spectral Density of Turbulence

The turbulence varies in a broad frequency range. Spectral density function of the turbulence has been investigated for several years and several models have been proposed. In this report, a so-called Kaimal turbulence model is used to represent the power spectral of turbulence [44], defined as:

$$\frac{f \cdot S(f)}{\sigma^2} = \frac{\dfrac{f \cdot x_L}{U_0}}{\left(1 + 1.5 \cdot \left(\dfrac{f \cdot x_L}{U_0}\right)\right)^{\frac{5}{3}}} \tag{3.26}$$

where f is the frequency of the turbulence, σ^2 is the variance, x_L is the turbulence length scale (proposed maximum 600 m) and U_0 is the average wind speed. Figure 3.15 presents the logarithm power spectra ($S(f)*f$) of the turbulence simulated with Kaimal model to an average wind speed of 10m/s, turbulence intensity of 10% and turbulence length scale 600m.
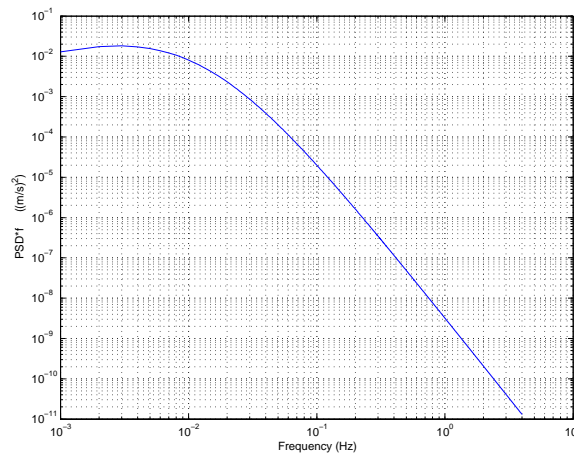
Figure 3.15. Kaimal PSD of Turbulence.

The Kaimal power spectra pattern was fitted based on several experimental data collected with neutral atmosphere over flat homogeneous terrain in Kansas as explained in [44]. The Kaimal power spectra has a peak when $x_L \cdot f/U_0 = 1$ and decreases with the $-5/3$ of the frequency, hence, the turbulence variations tend to zero in high frequency.

Several studies (e.g. the review presented in [55]) try to reveal the more accurate turbulence spectral model. Here, the Kaimal spectrum was selected to model turbulence. However, the application of other model is straightforward. The choice for Kaimal is done because it is widely accepted and because the Kaimal is suggested according to the *Danish standard for loads and safety of wind turbines construction* [56].

3.1.5.2 *Coherence of the Wind*

The coherence of the wind is relevant because it shows the correlation between wind speeds in different positions. The correlation of the wind in two different locations depends on the average wind speed, the distance between the positions and the frequency.

Near positions are well correlated but it reduces as the distance increases. In similar way, turbulence is highly correlated in lower frequency and decreases as the frequency increases, these characteristics have been measured as presented in [57].

The EWS uses the Davenport coherence type to simulate the coherence in the rotor area. The Davenport type coherence has the following form [57]:

$$\gamma(f,d) = e^{-k\frac{d \cdot f}{U_0}} \tag{3.27}$$

where γ is the coherence, U_0 is the mean wind speed, f the frequency, d is the distance between two positions and k is a decay factor. The decay factor has originally been expressed as a constant equal to 7.7 [57]. Measurements in other sites however reveal a different constant value that is in the range from 2 to 27 that is mostly related to the ratio d/h (distance divided between the two points and the height of the measurements (h)) as presented in [55].

Considering the application to wind turbines and the *Danish standard for loads and safety of wind turbines construction* [56], the EWS uses 12 for the decay factor constant.

3.1.5.3 *Power Spectral Density of a Rotating Blade – Rotational Turbulence*

The blades rotation generates special power variations. As for the deterministic part of the wind, the blades rotation will move energy contents of the turbulence from low frequency to multiple frequencies of the rotor speed, a process usually called *"rotational sampling of turbulence"*[59].

Wind turbine blades pass through different turbulences several times. It results that the power spectra of the turbulence on a blade section of a wind turbine has high energy content in the multiples of the rotational speed of the wind turbine. The rotational sampling of turbulence has been reported as the main cause of flicker from wind turbines, which makes its inclusion on wind speed model relevant to power quality assessments [60].

The rotational sampling of turbulence has been studied for several years and means to simulate it has been proposed by different ways. One of the methods includes the generation of several correlated time series of wind speed on the rotor area of the wind turbine, so called wind grid model. Then interpolation of appropriate points generates the wind on a rotating blade section, where the appropriate points comes from the expected position of the rotating wind turbine blade as presented in [47]. This method demands generation of several correlated time series of wind speeds, which result in large memory usage.

The method used here is based on equivalent wind speeds to each rotational sampling frequency, which is explained in the following sub-section.

3.1.6 Implementation of the Stochastic Component

The basic component of the stochastic component is the turbulence wind speed. The turbulence wind speed is simulated by applying a "Kaimal" filter to a random number generator. The Kaimal filter is fitted to output the Kaimal power spectral. The filter used in the EWS was fitted in [50].

The stochastic component includes the rotational sampling turbulence that is simulated the same way as the deterministic component, i.e. first, the azimuth expansion coefficients are simulated, and then they are used as amplitudes to the harmonics according to Equation (3.10) (only 0 and 3p). However, the azimuth expansion coefficients are time dependent in this case.

The azimuth expansion coefficients are random signals [49], and the PSD of the nth azimuth expansion coefficient $S_{w\{3n\}}(\Delta\omega)$ is equal to the PSD of the wind speed in a fixed point $S_w(\Delta\omega)$ (here Kaimal), multiplied by an admittance function $F_{\widetilde{w}\{3n\}}(\Delta\omega)$, i.e.:

$$S_{w\{3n\}}(\Delta\omega) = F_{\widetilde{w}\{3n\}}(\Delta\omega) \cdot S_w(\Delta\omega) \tag{3.28}$$

where S_w is the Kaimal distribution and the admittance function $F_{\widetilde{w}\{3n\}}$ can be determined by a triple integral, which is [49]:

$$F_{\widetilde{w}\{3n\}}(\Delta\omega) = \frac{\int_0^R \int_0^R \psi(r_1)\psi(r_2)F_k(f,r_1,r_2)dr_1dr_2}{\left(\int_0^R \psi(r)dr\right)^2} \tag{3.29}$$

where ψ is the aerodynamic function, f is the frequency, r is the radial position along the blade on the rotor area and F_k defined as:

$$F_k(f,r_1,r_2) = \frac{1}{2\pi}\int_0^{2\pi} \gamma(f,d)\cos(\phi)d\phi \tag{3.30}$$

where $\gamma(f,d)$ is the square root coherence according to Equation (3.27) where the distance d is $\sqrt{r_1^2 + r_2^2 - 2r_1r_2\cos(\phi)}$, r_1 and r_2 are two radial positions and ϕ is the angular difference between them.

In the EWS, the admittance function is represented by a second order filter with a transfer function $H_{adm\{0p\}}$ fitted in [50]. The EWS only accounts to the 0p and 3p as they are the most relevant to three bladed wind turbine rotor types.

The filter applied to the 0p harmonic component (from [50]) is:

$$H_{adm\{0p\}}(s) = \frac{4.7869 \cdot d_{TF}^2 \cdot s^2 + 0.9904}{7.6823 \cdot d_{TF}^2 \cdot s^2 + 7.3518 \cdot d_{TF} \cdot s + 1} \tag{3.31}$$

where $d_{TF} = R/U_0$ is the normalization parameter, R is the total radius of the wind turbine rotor and U_0 is the average wind speed. Figure 3.16 presents the normalised numerical and the fitted admittance function to the 0p (source: [50]).
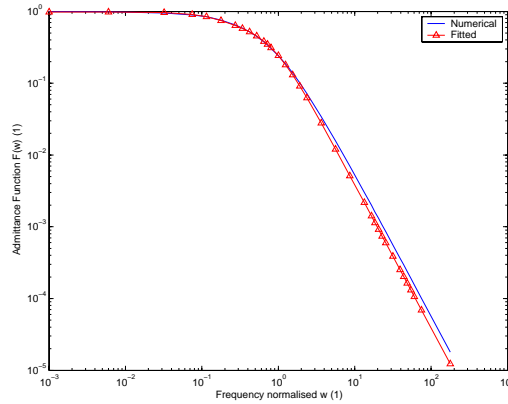
Figure 3.16 Normalised admittance function to 0p.

To find the real rotational frequency (in rad/s) in Figure 3.16 is necessary to scale the normalised frequency (w) with the constant of normalisation ($d_{T.F.}$), i.e. $w \cdot d_{T.F.}$. The admittance function to the 0p harmonic component can be understood as a smoothing function to the variations of the turbulence on a stationary reference frame that are transferred to the mechanical power. In low frequency, the turbulence variations are totally transferred to the aerodynamic power while on high frequency, the variations are filtered out due to the coherence of the turbulence.

To the 3p harmonic component, the transfer function $H_{adm\{3p\}}$ is fitted to [50]:

$$H_{adm\{3p\}}(s) = \frac{0.2766 \cdot d_{TF} \cdot s + 0.0307}{0.3691 \cdot d_{TF}^2 \cdot s^2 + 1.7722 \cdot d_{TF} \cdot s + 1} \tag{3.32}$$

Figure 3.17 presents the normalised numerical and fitted admittance function to the 0p (source: [50]).

It is important to remind that the normalised frequency to the 3p harmonic component is shifted by a frequency of 3p from Equation (3.10). Hence, to find the real frequency it is necessary to scale the normalised frequency (w) with the normalisation factor ($d_{T.F.}$) and with the 3p rotational speed (in rad/s – w_{3p}), i.e. $w_{3p} \pm w \cdot d_{T.F.}$.
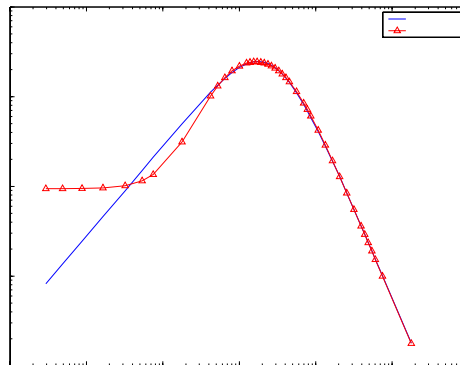
Figure 3.17 Normalised admittance function to 3p.

The admittance function to the 3p harmonic component can be understood as a smoothing procedure to the variations of the turbulence that are transferred to the mechanical power similar to the 0p. However, the reduction effect is much higher compared to the 0p admittance function because the coherence decays much more due to the higher frequency (3 times the rotational speed). At lower and above than 3p frequencies, the variations from turbulence are filtered out due to the coherence of the turbulence.

From Figure 3.17 it is possible to verify a poor agreement between the numerical result and the fitted admittance function at very low frequencies. The difference at very low frequency happens because the numerical results were fitted to a second order filter. However, at these lower frequencies, the 3p admittance function is quite small and, therefore not so important. In addition, a fourth order filter does an excellent fit but the improvements in terms of power variations on the results did not justify the use of higher order filter [50].

Finally, Figure 3.18 illustrates the total implementation of the stochastic part of the EWS implemented in Simulink/MATLAB®.
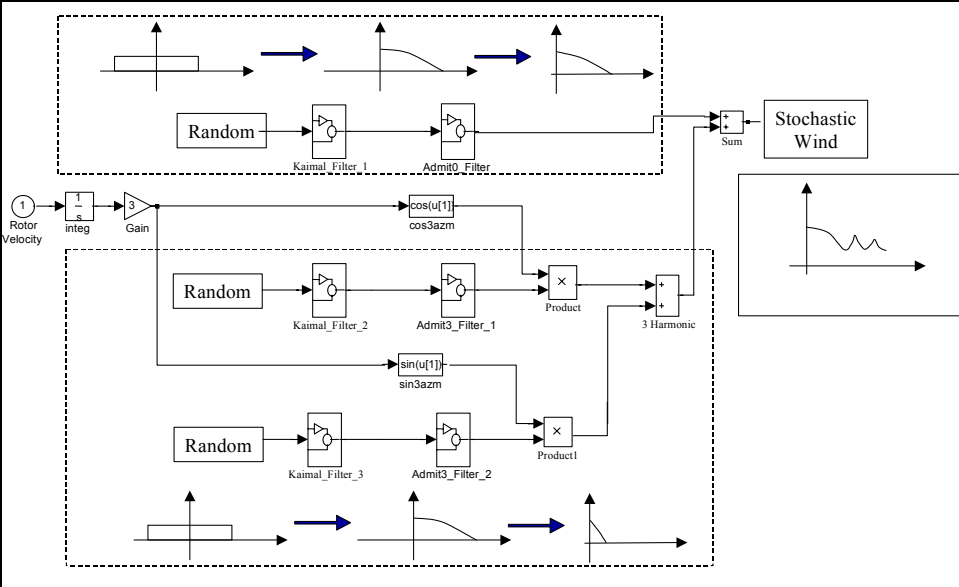
Figure 3.18 Implementation of the stochastic model in Simulink/MATLAB.

In Figure 3.18, the rotor position is first computed by integrating the rotor speed of the wind turbine. Kaimal filters applied to the random numbers simulate the turbulence wind speed, which is inputted to the admittance functions representing the smoothing effect on the rotor area to 0p and 3p. Finally, the three components are added resulting in the stochastic part of the EWS. The complete EWS is the sum of the stochastic and deterministic parts as presented in Equation (3.14).

3.2 Validation of the Equivalent Wind Speed Model

This section presents tests of the EWS, which is done in two parts: in the first part the deterministic and stochastic models are verified separately and in the second part the EWS is compared with measurements.

In the first part, the output of the EWS is compared to the ones from the Design Bases Program 2 – DBP2. The DBP2 is an integrated model of a horizontal axis wind turbine that the main aim is to analyse structural performance of wind turbines [61]. In this chapter, the DBP2 generates time series of the wind speed on blade sections of the wind turbine that are compared to the EWS.

The deterministic part of EWS is compared in terms of the normalised deterministic wind influenced by the tower shadow. Two winds are simulated using the EWS, the first one with the 0p and 3p harmonic components only and the second with all 3np harmonic components. The wind speed simulated in DBP2 is seen from a single blade section located at 2/3 of the total blade length. Therefore, the simulated wind speed in DBP2 was processed to reflect the average wind speed seen from three-bladed rotor. This was done by averaging the measured wind speed at times t-Δt, t and t+Δt, where Δt is the time corresponding to 120° in the rotational speed of the rotor of the wind turbine (40 rpm). Figure 3.19 presents the comparison and Table 3.2 presents the tower parameters from the wind turbine tested.
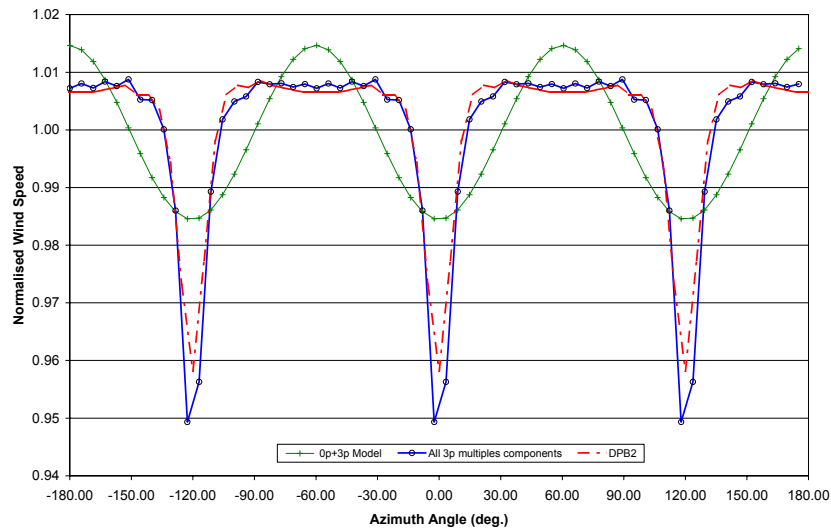
Figure 3.19 Normalised simulated deterministic wind component compared to a DBP2 model.

Figure 3.19 shows a good agreement between the "all 3np" simulation and the DBP2 calculation, whereas the agreement of the "0p+3p" simulation model is poor. This illustrates that the equivalent deterministic wind speed can replace the deterministic wind speed simulated with DBP2 but it requires that orders higher than 3p are included. Still, only 0p and 3p are included in the model because the mechanical structure reduces the corresponding simulated mechanical torque as discussed previously in this chapter.

Table 3.2 Parameters used in the simulation for tower shadow.

Physical geometric parameters	Size
Rotor diameter	29 m
Distance from tower to rotor	1.15 m
Tower diameter	1.70 m

The stochastic part of the model was simulated for an average wind speed of 8m/s, turbulence intensity of 0.10. In the EWS, the dynamics of the wind turbine was not modelled, so the rotational speed of the rotor was assumed constant 40 rpm while in the DBP2 the stochastic wind speed was simulated to a single blade section. The comparison of the stochastic behaviour is shown in Figure 3.20 in terms of PSD's.
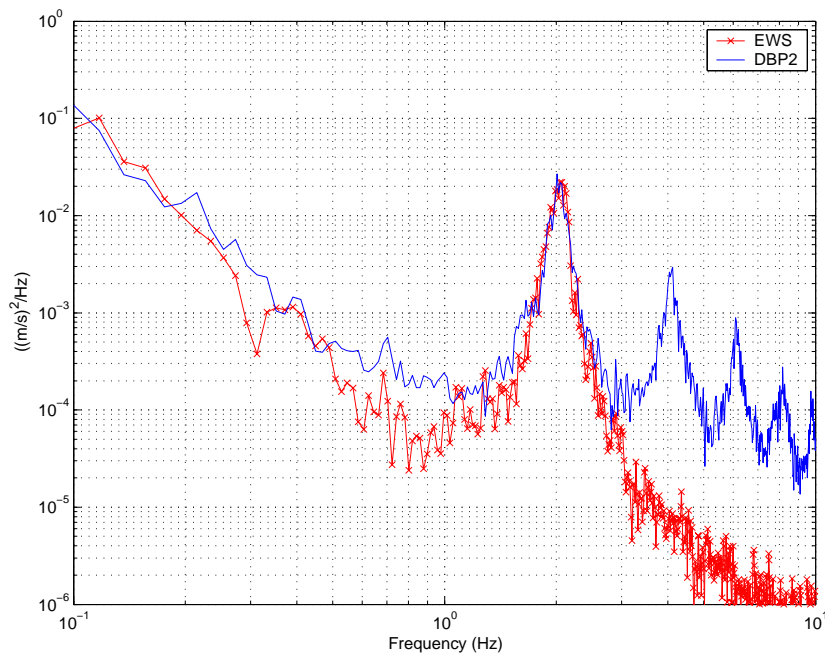
Figure 3.20 PSD comparisons of the stochastic model.

As previously mentioned, only the contributions from zero and 3rd harmonics are taken into account in the EWS and the frequency range of interest is from 0p to 4p. In this frequency range, the EWS model is close to the DBP2 model with only minor deviations. In the frequency range above 3Hz, the EWS differs from the DBP2 because the DBP2 shows the turbulence acting on a single blade section of a wind turbine including all physical aspects that are not presented in the electrical power measurements because they are filtered out by the wind turbines dynamics.

In the second part of the validation, the EWS output was compared with measured data. The wind speed was measured in a rotating blade with a five holes Pitot tube. The Pitot tube was mounted at 15 m of the rotor centre at an angle of 14° to the local chord and in a distance of about one chord length in front of the blade leading edge [48].

The wind measured at the hub height on a meteorological mast in front of the wind turbine was used to compute the mean wind speed and turbulence intensity (input parameters of the model). The turbulence intensity and the mean wind speed measured in a fixed point on a meteorological mast were 0.16 and 10.51m/s respectively and the rotor speed was 30 rpm. The main parameters of the wind turbine are shown in Table 3.3.

Table 3.3. Parameters of the wind turbine used in the measurement comparisons.

Physical geometric parameters	Size
Rotor diameter	41 m
Distance from tower to rotor disc	2.9 m
Tower diameter	1.70 m

The measured wind speed is seen from a single point on a rotating blade, whereas the reduced model describes the summed effect of the wind speed on all three blades. Therefore, the measured wind speed was processed to reflect the average wind speed from three blades before it was compared to the simulation. This was done by averaging the measured wind speed at times t–Δt, t and t+Δt, where Δt is the time corresponding to 120°

in 30rpm. The comparison of the measurement and simulation are shown in Figure 3.21 where the 1p frequency is approximately 0.5Hz.
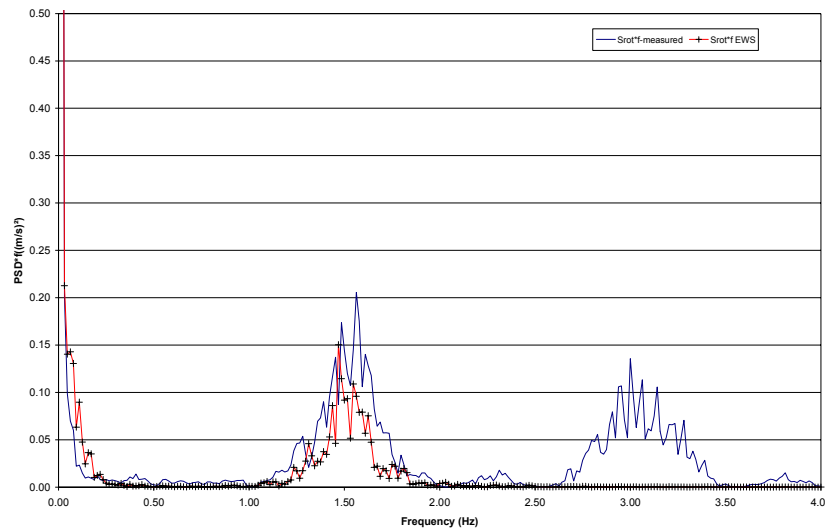
Figure 3.21 Measured and the simulated equivalent wind speeds on rotating blade section.

The comparison presents a reasonable agreement in the range from 0 to 3p. However, two aspects are different for the measurement and simulation, which could explain most of the difference.

First, the measurements are done in a single section of the blade, whereas the model intends to include the wind averaged along the blades. Hence, the standard deviation of the measured rotating wind speed is 1,7m/s, which is approximately equal to the standard deviation measured in the fixed point in the mast. This complies with the theory for rotational sampling described by Kristensen and Frandsen [59], where it is described how the rotation moves standard deviation from lower frequencies to higher frequencies. The standard deviation of the simulated equivalent wind speed is 1.08m/s, which is 40% lower than the fixed-point standard deviation as expected from the averaging process along the [50].

The second difference between the measurement and simulation is, that the wind speed is only measured on a single blade, so it was necessary to assume that the wind speed seen by blade 2 is the same at time $t+\Delta t$ as the wind speed seen by blade 1 at time t as described above. In addition, the same assumption is made for the blade 3. it is important to quote that the dynamic wind turbine was not modelled, so to the EWS (in this chapter only) the rotor speed f the wind turbine was assumed constant what is also pointed as one more reason to the difference between the model and measurements.

3.3 Equivalent Wind Speed Model Remarks

In this section, the EWS model was introduced. It has been reduced in complexity although is based on complex theory.

The EWS consists of a deterministic part and a stochastic part. Both of them have been compared with a verified model – DBP2. The EWS has also been compared to measurements.

The deterministic part does not present a good approximation using only the zero and the third harmonics. The higher components can be added to the model but measurements of the power indicate that they are filtered by the dynamics of the wind turbine. The deterministic part of the model was developed for tubular towers. In the case of a lattice tower, an approximate tower effect can be obtained by specifying an equivalent fictitious tubular tower.

The stochastic part was compared with a spectrum derived from the DBP2 model. It showed good agreement in the frequency range from zero to 4p. Finally, there is no significant difference considering the energy content of the DBP2 and the proposed model for the stochastic part.

The comparisons with measurements presented a good agreement in the range from 0P to 4P. The small difference of amount of energy in the range from 1P to 4P is associated to the single point measured compared with an equivalent wind simulated. The difference also presented in the range above 4p was expected as a result from the initial assumptions that the wind turbine acts as a low order pass filter.

The implementation of the model as a function of the rotor position enables the program to be applied for variable or constant rotor speed wind turbine models without additional modifications.

The fast computation and reduced memory usage are very suitable for simultaneous simulation of a large number of wind turbines making it possible to efficiently estimate the impact of a large wind farm on the power quality.

The increased speed and reduced memory usage could be compared in terms of wind time series generated. As the conventional models generate several wind time series, the presented model only generates one resulting in a small memory usage and a decrease in the time computation.

Chapter 4

4   Wind Turbine Model

The produced electrical power from wind turbines does not have the same behaviour in terms of variation as the wind. Wind turbines are dynamic generators with several components that influence the power conversion from the wind. As mentioned before, the dynamics of the wind turbine filter out the high frequency power variations but it also includes new components due to its dynamics itself.

There are several types of wind turbines commercially available. Each one of them has a special configuration and specific power dynamics. Here a dynamic wind turbine model to a conventional wind turbine is presented. The conventional wind turbine has a stall-regulated rotor connected to an induction generator through a gearbox. The electrical generator is directly connected to the network. A soft-start is used to start-up the wind turbine. The reactive power demanded from the generator is partial compensated using a capacitor bank. Finally, the integration of the electrical power into the grid is done at medium voltage (e.g. 10kV), so a step-up transformer is used.

From the basic components of the conventional wind turbine, the relevant ones are classified as:

- Aerodynamic rotor – converts the wind power into mechanical power;

- Transmission system – connects the aerodynamic rotor to the electrical generator using shafts and gearbox;

- Generator – converts the mechanical to electrical power using an asynchronous generator synchronized with the network;

- Controller – controls and optimise the wind turbine operation;

- Reactive power compensation – partial or total compensation of the reactive power demanded by the generator;

- Step-up transformer – integrates the power produced in the medium voltage electrical network;

- Network – medium voltage grid that transmit the power.

Each one of the components influences the dynamic operation of the wind turbines. In addition, the elements of the wind turbine interact with each other, e.g. the aerodynamic rotor output depends on the wind speed and on the rotor speed.

The Equivalent Wind Speed model (presented is chapter 03) is the input to the dynamic wind turbine model. The dynamic wind turbine model is intended for power quality assessment of wind turbines. This chapter presents a dynamic wind turbine model for a three-bladed stall regulated wind turbine with induction generator connected directly to the network.

4.1 Simulation Tool

The dynamic wind turbine model can be implemented in any simulation program. Here, the wind turbine model is implemented in the Power System Simulation software

SIMPOW from ABB because it has built in an extensive library of electrical components and it can solve the network equations outputting the relevant characteristics of the electrical power system. Therefore, the focus is on developing appropriate models of the aeroelastic parts of the wind turbine. The dynamic aeroelastic model must simulate the power conversion from the aerodynamic rotor and the transmission to the electrical generator.

Once an appropriate induction machine model is chosen, the mechanical torque from the wind turbine model is the input and the SIMPOW simulates all the electrical and mechanical characteristics of the power system equipments modelled. SIMPOW has some limitations in handling stochastic processes. Random numbers are not available in the library. Hence, the wind speeds are time series, which are input to SIMPOW.

The total dynamic wind turbine model is composed of several modules: the first module is the wind speed generation (described in chapter 3) that is implemented in Matlab$^{\circledR}$, the Matlab module outputs time series of wind speed that is read by SIMPOW. The second module is the aeroelastic model of the wind turbine that reads the wind speed from a file and outputs the mechanical torque on the electrical machine shaft. The third module comprises the load flow and dynamic simulation of all electrical equipments. The second and third modules are implemented in SIMPOW. Finally, the last module is the data processing that is implemented in Matlab, so SIMPOW exports time series of selected variables

4.2 Wind Turbine Model

Each component of the wind turbine has some relations with other components. Figure 4.1 presents the main relations among different components. The aerodynamic rotor depends on the transmission system; the transmission system depends on the electrical generator and aerodynamic rotor; and so on.
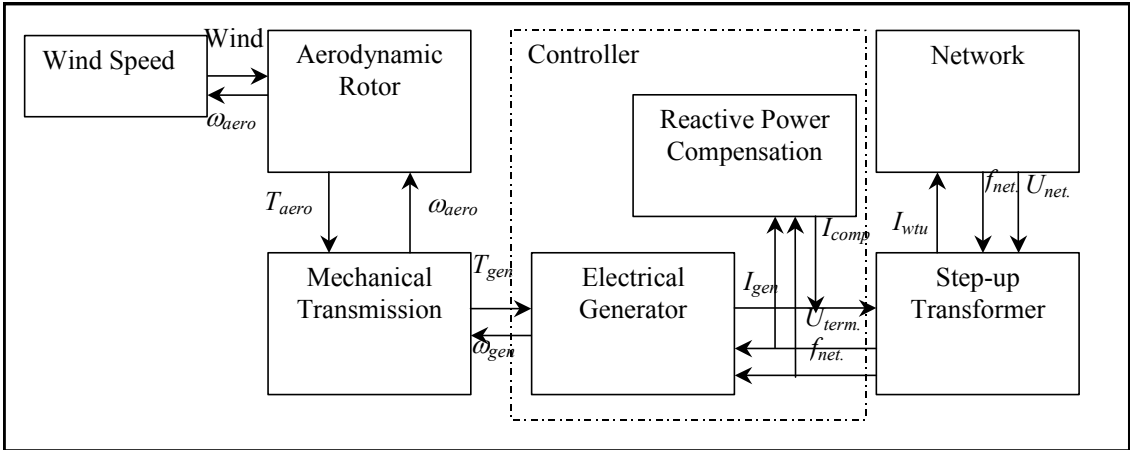
Figure 4.1 Interaction between each components of a wind turbine unity.

In Figure 4.1, ω is the rotational speed, T is the torque, U is the voltage, I is the current and f is the frequency where the subscripts *aero* means to the aerodynamic rotor and *gen* means electrical generator, *comp* means compensation unity, *net* means network and *wtu* means wind turbine unity.

The wind turbine components are classified in electrical and aeroelastic parts. The aeroelastic part comprises the aerodynamic rotor and the mechanical transmission system.

The electrical part comprises all the electrical components, i.e. the generator, reactive power compensation, step-up transformer, and network.

4.2.1 Aeroelastic Components

4.2.1.1 Aerodynamic Rotor

The aerodynamic rotor converts the wind into mechanical power. Aerodynamic effects throughout the blades convert the wind flow in aerodynamic torque. Each blade section contributes to the total aerodynamic torque in a single blade. Integrating the torque along the blade sections and adding up the effects of all 3 blades results in the aerodynamic torque on the main shaft.

The aerodynamic model uses the Equivalent Wind Speed (EWS) as input to compute the available power and it uses the speed of the rotor to compute the torque on the main shaft.

The aerodynamic power on the main shaft can be expressed in per unit as:

$$P_{aerdynamic} = \frac{\frac{1}{2} \rho \cdot \pi \cdot R^2 \cdot W^3 \cdot C_p\left(\lambda, \theta_{pitch}\right)}{P_{baserotor}} \tag{4.1}$$

where ρ is the air density; R is the rotor radius, W is the wind speed, C_p is aerodynamic power coefficient and $P_{baserotor}$ is the rated power of the rotor in order to give the torque in per unit. The power coefficient is a normalized function of the pitch angle θ_{pitch} and the tip speed ratio λ, which is defined as the ratio between blade tip speed and the wind speed as follows:

$$\lambda = \frac{\omega_{rotor} \cdot R}{W} \tag{4.2}$$

where ω_{rotor} is the rotational speed of the rotor. Using Equation (4.1), and the power coefficient of a stall regulated wind turbine, the aerodynamic torque in per unit can be expressed as:

$$T_{aerodynamic} = \frac{P_{aerodynamic}}{\omega_{rotor} \cdot P_{baserotor}} = \frac{\rho \cdot \pi \cdot R^2 \cdot W^3 \cdot C_p(\lambda)}{2 \cdot \omega_{rotor} \cdot P_{baserotor}} \tag{4.3}$$

where in this case the C_p is a function only of the λ because stall regulated wind turbines have a fixed pitch angle. This model fairly represents the power conversion in wind speeds below the stall region [62]. However, during stall conditions the aerodynamics has been reported to be quite different from static conditions because Equation (4.3) corresponds to steady state aero loads. It underestimates the power fluctuations in the stall condition because the stall effect does not happen instantaneously as the wind changes but after a time lag [62].

A dynamic stall model is implemented in the aerodynamic module. The model is based on time lags of separation [62]. The power conversion in an aerodynamic rotor can be decomposed in three conditions:

- Static power conversion condition – is the stead-state power conversion curve of an aerodynamic;

- Totally attached condition – is an extreme dynamic condition that considers that the flow does not stall in any wind speed, hence the power converted is proportional to the cubic of the wind speed;

- Totally separated condition – another extreme dynamic condition where in all wind speeds the flow is totally separated of the wind turbine blades.

So, during stall condition, when the wind speed changes instantaneously, the power conversion follow instantaneously the present degree of separation and after the time delay it come back to the steady state curve. The power coefficient computation is done by dedicated aerodynamic program. Figure 4.2 illustrates the three power coefficients to a 660kW stall regulated machine.
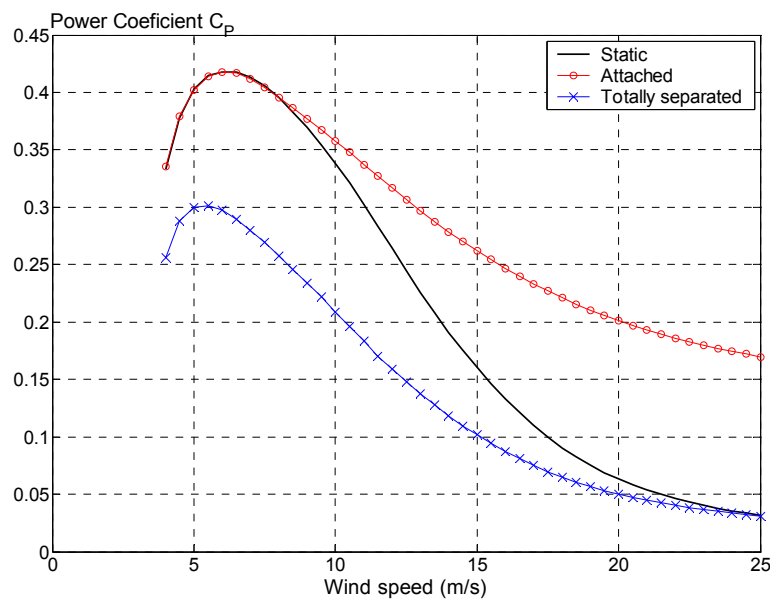
Figure 4.2 Power coefficients to compute the dynamic power coefficient.

The static (or steady state) power coefficient tends in low wind speed to follow the totally attached curve and in high wind speed to follow the totally separated curve. In low wind speeds, the blade profiles are designed to extract the power based on aerodynamic coefficients that depend on the attached flow to generate lift. On high wind speeds, the blade profiles are designed to start to stall (or separate) hence reducing the lift generated and the extracted power from the wind, which is important to avoid overload of the wind turbine.

The first step to compute the dynamic power coefficient, $C_p(\lambda)$ is to find the static interpolation factor (f_{static}) that represents the static curve as a combination of the others two as follow

$$C_{p_{static}}(\lambda) = f_{static} \cdot C_{p_{attached}}(\lambda) + (1 - f_{static}) \cdot C_{p_{separated}}(\lambda)$$ (4.4)

Then the dynamic interpolation factor (f) is computed as a time lag according to:

$$\frac{\partial f}{\partial t} = \frac{(f_{static} - f)}{\tau_{ds}} \tag{4.5}$$

where the time constant $\tau_{ds} = 4/U_0$ is computed from experimental tests as defined in [62]. U_0 is the average wind speed. Finally, the dynamic power coefficient is defined as:

$$C_p(\lambda) = f \cdot C_{p_{attached}}(\lambda) + (1 - f) \cdot C_{p_{separeted}}(\lambda) \tag{4.6}$$

The dynamic power coefficient applied to Equation (4.3) gives the torque.

4.2.1.2 Drive Train

The aerodynamic torque, in a wind turbine, varies all the time due to wind turbulence and tower shadow. The variations however are not directly transferred to the electrical power output because of the dynamic mechanical transmission system.

The electrical generators run in a relatively high speed compared to the aerodynamic rotor. The drive train connects high speed in the electrical generator side and slow speed in the aerodynamic rotor using a gearbox. The drive train includes a gearbox; shafts and disc brakes that can be positioned in the low or in the high-speed shaft depending on the size of the wind turbine. On small wind turbines the brakes are positioned in the low speed shaft that reduces the stresses on the gear box during shut down of wind turbines, on large wind turbines, however, the torques in low speed shaft are very high hence the disc brakes are located in the high speed shaft. Figure 4.3 illustrates the drive train of a small wind turbine size.
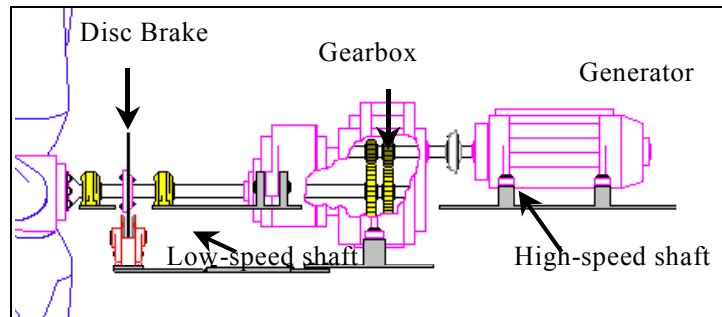
Figure 4.3 Example of drive-train components.

In the left side of Figure 4.3, the aerodynamic rotor is presented that is connected to the electrical generator in the right side through a gearbox. The gearbox is analogue to an electrical transformer where the torques are like the currents and the rotational speed are like the voltages. An ideal gearbox has no losses and does not modify the dynamics of the system. The drive train modifies the dynamics of the system because they include torsional modes. The shaft torsional modes are related to the aerodynamic rotor mass swinging with the induction generator mass through the flexible transmission shaft.

Figure 4.4 presents a simplified dynamic drive train model where the gearbox is considered ideal hence omitted here and the speeds and torques are in p.u.
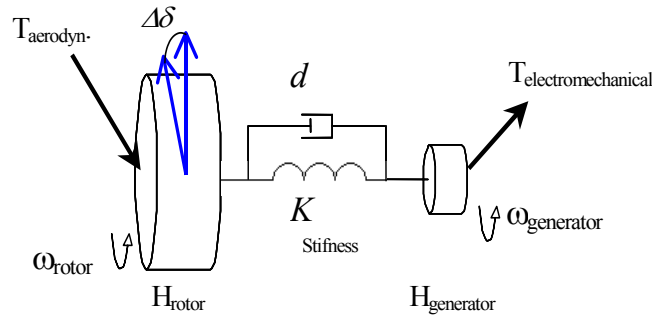
Figure 4.4 Dynamic representation of the drive train model.

In Figure 4.4, $T_{aerodyn}$ is the aerodynamic torque computed from the aerodynamic module, ω_{rotor} is the rotational speed of the aerodynamic rotor, $\omega_{generator}$ is the rotational speed of the induction generator, $T_{electromechanical}$ is the electromechanical torque in the induction generator, H_{rotor} is the inertia of the aerodynamic rotor, $H_{generator}$ is the inertia of the induction generator, $K_{stifness}$ is the equivalent stiffness of the shaft connecting the two masses, d is the equivalent damping coefficient that includes the losses in the system and an aerodynamic damping and Damping losses are the torque losses related to the damping coefficient.

The equations of motion in to the dynamic drive train in Figure 4.4 can be expressed according to:

$$2H_{rotor}\frac{d(\omega_{rotor})}{dt} = T_{aerodyn.} - K(\delta_{rotor} - \delta_{generator}) - d(\omega_{generator} - \omega_{rotor}) \qquad (4.7)$$

$$\frac{d(\delta_{rotor})}{dt} = \omega_{rotor} \cdot \omega_0 \qquad (4.8)$$

$$2H_{generator}\frac{d(\omega_{generator})}{dt} = K(\delta_{rotor} - \delta_{generator}) - T_{electromechanical} + d(\omega_{generator} - \omega_{rotor}) \qquad (4.9)$$

$$\frac{d(\delta_{generator})}{dt} = \omega_{generator} \cdot \omega_0 \qquad (4.10)$$

where the constants are explained as follow:

H_{rotor} − is the total inertia of the aerodynamic rotor expressed in per unit. The rotor inertia includes the blades and the hub in the low speed shaft. The inertia is then converted to the high speed side of the shaft and finally converted to the per unit system using the following equation (4.11):

$$H_{rotor} = \frac{1}{2} \cdot \frac{J_{rotor}(\omega_0)^2}{q_{gear}^2 \cdot S_{base}} \qquad (4.11)$$

where J_{rotor} is the rotor inertia in physical units on the low speed side of the gearbox, q_{gear} is the ratio between low and high speeds in the gearbox, $\omega_0 = 2\pi f_0/poles$ is the mechanical

synchronous speed on the generator side and S_{base} is the base power of the electrical generator.

$H_{generator}$ – is the inertia of the electrical generator in per unit defined as:

$$H_{generator} = \frac{1}{2} \cdot \frac{J_{generator} (\omega_0)^2}{S_{base}}$$

(4.12)

where $J_{generator}$ is the generator inertia in physical units.

K is the equivalent stiffness of the shaft connecting the two masses and can be expressed as:

$$K = \frac{k_{stiffness}}{T_{base}}$$

(4.13)

where T_{base} is the mechanical base torque and $k_{stiffness}$ is the stiffness constant in physical units, which can be computed using the first torsional eigen-frequency ($\omega_{transmission}$) as follow:

$$k_{stiffness} = (\omega_{transmission})^2 \cdot J_{rotor}$$

(4.14)

where $\omega_{transmission}$ is the first torsional eigen-frequency. The transmission system eigen-frequency is measured in tests of the wind turbine. In the tests, the generator side has the brakes on (i.e. fixed end) and the torque is measured.

d is the damping coefficient expressed as:

$$d = \frac{c_{damping}}{T_{base}}$$

(4.15)

where $c_{damping}$ is damping coefficient computed in physical units, which is computed as follow:

$$c_{damping} = 2\delta_{\log} \frac{\sqrt{k_{stiffness} \cdot J_{rotor}}}{\sqrt{(2\pi)^2 + (\delta_{\log})^2}}$$

(4.16)

where δ_{log} is the logarithmic decrement in terms of few percents, which is very difficult to determine and in general it is measured from the tests of the wind turbines.

The main intention is to model the first torsional mode of the mechanical transmission system but actually, the model includes the first and second modes due to the use of two masses system (second order model). There are several other models to simulate the drive train module (e.g. [10], [63] and [64]). The complexity of the model depends on the aim of the model. Considering the power quality assessment of wind turbines, a two masses model and a flexible shaft simulate the most relevant torsional moment from wind turbines [63].

The first torsional mode of a medium sized wind turbine is around 1Hz and it is considered the most relevant for power quality from wind turbines. The second mode is related to the interaction between the rotor and generator masses oscillating against each other due to the stiffness of the shaft, which is around 2 Hz.

4.2.2   Electrical Components

The electrical components comprise the electrical generator, the reactive power compensation, control system, step-up transformer. In this thesis, they are modelled using the standard library of SIMPOW/ABB, which has verified models of most of the conventional electrical components in power systems including electrical machines, transmission lines, transformers and power electronics and controllers.

Details of the electrical power system including the wind farm depend on the purpose of the simulation. Here only some characteristics of the electrical generator are presented and Annex 9.1 presents the some characteristics of the models used here from the SIMPOW.

4.2.2.1   Electrical generator

The induction generator is the most common type of electrical machine. It is mostly applied as motor. As generator, however, it has been used for many years in wind turbines. The reliability, low price, and low maintenance made this type of machine the most suitable for wind turbines. Allied to those characteristics, the speed flexibility (slip), when compared to the synchronous machines, reduces the current spikes due to wind gusts.

In the asynchronous generators, the rotational speed of the rotor is not fixed as it is in the synchronous machines, but it is related to the torque from the prime mover and to the network frequency.

The rotational speed of the asynchronous generator must be above the synchronous speed in order to force the power flux to the network. Figure 4.5 presents an example of power relation to the speed and voltage terminals in an asynchronous generator based on static models [65].
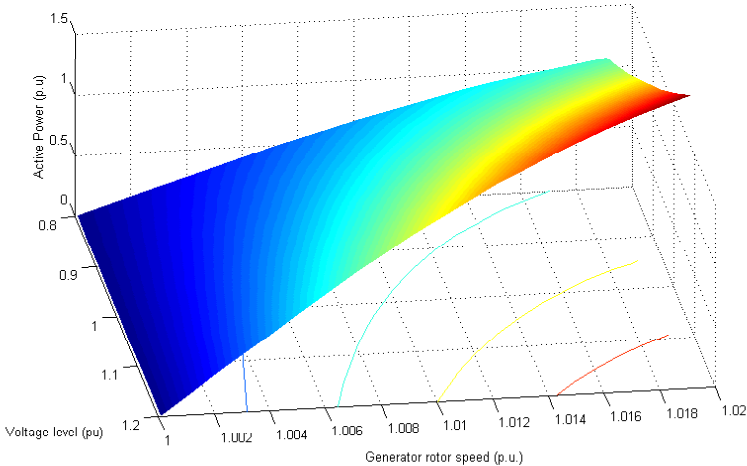
Figure 4.5 Active power as function of speed and voltage terminals for an asynchronous generator.

In Figure 4.5, positive signal means power produced from the machine. The active power is mainly related to the prime mover torque on the mechanical shaft and the voltage

influences the electrical characteristic of the induction machine, i.e. the excitation (reactive power) modifies with the voltage. The reactive power of induction machines as generator varies with the voltage. Figure 4.6 illustrates the reactive power from an induction generator.
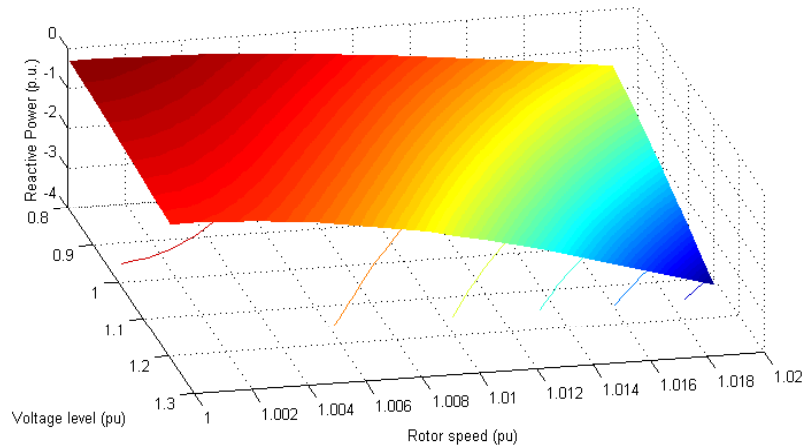
Figure 4.6 Reactive power as a function of the speed and voltage for an asynchronous generator (1p.u. = rated reactive power at 1pu volts).

In Figure 4.6, negative power means the power system supplies power and 1p.u. of reactive power means the rated reactive power. The asynchronous machine does not have an independent excitation control system, hence the excitation is supplied from the power system, which means reactive power consumption. The reactive power demanded of an induction machine depends mainly on the voltage at its terminals and on the active power supplied to the power system.

Keeping the active power constant and increasing the voltage lead to an increase in the reactive power because the excitation is a shunt element proportional to the voltage. Still keeping the active power constant and at this time reducing the voltage lead to a small reduction on the reactive power consumption, however decreasing further the voltage leads to an increase in the reactive power because of the losses that are increased due to the higher currents flowing in the machine.

4.3 Verification of the Complete Wind Turbine Model

In order to verify the Dynamic Wind Turbine Model, a 500kW stall regulated wind turbine directly connected to the grid is modelled and compared to measurements. The wind turbine is installed at the test station facility of the RISØ laboratory. Table 4.1 presents a resume of the most relevant information to the wind turbine.

Table 4.1 Basic characteristics of the Nortank 500kW wind turbine modelled.

Nominal Power	500kW
Rotor diameter	35 m
Generator speed	1500 rpm
Rotor speed	27 rpm
Capacitor Bank	300kVAr
Generator terminal voltage	400V
Electrical frequency	50Hz
Tower height	36 m
Gearbox ratio	55.55
First torsional frequency	1.08Hz
Estimated logarithmic damping to drive train	5%
Number of blades	3
Constant of inertia of the aerodynamic rotor	1.15 s
Constant of inertia to the generator	0.15 s
Tower shadow 3p effect	1.5%

Figure 4.7 presents the static power coefficient to this wind turbine.
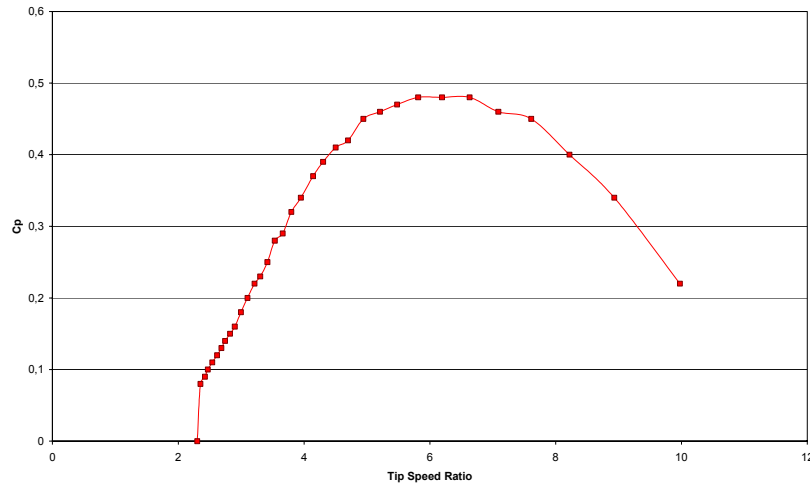
Figure 4.7 $C_p(\lambda)$ static characteristic of the wind turbine Nortank 500kW.

To this verification, the wind speed measured in the hub high is used as input to the dynamic wind turbine model and admittance filters (as introduced in chapter 2) representing the coherence smoothing effect on the rotor area of the wind turbine are applied. In addition, time series of wind speeds to the 3p effect are simulated based on the average wind speed and turbulence intensity measured.

The average wind speed measured is approximately 8m/s and turbulence intensity of 13.3%. The low wind speed is far from the stall condition and the dynamic stall module is not implemented in this case. Figure 4.8 presents the measured wind speed applied to the dynamic wind turbine model.
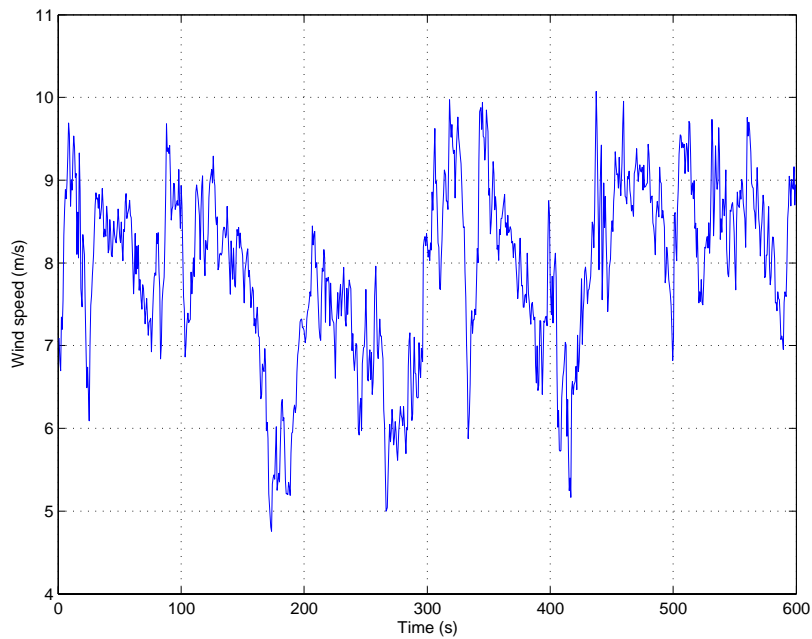
Figure 4.8 Measured wind speed.

Figure 4.9 presents the time series of powers simulated and measured in the wind turbines terminals during 600s. A general good agreement is seen between the simulated and measured power from the wind turbine.
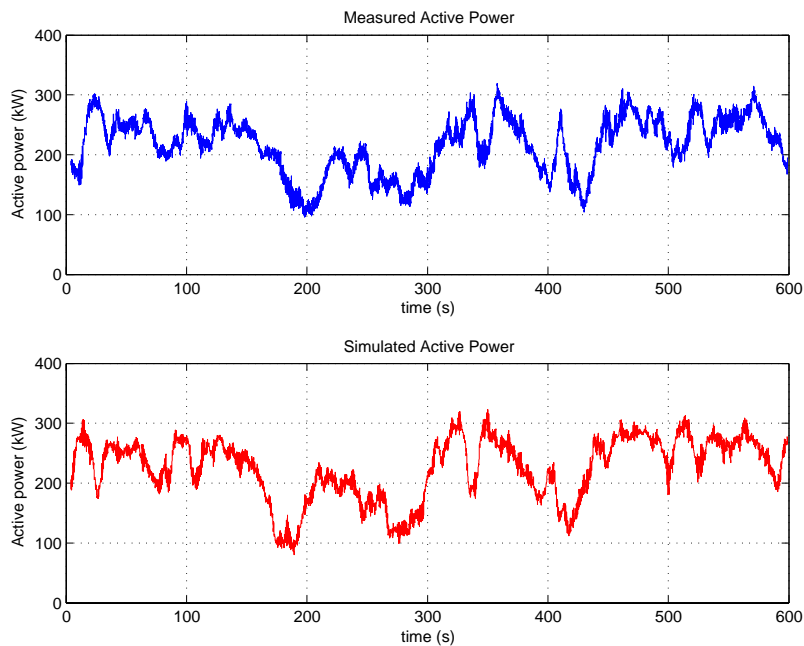
Figure 4.9 Time series of simulated and measured power to the Nortank 500kW.

The mean wind speed was adjusted to simulate the same mean power in the period of 10 minutes. The measured wind speed directly applied to the model resulted in a mean power difference of -75kW (–15% related to the rated power) when compared to the measured power. One possible reason for the difference can be that the ambient wind speed is measured 100 meters from the wind turbine because it cannot be measured on the rotor

plane. Hence, the wind speed acting on the rotor of the wind turbine is not necessarily the same as the measured one. The adjustments in the wind speed are composed of modifying the mean wind speed and to scale the turbulence to modify the standard deviation. Another possible reason for the difference may be that the actual aerodynamic characteristics are different from the modelled ideal characteristics.

With the mean wind speed adjusted (Figure 4.9), the mean and maximum powers and the standard deviation are overestimated while the minimum power is underestimated. The simulated mean power is 1.45% higher than the measured power the normalisation used in this section is related to the rated power. The simulated instantaneous maximum power is 0.92% higher than the measured and the simulated standard deviation is 1.07% higher than the measured. The simulated instantaneous minimum power is 3.19% lower than the measurements. Those results indicate that the mean wind speed and the turbulence could still require some adjustments, however, the differences are assumed reasonable here.

The power spectral distribution (PSD) of the active power is one of the relevant characteristics from the wind turbines because of the stochastic nature of the process, hence Figure 4.10 presents PSD of the measured and simulated power that corresponds to the time series presented in Figure 4.9. In the upper part of Figure 4.10 the spectral power, i.e. $S(f)\cdot f$, has been chosen because it shows the power variance from each frequency that helps to illustrate the significance of each frequency component. The middle part shows the cumulative standard deviation of the measured and simulated active power computed from the power spectra in the upper part. Finally, the lower part of Figure 4.10 shows the normalised difference between the standard deviation simulated and measured, where the normalisation refers to the rated power of the wind turbine.
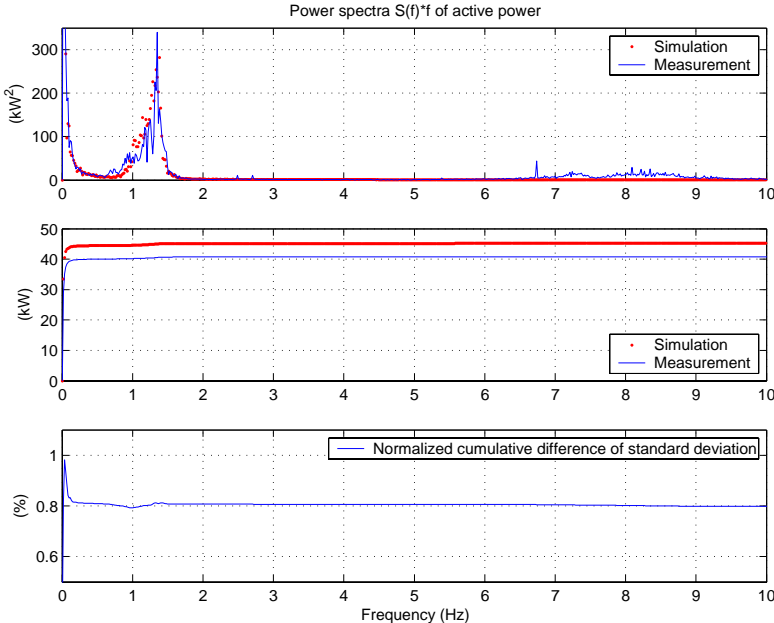
Figure 4.10 Verification of the standard deviation of the dynamic wind turbine model.

From 0 to 6Hz there is a general good agreement between the simulated and measured power spectra that is verified in terms of the cumulate standard deviation (middle part of the figure). In the power spectra, at the frequency of approximately 0.8Hz, the measurements have a power variation related to the first tower bending moment. This mode

was not included in the dynamic wind turbine model because it is small the power contribution. The power on the frequency around 1.08 is related to the first torsional mode from the drive train. The simulated drive train has more variations than the measured one. In the frequency range below 3p (1.5Hz), the measured and the simulated active powers agree.

In the frequency range from 6.7Hz up 9.5Hz, the power spectral distribution of the measured power shows a power variation related to complex modes of oscillation that have been related to the flexible complex aerodynamic rotor and the induction generator [66]. These effects have not been implemented in the dynamic wind turbine model because they are small compared to the relevant power variations for power quality assessments as the difference between the simulated and measured standard deviations accumulated is less than 0.8% (normalisation to the rated power).

The last relevant parameter compared in this section is the flicker emission. The short-term flicker emission can be computed based on the time series of active and reactive power [34]. The flicker short-term emission (P_{st}) from the measurements is 0.1834 and from the simulation, P_{st} is 0.1681, the total difference was small and because it is not linear, it cannot be directly compared.

In order to detail the flicker estimation using the dynamic wind turbine model, the P_{st} flicker is computed again where different power contributions in frequency domain are included as presented in Figure 4.11. This is done by applying a sharp cut-off filter to the measured and simulated active and reactive powers at different frequencies and then those time series are applied to the flicker program that computes the P_{st}.
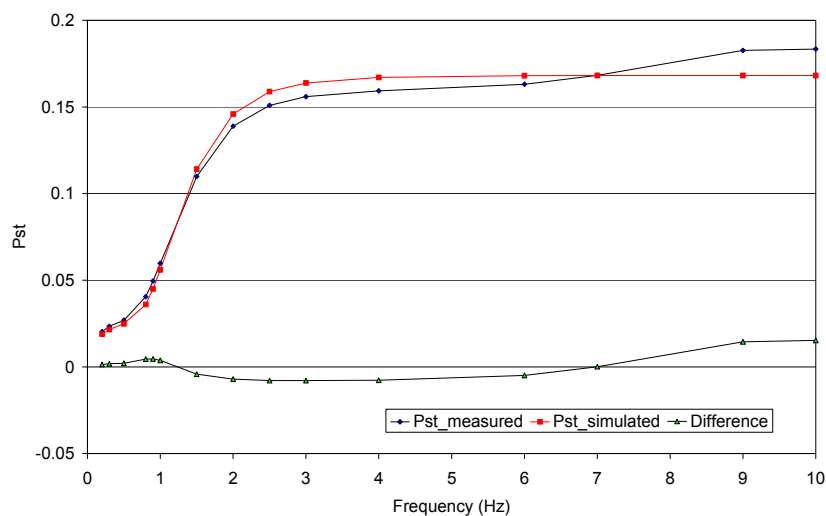
Figure 4.11. Verification of the flicker P_{st} to different frequencies.

The simulated flicker is very similar to the measured one. The flicker as a function of the power contributions bellow different frequencies shows that the 3p is the most relevant effect on the flicker while in the frequency range from 5Hz to 10Hz the contribution to the total flicker is reduced (less than 0.02 compared to 0.18). The dynamic wind turbine model only includes the effects up to 4Hz that is the most relevant to power quality assessment.

4.4 Dynamic Wind Turbine Model Remarks

A dynamic wind turbine model has been presented, which is intended to power quality assessment of wind turbines. This chapter focus on the aeroelastic model because the electrical components are modelled by a dedicated conventional power system simulation program.

The model was applied to a 500kW machine and the simulated electrical power was compared to the power measured. The results showed a general good agreement. The power spectral density, however, present some differences.

The main differences are related to basic assumptions done in the model. The first difference is related to the tower bending moment that is not included in the aeroelastic model therefore the differences were expected.

Finally, the model is suitable to power quality assessment. The model can be applied to different simulation tools with small modifications. The model also is fast and permits the simultaneous simulation of several wind turbines representing wind farms.

Chapter 5

5 Aggregate Wind Farm Model

Proper and successful integration of wind farms into the power systems rely on good understanding of the power variations from wind turbines. Wind turbines deliver a fluctuating power caused by turbulence and machine dynamics. Several wind turbines compose a wind farm where each wind turbine contributes to the net power output variations.

Power utilities usually are concerned about power quality deviations and stability issues from wind farms operation. The power produced by wind turbines varies in a broad range of frequencies and can cause undesirable voltage variations as well as frequency variations in large-scale integration.

Recently, the power quality assessment from wind turbines has been addressed in IEC61400-21 [1]. In IEC 61400-21 the most relevant power quality characteristics from wind turbines has been indicated. It gives also tools to estimate power quality deviations due to the wind turbines connection as pointed in chapter 2.

The tools presented in [1] can estimate the power quality deviations, however, simulations of the wind farms are still recommended to some specific conditions, e.g. when large amount of wind energy is connected to the local capacity or when the networks are weak. In those cases, the wind farms power production must be simulated and power quality, power stability, and proper operation of the protections must be assured.

A wind farm model to support power quality assessment of wind farms based on aggregate representation of the wind farm is presented. The Aggregate Wind Farm (AWF) is a scale up of a wind turbine where the wind speed is an average of the wind acting on each wind turbine in the wind farm. The aggregate wind farm represents the entire wind farm.

The AWF reduces the simulation time and it has been implemented in a commercial power system simulation tool SIMPOW/ABB® using available library models of the electrical components as presented in chapter 4. The time inexpensive implementation of the AWF makes the analysis of integration of large-scale wind farms in the power system more effective and feasible.

5.1 Aggregate Wind Speed Model

An appropriate wind speed model is essential to obtain realistic simulations of the power fluctuations from wind farms [67]. The turbulence model was defined in chapter **3**, and here the main aspects of the wind in the park scale are presented.

The Aggregate Farm Wind Speed (AWFWS) model is an average of the wind speed of the wind acting on each wind turbine in the wind farm. The AWFWS is based on a linear system assumption. Considering the power from the wind farm is the sum of the power produced from each wind turbine in the wind farm, the AWFWS is defined as the average of the wind speeds in each wind turbine that applied to the scaled wind turbine simulates the wind farm power produced.

Currently, the AWFWS represents the stochastic part of the longitudinal wind. The longitudinal wind is the most relevant for power production in wind turbines, which is a reasonable assumption. Here, it is also assumed that all wind turbines have the same average wind speed and there is neither deterministic influences nor wake effect in the wind farm.

5.2   Coherence of Turbulence in a Park Scale

The turbulence between two positions is correlated. The degree of correlation depends on the distance between the two positions, the average wind speed and the turbulence intensity very similar to the case on the rotor area of a wind turbine as presented in chapter 3.

Similar to the coherence on the rotor plane in Equation (3.27), the Davenport type coherence [57] also represents the coherence between two wind turbines however the decay factors are modified to account larger distances. The Davenport type coherence between two positions x and y is rewritten here as:

$$\gamma\left(f, d_{xy}\right) = e^{\left(-a_{xy}\frac{d_{xy} \cdot f}{U_0}\right)} \tag{5.1}$$

where a_{xy} is the decay factor; d_{xy} is the distance between the wind turbine in position x and wind turbine in position y as presented in Figure 5.1, f is the frequency of the turbulence and U_0 is the mean wind speed. In this case, the prevailing wind direction influences the coherence factor, where the inflow wind speed angle for each wind turbine (α_{xy}) is defined as in Figure 5.1.
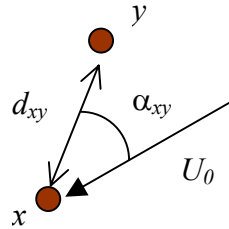
Figure 5.1 Spatial disposition of the two wind turbines ($\alpha_{xy} = 90°$ means lateral disposition).

where d_{xy} is the distance between the wind turbines in positions x and y, α_{xy} is the inflow wind speed angle to wind turbine in x that it is the relative angle of the wind speed to the wind turbine in the position y and U_0 is the mean wind speed.

The decays factors a_{xy} for the park scale includes the distances up to kilometres and have been experimentally studied in [58], which suggests the following expression:

$$a_{xy} = \sqrt{\left(a_{long}\cos\left(\alpha_{xy}\right)\right)^2 + \left(a_{lat}\sin\left(\alpha_{xy}\right)\right)^2} \tag{5.2}$$

where α_{xy} is the wind inflow angle (see Figure 5.1) and a_{lat} is the lateral component:

$$a_{lat} = \left(17.5 \pm 5\right) \cdot \frac{\sigma}{1m/s} \tag{5.3}$$

where σ is the standard deviation of the wind speed in m/s. Moreover, a_{long} is the longitudinal component:

$$a_{long} = (15 \pm 5) \cdot \frac{\sigma}{U_0} \tag{5.4}$$

Figure 5.2 presents an example of coherence simulated with different separations from 100m up to 1300m all with average wind speed of 15m/s and turbulence intensity of 15%, inflow angle = 0°, a_{lat} = 17.5 and a_{long} = 15.
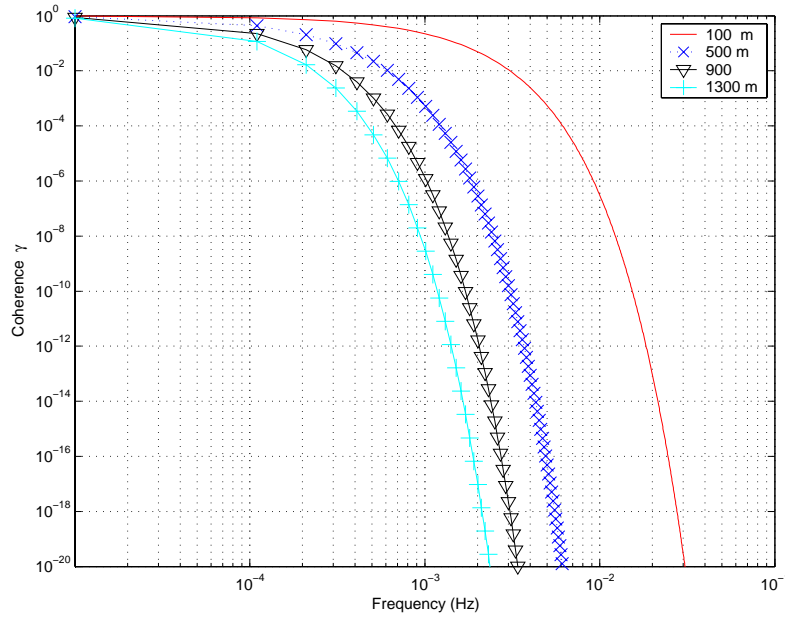
Figure 5.2 Coherence factor for different distances between two points.

The separation and the frequency have strong influences on the coherence. The distances in a wind farm are in the range from hundred meters up to kilometres, in which the turbulence will be highly correlated at very low frequencies up to 0.001Hz. At the 3p frequency, which is around 1Hz in medium sized wind turbines, the turbulence can be considered uncorrelated because of the strong reduction from the coherence. These facts are important to the implemented AWFWS as presented in the following section.

5.3 Aggregate Turbulence

The wind field acting on the rotor of a wind turbine can be expressed as an equivalent time series of wind speed as explained in chapter 3.

The equivalent wind speed ($w_{eq,i}(t)$) for the wind turbine i can be expressed as sum of harmonics on the rotor azimuth angle as follow:

$$w_{eq,i}(t) = \sum_{k=-\infty}^{\infty} \widetilde{w}_{3k,eq,i}(t) e^{j3k\phi_{rotor,i}} \tag{5.5}$$

where the $\widetilde{w}_{3k,eq,i}$ is the $3k^{th}$ term of the expansion of the wind, k is the multiple for the third harmonic component in terms of azimuth angle ϕ_{rotor} for wind turbine i.

Power spectral analysis of power measurements from three-bladed wind turbines revealed that the harmonic components at three times the azimuth speed are the most significant that are converted to the electrical power (chapter 3). Equation (5.5) is then rewritten as:

$$w_{eq}(t) \approx w_{0p}(t) + 2\,\mathrm{Re}\{w_{3p}(t)\}\cos(3\phi_{rotor}) + 2\,\mathrm{Im}\{w_{3p}(t)\}\sin(3\phi_{rotor}) \tag{5.6}$$

where, the PSD of the w_{np}'s are computed as admittance functions applied to the PSD of turbulence (e.g. Kaimal [44]) as pointed in chapter 3.

Using the Aggregate Wind Farm Wind Speed (AWFWS), its harmonic components can be rewritten as:

$$w_{AWFWS}(t) = \frac{1}{N_{W.T.}}\left(\sum_{i=1}^{N_{W.T.}} w_{eq,i}(t)\right) \tag{5.7}$$

Inserting Equation (5.6) in Equation (5.7):

$$w_{AWFWS}(t) =$$
$$\frac{1}{N_{W.T.}}\sum_{i=1}^{N_{W.T.}}\left(w_{0p,i}(t)\right) + \frac{2}{N_{W.T.}}\sum_{i=1}^{N_{W.T.}}\mathrm{Re}\{w_{3p,i}(t)\}\cos(3\cdot\phi_{rotor,i}) + \frac{2}{N_{W.T.}}\sum_{i=1}^{N_{W.T.}}\mathrm{Im}\{w_{3p,i}(t)\}\sin(3\cdot\phi_{rotor,i}) \tag{5.8}$$

where $N_{W.T.}$ is the number of wind turbines in the wind farm. Rewriting (5.8):

$$w_{AWFWS}(t) \approx$$
$$w_{0p,AWFWS}(t) + 2\,\mathrm{Re}\{w_{3p,AWFWS}(t)\}\cos(3\cdot\phi_{rotor,AWF}) + 2\,\mathrm{Im}\{w_{3p,AWFWS}(t)\}\sin(3\cdot\phi_{rotor,AWF}) \tag{5.9}$$

Here, it is assumed that the azimuth position of the aggregate wind farm $\phi_{rotor,AWF}$ can replace the azimuth position of each wind turbine. Since the winds at 3p frequency are totally uncorrelated because of the higher frequency and distances between the wind turbines, the assumption is valid. $w_{0k,AWFWS}$ and the $w_{3k,AWFWS}$ are the harmonic amplitudes of the AWFWS, defined as:

$$w_{0p,AWFWS}(t) = \frac{1}{N_{W.T.}}\left(\sum_{i=1}^{N_{W.T.}}\left(w_{0p,i}(t)\right)\right) \tag{5.10}$$

$$w_{3p,AWFWS}(t) = \frac{1}{N_{W.T.}}\left(\sum_{i=1}^{N_{W.T.}}\left(w_{3p,i}(t)\right)\right) \tag{5.11}$$

5.4 Simulation of Wind Speeds

The wind speed simulator has six main inputs parameters:

- Wind speed parameters – e.g. average wind speed, wind direction turbulence length scale, turbulence intensity, coherence factors, etc.

- Wind turbine diameter.

- Wind farm layout.

- Turbulence Power Spectral Density model, e.g. Kaimal [44].

- Coherence model – e.g. Davenport [57].

- Admittance functions – to 0p and 3p harmonic components.

The model outputs three time series that compose the Aggregate Wind Farm Wind Speed – AWFWS – as defined in Equation(5.9). Figure 5.3 presents the main structure of the AWFWS.
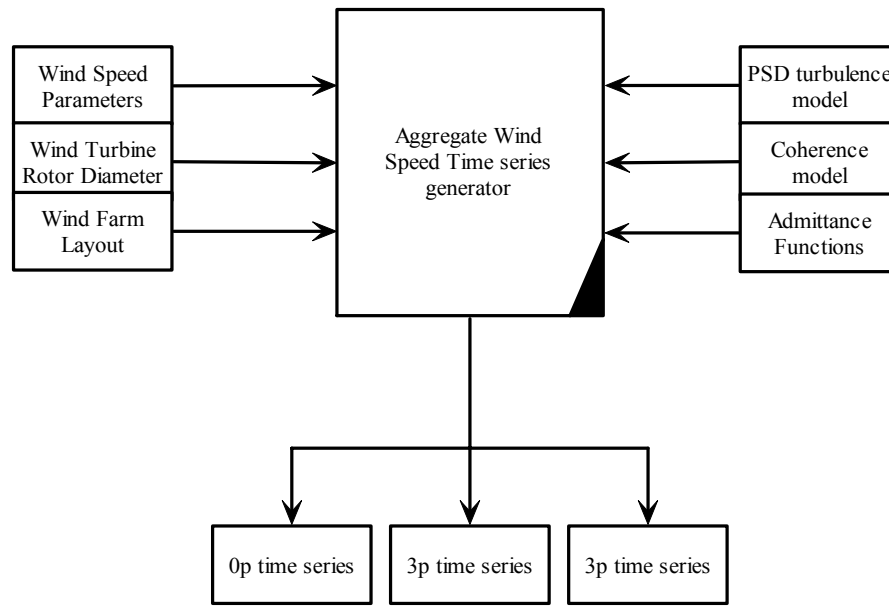
Figure 5.3 Structure of the AWFWS generator.

The aggregate wind speed times series generator in Figure 5.3 is based on the Shinozuka method using a cross-spectral matrix similar to the method used in [68]. The Shinozuka method purpose is to compute a realization of a stochastic process given the spectral density function of the process.

Here a cross-spectral matrix represents the correlated turbulence processes. The cross-spectral matrix contains all energy from the turbulence on each wind turbine position in the wind farm and the contributions due to the correlation between two positions. The cross-spectral matrix $S(f)$ is NxN, which corresponds to a wind farm with N wind turbines. The $S(f)$ has the following structure

$$(S(f)) = \begin{pmatrix} S_{1,1}(f) & S_{1,2}(f) & \cdots & S_{1,n-1}(f) & S_{1,n}(f) \\ S_{2,1}(f) & S_{2,2}(f) & \cdots & \cdots & S_{2,n}(f) \\ \vdots & \vdots & \ddots & & \vdots \\ S_{n-1,1}(f) & \vdots & & S_{n-1,n-1}(f) & S_{n-1,n}(f) \\ S_{n,1}(f) & S_{n,2}(f) & \cdots & S_{n,n-1}(f) & S_{n,n}(f) \end{pmatrix} \tag{5.12}$$

where the diagonal elements are the spectral density of turbulence on each wind turbine. The non-diagonal elements are the cross-spectral densities of the turbulence for the pairs x,y. The cross power spectral density includes a time delay and it is written as [19]:

$$S_{xy}(f) = \left| S_{xy}(f) \right| e^{-2\pi f \tau_{xy}} \tag{5.13}$$

where , $S_{xy}(f)$ is the cross spectrum between the turbulences in x and y, f is the frequency, γ_{xy} is the coherence function between x and y defined in Equation (5.1) and τ_{xy} is the travelling time of the wind travel from wind turbine x to y, which can be determined according to Figure 5.1 as

$$\tau_{xy} = \frac{\cos(\alpha_{xy}) d_{xy}}{U_0} \tag{5.14}$$

where U_0 is the mean wind speed. Thus, the cross-spectral density can be expressed as

$$S_{xy}(f) = \gamma(f, d_{xy}) \sqrt{S_{xx}(f) S_{yy}(f)} \cdot e^{-j2\pi f \tau_{xy}} \tag{5.15}$$

Hence, using the spectral matrix and taking the definition of the AWSWF from Equation (5.10) and Equation (5.11) the spectral density terms to the Aggregate Wind Farm Wind Speed ($S_{AWFWS,k}(f)$) for each harmonic component is written as:

$$S_{AWFWF,0p}(f) = \frac{1}{N_{W.T.}^2} \sum_{x=1}^{N_{W.T.}} \sum_{y=1}^{N_{W.T.}} S_{xy,0p}(f) \tag{5.16}$$

$$S_{AWFWF,3p}(f) = \frac{1}{N_{W.T.}^2} \sum_{x=1}^{N_{W.T.}} S_{xx,3p}(f) \tag{5.17}$$

Where $S_{xy,k}$ are the cross spectral elements of the kth harmonic component and $S_{xx,k}$ is the spectral density of each kth harmonic component for each wind turbine. The main difference between the terms to the $0p$ and $3p$ is that for the 3rd harmonic the cross spectral elements $S_{xy,k}$ are assumed to be zero due to the high frequency and relative large distance between wind turbines x and y (coherence is zero).

After having defined the spectral terms of the aggregate wind speed, it is necessary to discretise the frequency in order to use a computer code to generate the wind speeds. The discrete step of the frequency to simulate a time series with length T_p is $\Delta f = 1/T_p$, so the ith frequency is $f[i] = i\Delta f$. The corresponding discrete value of $S_{xy}(f)$ is $S_{xy}[i] = S_{xy}(\Delta f\, i) \cdot \Delta f$.

The corresponding time series is discrete by the sampled representation of the wind speed with time steps of $\Delta t = 1/f_s$ where f_s is the sampling frequency in Hz. The sampling frequency limits the frequency to $\pm f_s/2$ and consequently the frequency index i to $\pm Ns/2$, where $Ns = T_p \times f_s$ is the number of samples in the simulated time series. Ns must be integer and in order to use FFT it should be an exponent of 2.

The next step is for each frequency index k to generate random complex numbers $c_k = A_k + jB_k$ to finally use the inverse Fourier Transformation with Fourier coefficients c_k, i.e.

$$w(t) = A_0 + \sum_{k=1}^{N} 2 \cdot A_k \cos(k \cdot \Delta f) - \sum_{k=1}^{N} 2 \cdot B_k \sin(k \cdot \Delta f) \tag{5.18}$$

Then the energy content to the kth component from Equation (5.18) can be rewritten as:

$$E_k(w) = 2\left(A_k^2 + B_k^2\right) \tag{5.19}$$

It is imperative that this method preserves the variance σ^2 of the process. Thus, using a single sided spectrum, the variance can be defined as:

$$\sigma^2 = \int_0^\infty S_{xx}(f)df \approx \int_0^{f_s/2} S_{xx}(f)df \approx \sum_{K=0}^{N_s/2} S_{xx}(k \cdot \Delta f) \cdot \Delta f \tag{5.20}$$

The discrete part of the energy content of the frequency $k \cdot \Delta f$ must then have the same mean value of the energy content E_k,

$$E\{E_k\} = S_{xx}(k \cdot \Delta f) \cdot \Delta f \tag{5.21}$$

Assuming $E\{A_k^2\} = E\{B_k^2\}$ then,

$$E\{A_k^2\} = E\{B_k^2\} = \frac{S_{xx}(k \cdot \Delta f)\Delta f}{4} \tag{5.22}$$

Assuming that the mean value of A_k and B_k are zero, i.e. $E\{A_k\} = E\{B_k\} = 0$, the standard deviation $\sigma\{A_k\}$ and $\sigma\{B_k\}$ can be determined as

$$\sigma\{A_k\} = \sigma\{B_k\} = \sqrt{E\{A_k^2\} - (E\{A_k\})^2} = \frac{\sqrt{S_{xx}(k \cdot \Delta f)\Delta f}}{2} \tag{5.23}$$

Thus, A_k and B_k can be determined from a normally distributed stochastic process with mean value zero and standard deviation: $\frac{\sqrt{S_{xx}(k \cdot \Delta f)\Delta f}}{2}$. Figure 5.4 presents a comparison between the formal Shinozuka random phase angle method and the use of the two random numbers
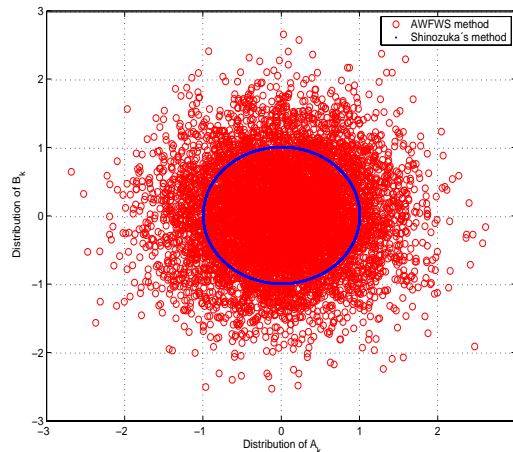
Figure 5.4 Distribution of random constants.

From Figure 5.4 it is possible to see that the terms to the Inverse Fourier Transformation are more random than the random phase angle method.

5.5 Aggregate Wind Turbine Machine

The aggregate wind turbine replaces the entire wind farm with a single wind turbine. The single wind turbine is modelled as presented in chapter 4.

The aggregation procedures have been extensively applied to power system analysis particularly to stability analysis of large power systems. The method has been applied to represent groups of similar machines in areas of the power system.

The aggregation procedures of induction motors applied to power quality analysis have been successfully reported, e.g. [69], [70] and [71].

Here, the aggregation procedure is applied to similar wind turbines, hence the equivalent wind turbine to the entire wind farm is a scale up of a single wind turbine, i.e. the base power becomes N_{wt} times the base power of a single wind turbine in the farm, where N_{wr} is the number of turbines in the wind farm.

5.6 Results and Discussions

Here, the simulated power using the AWF is compared with a simulation that models individually each wind turbine in a wind farm, hereafter called IWF. The IWF simulates all wind turbines in the farm applying to each of them a correlated time series of wind.

The IWT models each wind turbine in the wind farm with accurate models to the wind turbine dynamics. The Parksimu model [19] generates correlated time series of wind speed to each wind turbine in the wind farm.

The AWF model uses a single aggregate wind turbine that replaces all wind turbines in the wind farm.

5.6.1 Case Description

The wind farm is composed of six 660kW stall regulated directly connected wind turbines type. The wind turbine is composed of an aerodynamic module, a mechanical

transmission system, an asynchronous generator, a capacitor bank, and a step-up transformer.

The aerodynamic module uses power coefficients as introduced in chapter 4 and dynamic stall effects are included. The drive train of the wind turbine has the first torsional moment in 1Hz and inertias of 3.05 and 0.2 per units (seconds) of the aerodynamic rotor and induction generator respectively. The stiffness and damping constants are computed using the definitions from chapter 4. The logarithmic decrement damping coefficient is assumed to be 5%. Table 5.1 presents a resume of the most relevant information to the single wind turbine.

Table 5.1 Basic characteristics of the 660kW wind turbine modelled.

Nominal Power	660kW
Rotor diameter	48 m
Generator speed	1500 rpm
Rotor speed	21 rpm
Capacitor Bank	200kVAr
Generator terminal voltage	400V
Electrical frequency	50Hz
Tower height	36 m
Gearbox ratio	71.43
First torsional frequency	0.8Hz
Estimated logarithmic damping to drive train	5%
Number of blades	3
Constant of inertia of the aerodynamic rotor	3.05 s
Constant of inertia to the generator	0.2 s

The electrical generator is a squirrel cage induction machine, modelled with a 3rd order model where current displacement module is not active (i.e. the rotor resistance is constant).
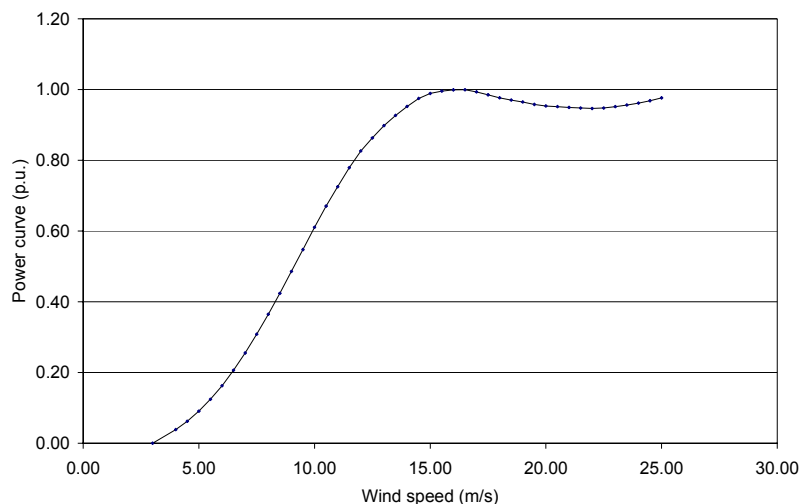
Figure 5.5. Static power curve of the wind turbine.

Figure 5.6 presents the wind farm layout. Where the lateral space between wind turbines is 4 times the rotor diameter and the longitudinal space is 10 times. The wind direction is measured relatively to the North as indicated.
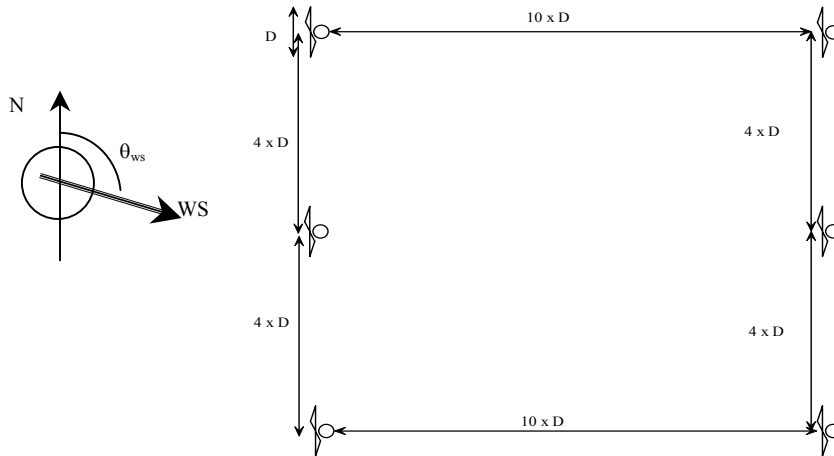
Figure 5.6 Wind farm layout.

The power system is very strong at the Point of Common Coupling (PCC), 400 times the rated power of the wind farm. The Thevenin equivalent at the PCC has an angle of approximate 50°. The PCC is the same to both simulations: AWF and IWF.

5.6.2   Results

5.6.2.1   Wind Speed Simulator

The wind speed simulator is verified here compared to Parksimu [19]. The Parksimu is a program to simulate correlated time series of wind speeds of each wind turbine in a given wind farm based on the layout of the wind farm, the mean wind speed and turbulence intensity as well as on the spatial coherence. The admittance filters are disabled and only one wind speed is simulated in order to compare to the wind speed for a single point as in the Parksimu.

Figure 5.7 presents a general comparison between the wind speed simulated with the Aggregate Wind Farm Wind Speed (AWFWS) and the Parksimu. In the upper part, time series of wind speed simulated with both models are presented. The middle part presents the power spectral of the simulated wind speed using the AWFWS simulator and the one produced from Parksimu described in [19]. In addition, the Kaimal turbulence model is plotted. Kaimal is the target power spectral of turbulence used in both simulation programs. In the lower part of the figure, the cumulative normalised differences of standard deviation of the AWFWS and Parksimu to the Kaimal target spectrum are presented. The same characteristics are applied for both simulations, i.e. average wind speed of 10 m/s at 30 meters height, turbulence intensity of 10%, and turbulence length scale of 600m.
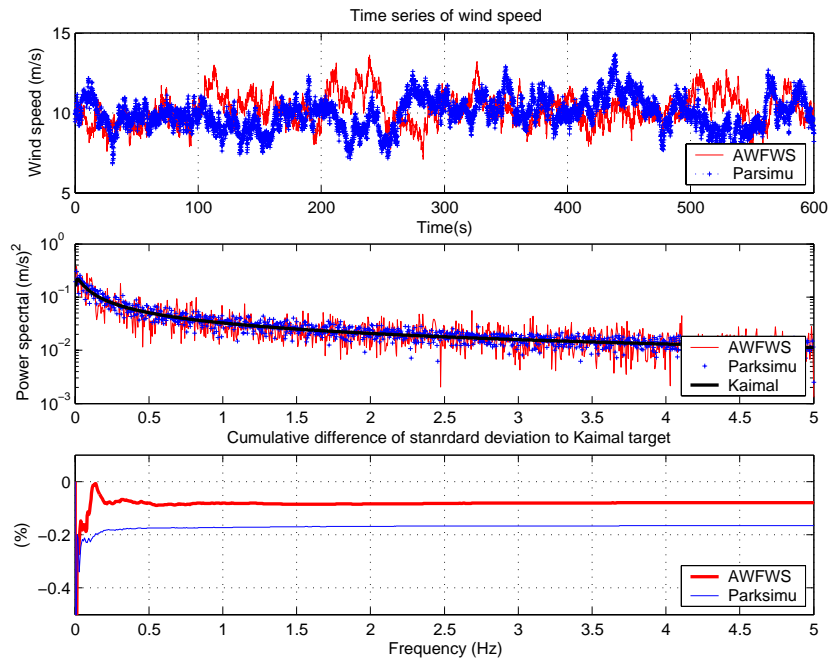
Figure 5.7 Comparisons of the wind speed simulator.

The upper part of Figure 5.7 shows two wind speeds uncorrelated with similar range of wind speed variations. The power spectra reveal general agreement of both wind speed simulations with the target power spectra (Kaimal), in addition, the AWFWS presents more variations than the Parksimu around the target power spectrum. The high variation around the target spectral is a consequence of using two random numbers instead of a random phase angle as used on the Parksimu.

In the lower part of Figure 5.7, the normalised cumulative differences of standard deviation show small difference with a total difference less than 0.2%. In this case, the normalisation factor is the mean wind speed (10m/s). Despite the high variation of the power spectrum of the AWSWF, both simulated wind speeds have similar energy content and slightly difference to the target standard deviation. From Figure 5.7, the AWFWS appears to represent better the turbulence, the difference relative to the target power spectral distribution (Kaimal) is mostly related to the random seeds, and in this particular case the random seed chose to the AWSWF represented better the turbulence than the Parksimu, anyway the total accumulated difference in terms of standard deviation is small.

5.6.2.2   Wind Farm Power Production

This section presents comparisons of the wind farm power simulated using the AWF to the IWT. Six cases are discussed: three different average wind speeds (10,13 and 16m/s) and two different turbulence intensities (10 and 20%). Those relative high wind speeds have been selected because the power curve at those wind speeds is non-linear.

The average power, maximum power in 0.2 seconds and flicker emission in short term were the parameters selected to compare the different models, in accordance to the IEC 61400-21 [1], in addition the standard deviation and minimum power are presented in order to give more information on the AWF usage. Table 5.2 presents the main power characteristics and flicker emission in short term (P_{st}) simulated using the AWF and the IWF.

Table 5.2 Representative power characteristic values of all simulations

Mean Wind speed		10m/s		13m/s		16m/s	
Turbulence intensity (%)		10	20	10	20	10	20
IWF (kW)	Mean Value	2419.73	2403.85	3501.37	3411.19	3870.91	3769.75
	Max Value	2804.95	3158.64	3791.55	3970.79	4014.85	4107.99
	Min Value	1921.04	1602.02	2992.91	2395.15	3589.11	2786.66
	Standard Deviation	131.36	248.62	114.66	244.47	54.65	164.07
AWF (kW)	Mean Value	2430.11	2454.74	3533.61	3519.13	3903.02	3868.42
	Max Value	2892.29	3477.01	3914.87	4152.74	4061.64	4256.20
	Min Value	1830.25	1492.88	3153.48	2615.11	3713.48	3358.08
	Standard Deviation	162.93	370.92	132.61	255.30	41.251	96.01
Flicker P_{st}	IWT	0.094	0.185	0.071	0.164	0.0474	0.120
	AWF	0.086	0.181	0.064	0.140	0.0468	0.100

In low turbulence intensity, the power characteristics simulated with the AWF agree well with the ones simulated with the IWF. Figure 5.8 illustrates the power characteristics simulated on low turbulence intensity.
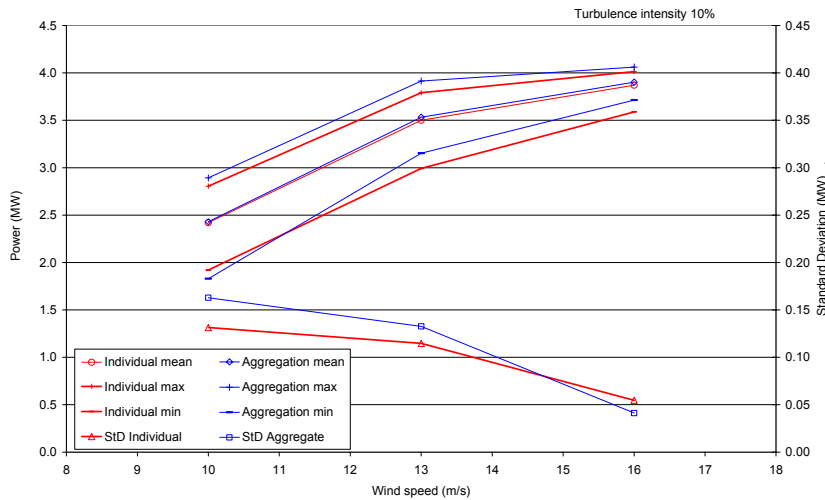
Figure 5.8 Power characteristics evolution with the wind speed (10% turbulence intensity).

In general, the power simulated with the AWF is slightly higher than the IWF. A possible reason for the power differences may be that the wind speed simulated with the AWF has slightly high standard deviation then the ones simulated with the Parksimu as introduced in Figure 5.7. Both simulations show that the power variations reduce with the increased wind speed because of the non-linearity of the aerodynamic power conversion (Figure 5.5).

In high turbulence intensity, the differences are large than the ones in the low turbulence but it is still presenting good agreement except to minimal power. Figure 5.9 illustrates the power characteristics from both simulations on high turbulence intensity.
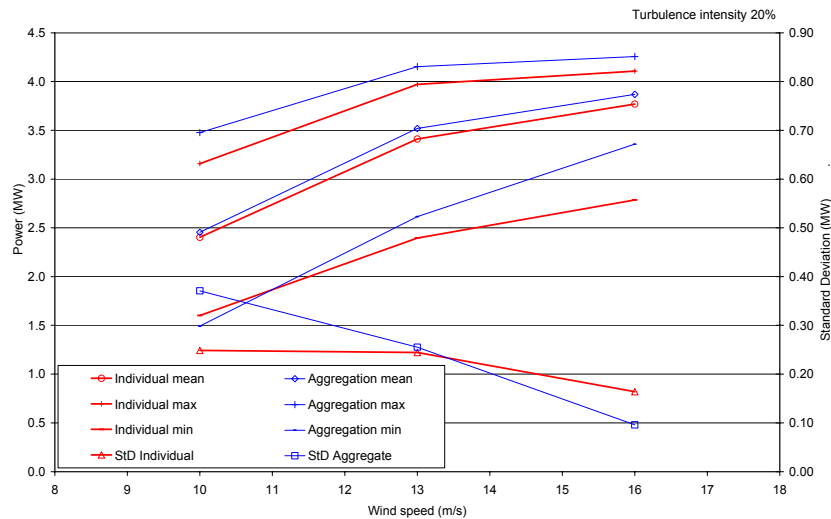
Figure 5.9 Power characteristics evolution with the wind speed (20% turbulence intensity).

Similar to the characteristics presented in low turbulence intensity, the AWF in general simulates higher power than the IWF and the power variations reduces with high wind speed. The differences are related to the same reasons as in the low turbulence intensity case. However, in this case, the high turbulence intensity in high wind speed strongly influences the simulated minimum power and the standard deviation in the AWF.

The high turbulence intensity means that the wind speed will vary in a broad wind speed range on top of the mean wind speed. In the high mean wind speed (16m/s), the power conversion on the aerodynamic rotor is extremely non-linear (see Figure 5.10). Hence, the power variation in a single wind turbine in the IWF can be very different from the one simulated with the AWF because the AWF is an average wind speed that smoothes the wind variations leading to less power variation and a concentration around the high mean value.
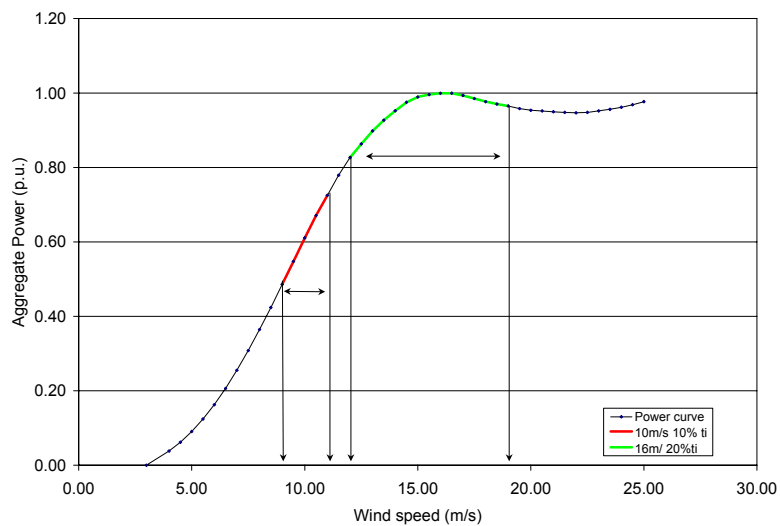
Figure 5.10. Non linear effects on the power variations.

Following, samples of time series of active power simulated are presented that illustrates the processes described above. Figure 5.11 presents the power produced by IWF and AWF with 13 m/s average wind speed and 10% turbulence intensity.
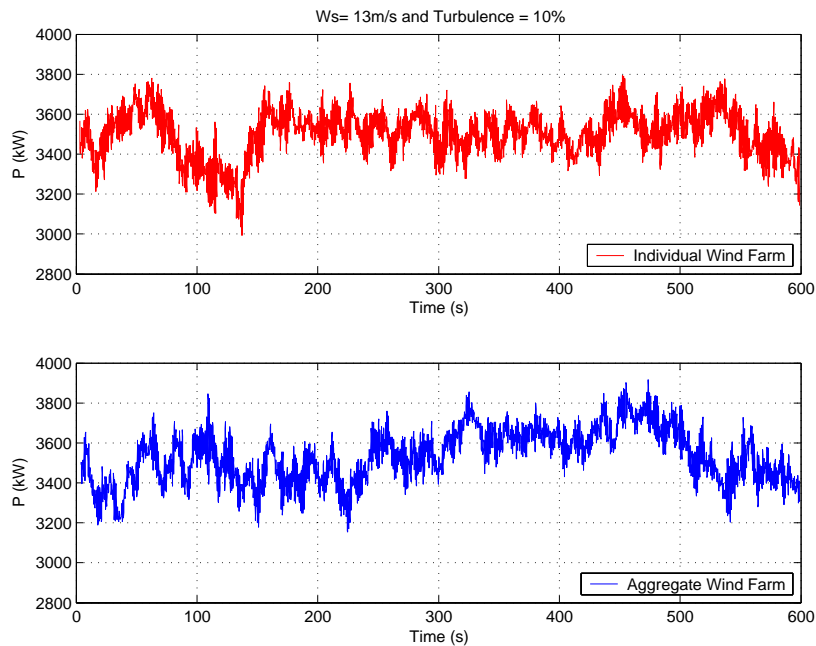
Figure 5.11 Power simulated 13 m/s and 10% turbulence intensity.

The simulated active powers presented in Figure 5.11 are uncorrelated and have similar ranges of power variations. At 13m/s and 10% turbulence intensity, the aerodynamic power conversion is reasonable linear. Power spectral analyses reveal small differences in frequency that are presented in Figure 5.12.
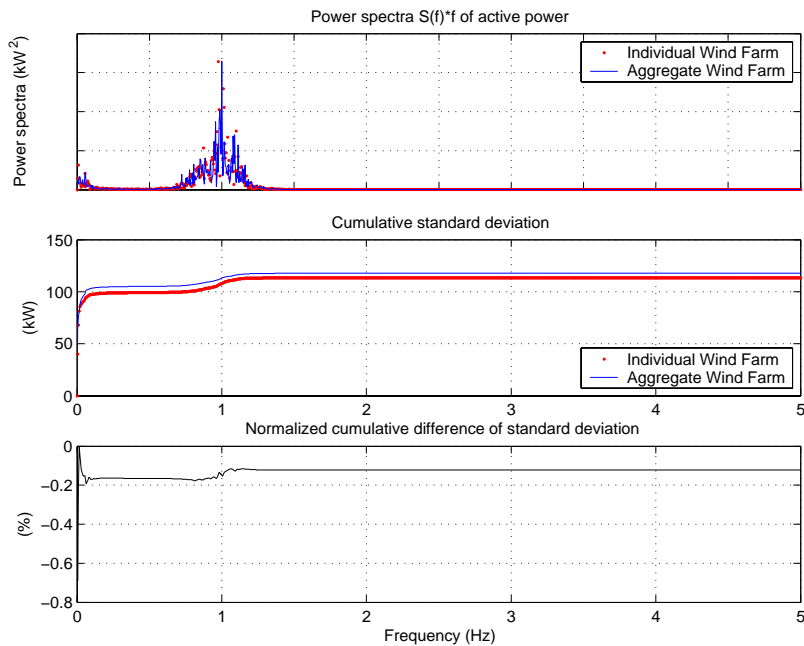
Figure 5.12 Power spectral comparisons at 13 m/s and turbulence intensity 10%.

At 13m/s, the power spectrum of the AWF presents a good agreement with the IWF as showed in the upper part of Figure 5.12. The cumulative difference of the standard deviation from both simulations agree well as presented in the middle part of Figure 5.12 with a steady difference that does not significantly changes with the frequency, that means that the main difference of the standard deviation (power variations) are concentrated on the low frequency range. The lower part in Figure 5.12 presents the normalised difference of the standard deviation between the powers simulated with the AWF and with the IWF, where the negative signal means that the AWF overestimates the standard deviation and the normalisation factor is the rated power of the wind farm.

As one can notice, the overall difference is small (less than 0.2%) and the main difference is on the lower frequency range (less than 1Hz). At frequencies above 1Hz, the power variations from the IWF are slightly higher than the power variations from the AWF that reduces the cumulative standard deviation difference. The reduction on the standard deviation difference is very small.

When the wind speed and the turbulence intensity are increased, the differences become more noticeable. Figure 5.13 presents the active power simulated at 16m/s and turbulence intensity 20%.
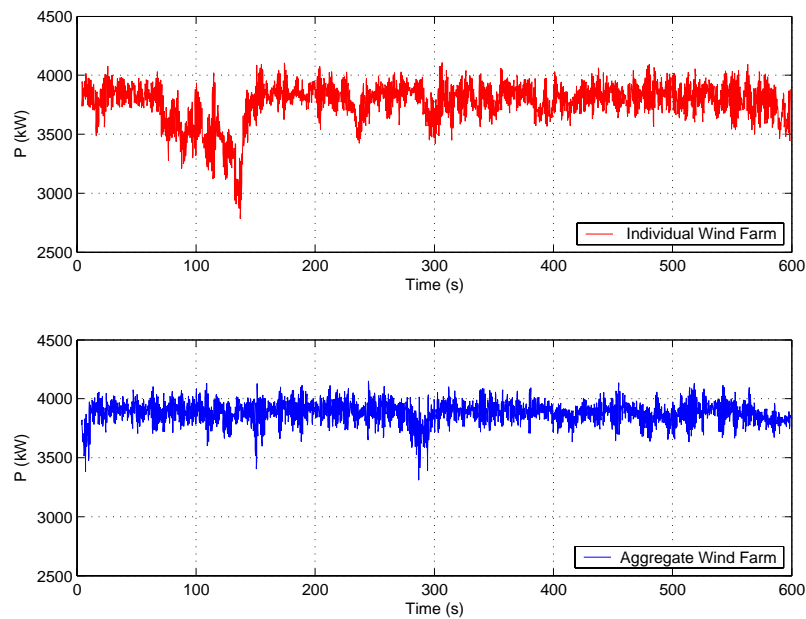
Figure 5.13 Power simulated at 16 m/s and turbulence intensity 20%.

In Figure 5.13, the IWF simulates a steady power reduction in 120 seconds while the AWF does not. This is related to the averaging wind speed process of the AWF added to the non-linear rotor as explained before. The power spectra of the powers reveal more information as presented in Figure 5.14.
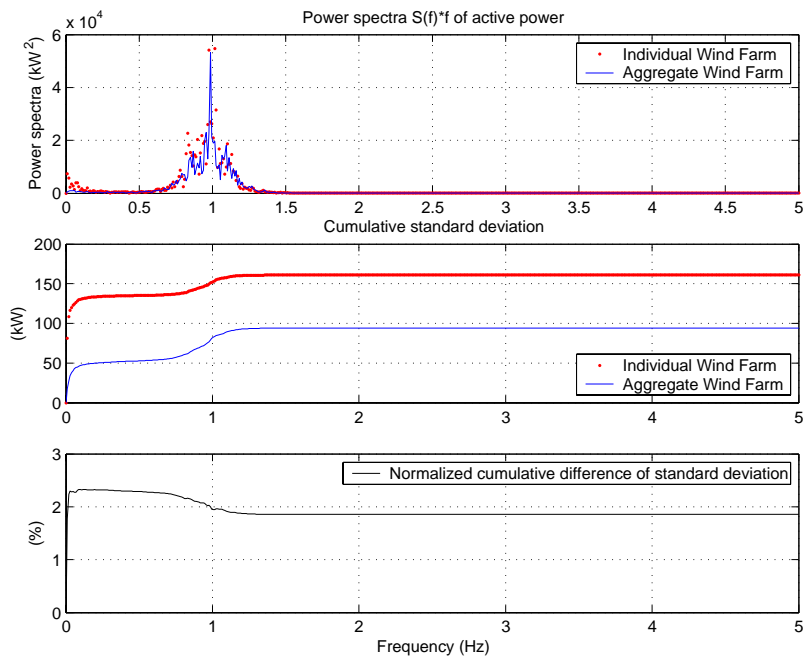
Figure 5.14 Power spectral comparisons at 16 m/s and turbulence intensity 20%.

The power produced from the AWF is smother than the power produced by the IWF that is related to the high non-linear power curve of the wind turbine. The standard deviation of the AWF is very different of the one in the IWF. The differences are very noticeable in the lower frequency range, i.e. less than 1Hz. In the lower frequency range, the wind speed variations are significant, which in this case acts on the high non-linear area of the power curve leading to greater differences on the standard deviation and minimum power.

The difference of standard deviation actually decreases with the frequency. At the frequency range above 3p, the differences on the standard deviation change very little because at this frequency range the wind speed variations are relatively small hence the dynamic stall provides a better power relation between the active power variation and the wind speed variation.

The power variations on low frequency range presented the most significant differences between the AWF and IWF. In the higher frequency rage, the power differences were relatively small that support the use of the aggregate model to flicker estimation from large wind farms. Following, the flicker estimated in the AWF is compared to the one in the IWF.

Using the short-term flicker presented in Table 5.2, the rated power of the wind farm and the number of wind turbines in the wind farm, the flicker coefficient (c) to the wind turbine in the wind farm is computed. The flicker coefficient from a wind turbine is a normalised measure of the flicker from a wind turbine as introduced in chapter 2 that can be computed using Equation (2.3) [1]. Following, Figure 5.15 presents the flicker coefficients for the wind turbine using the P_{st} simulated with the AWF and IWF.
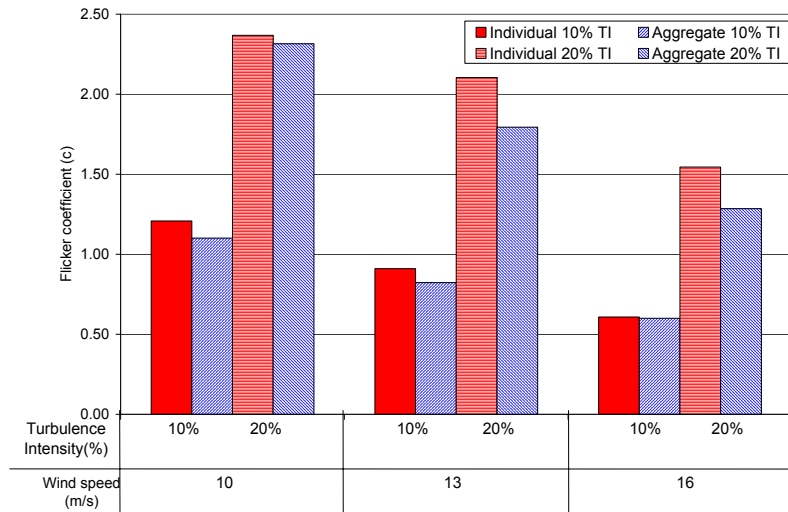
Figure 5.15 Flicker coefficients comparisons (computed according to [34]).

The flicker coefficients computed using the AWF are quite similar to those simulated with the IWF, particularly on the low turbulence intensity. In high turbulence intensity, the non-linear behaviour of the power conversion leads to greater differences between the AWF and the IWF but still god agreement.

In order to verify the contributions from the power variations in frequency domain to the flicker coefficient, following, the flicker estimation is detailed to two different wind speed conditions (13m/s, 20% turbulence intensity and 16m/s 10% turbulence intensity).

The flicker estimated at 13m/s and 20% turbulence intensity with the AWF presented the higher difference to the one simulated with the IWF. Figure 5.16 presents the evolution of the flicker coefficient computed with the P_{st} that included the contributions of the power variations with different frequencies. The active and reactive powers simulated in the AWF and IWF were filtered out with different low-pass cut-off frequencies and then applied to the flicker code that simulates the short-term flicker emission.
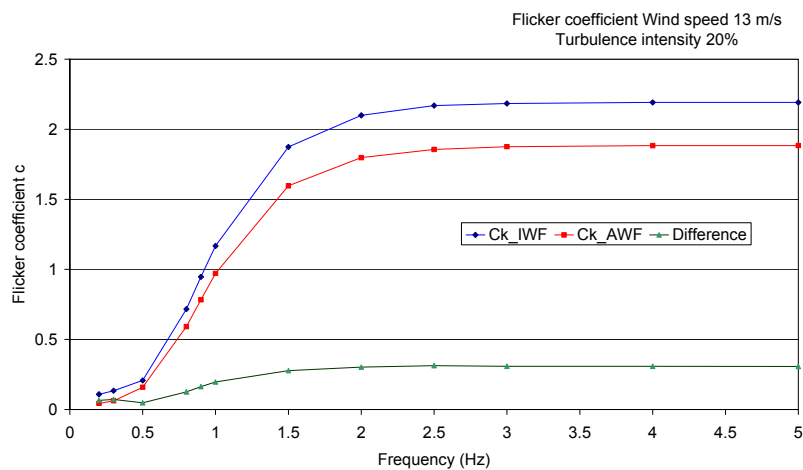
Figure 5.16 Evolution of flicker coefficients at 13m/s 20% turbulence intensity.

The flicker estimated in the AWF poorly agrees with the flicker coefficient estimated in the IWF at 13m/s and 20% turbulence intensity. The main difference appears to be

related to the 3p area, but the flicker procedure is not linear and the curve in Figure 5.16 must be used with caution.

The flicker estimated at 16m/s and 10% turbulence intensity presented the best agreement. The evolution of the flicker coefficient presents very small differences as showed in Figure 5.17.
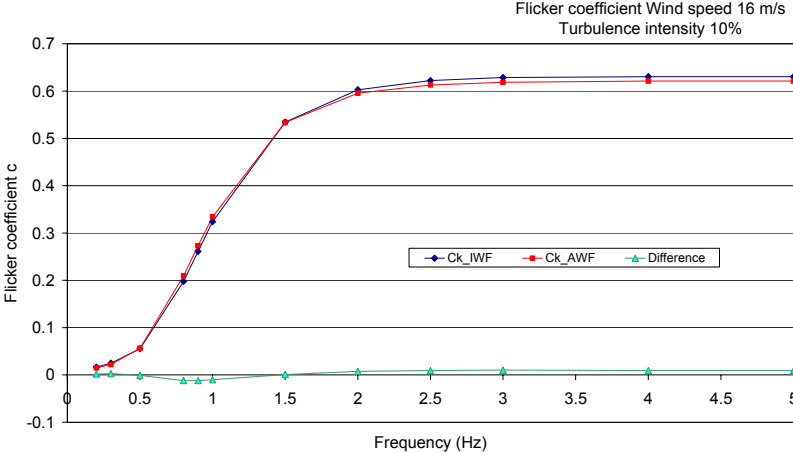
Figure 5.17 Evolution of flicker coefficients at 16m/s 10% turbulence intensity.

The relevant differences encountered here are related to the non-linear rotor under stall conditions and high turbulence intensity. The high turbulence intensity leads to large wind variations that when added to high wind speeds lead to large incursions on the non-linear region of the power conversion. The dynamic stall improved the aggregation model because it generates a relation between wind speed variation and power variation on the stall condition. However, it is not enough to compensate to the 6 wind turbines in high turbulence intensity.

5.6.2.3   *Extension to Large Wind Farms and Different Random Seeds*

In order to verify the usage of the AWF to large number of wind turbines, wind farms with sizes of 6, 12, 15, 21 and 30 wind turbines have been implemented in Matlab/Simulink®. Moreover, it had also been indicated that the random seeds can modify the results, and until now, the AWF has been applied to a small wind farm keeping the same random seeds in the simulations in order to trace the results. In this subsection, the model is extended to a large number of wind turbines and different random seeds are applied to two different wind speed conditions (13 and 16m/s 20% turbulence intensity).

In this case, the wind farm model does not have the electrical dynamic components and only the aerodynamic power is computed using the dynamic stall module. This is done because on the aerodynamic rotor resides larger part of the no-linear conversion and the simulation of larger wind farms including the electrical components would demand extensive simulations not giving much information because the main differences reside on the wind speed conversion. In addition, the cases presented in the previous section supported that the differences found were related to the wind speed variations at low frequency range (lower than 1Hz).

In this section, The wind farm layouts are similar to Figure 5.6 where the new wind turbines are included in groups of three in the end of the rows keeping the same distance

between them and the same wind speed inflow angle, which makes the power extremely correlated.

The mean power, standard deviation, maximum and minimum powers are the power characteristics investigated in the following section, where they are normalised with the rated power of the wind farm. Positive values stand for the AWF lower than the IWF.

Starting with the mean wind speed at 13m/s, Figure 5.18 presents the normalised power characteristics as a function of different number of wind turbines.
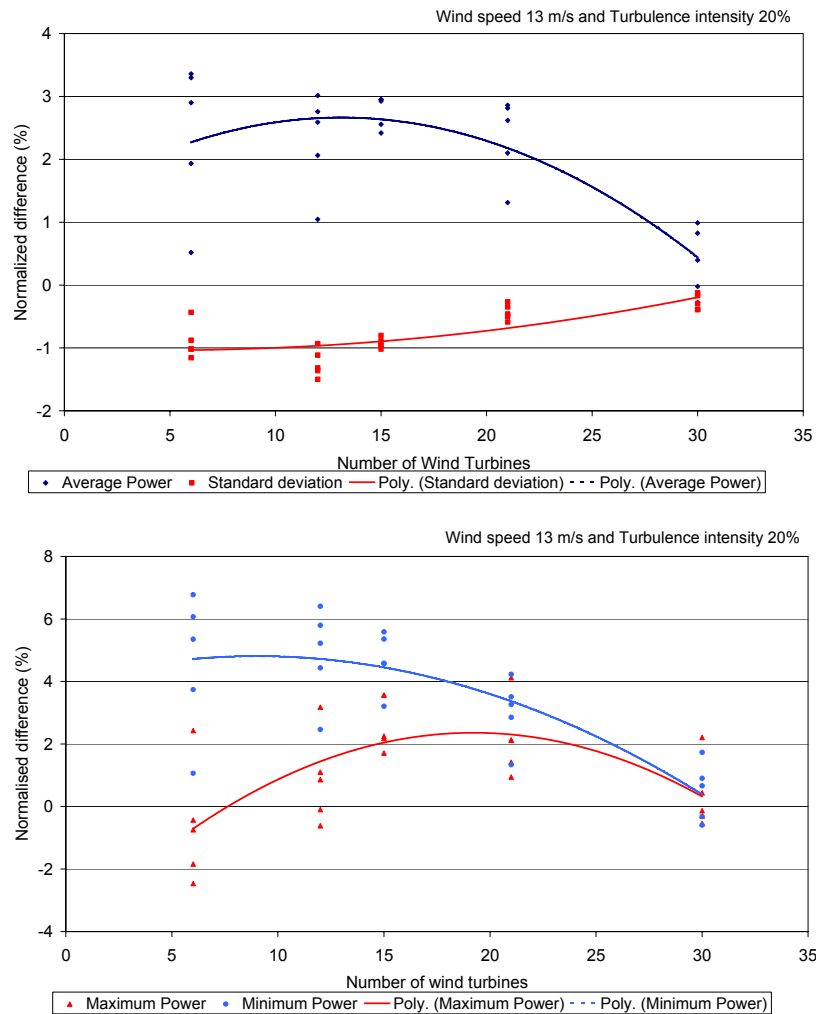
Figure 5.18 Influences of different sizes of aggregate wind farms to the power characteristics at 13m/s, 20 % turbulence intensity

The upper part of Figure 5.18 presents the normalised differences of the standard deviation and mean powers. Increasing the number of wind turbines in the aggregation procedure improves the performance of the AWF. In addition, the random seeds have strong influences on the results that reduce with the number of wind turbines in the aggregation procedure. These two main factors are related to the fact that increasing the number of wind turbines in this particular non-linear part of the power curve decreases the influence of a single wind turbine on the total results.

One can notice in this sub-section, that the standard deviation in the AWF is higher than the IWF in agreement with the complete model presented in the previous sub-section,

however, the mean power in the AWF is lower than the IWF, which is different from the complete model in SIMPOW (Figure 5.9). This difference is related to the strong influence of the random seed in the mean value. Probably in the complete model in SIMPOW, random seeds used to generate the wind speeds in both Parksimu and AWFWS were two extreme cases.

The lower part of Figure 5.18 presents the normalised differences of the maximum and minimum power. In general, the differences between the IWF and AWF reduce when increasing the number of wind turbines in the aggregation procedure. These conclusions are also related to the reduced significance of a single wind turbine when increasing the high number of wind turbines.

Following the analyses with the mean wind speed at 16m/s are presented.
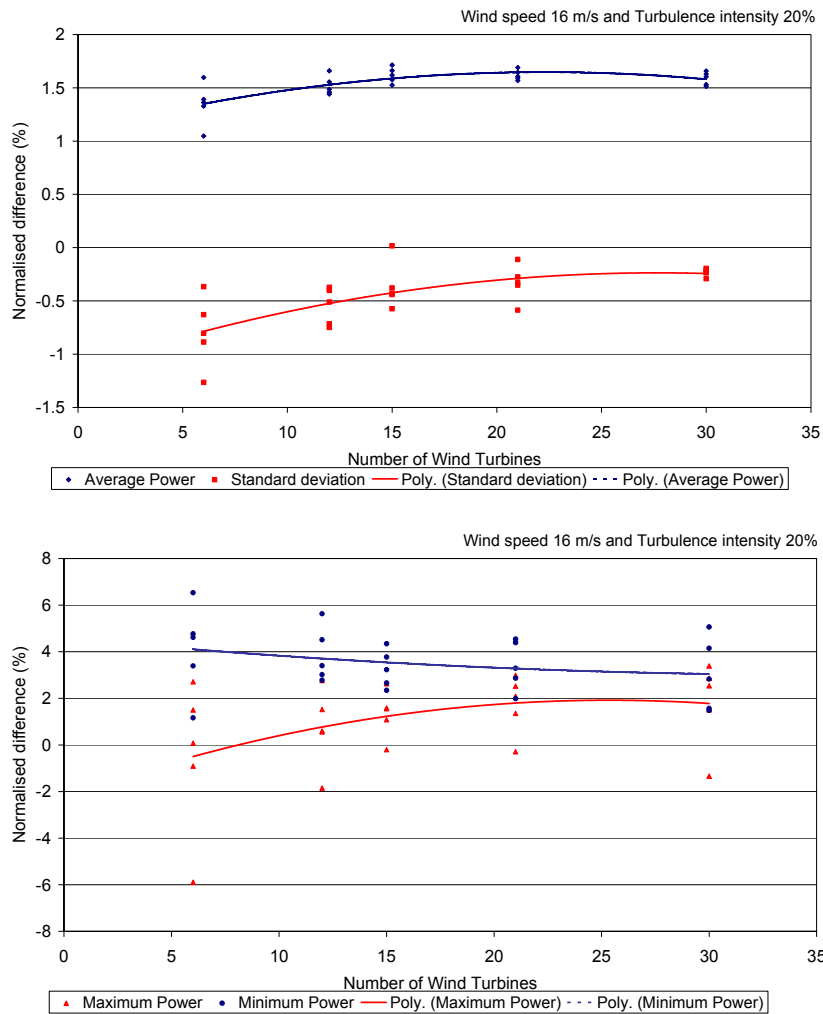
Figure 5.19 Influences of different sizes of aggregate wind farms to power characteristics at 16m/s, 20 % turbulence intensity

Similar to Figure 5.18, the upper part of Figure 5.19 presents the normalised differences of the standard deviation and the mean power. Increasing the number of wind turbines in the aggregation procedure improves the performance of the AWF. The random seeds have strong influences on the results that in general reduce with the number of wind turbines in the aggregation procedure. These two main factors are also related to the fact

that increasing the number of the wind turbines decreases the influence of a single wind turbine on the total results.

The lower part of Figure 5.19 presents the normalised differences maximum and minimum power differences between the AWF and the IWF. In general, the differences between the IWF and AWF as well as the random seeds influences on the results tend to reduce when increasing the number of wind turbines in the aggregation procedure. These conclusions are also related to the reduced significance of a single wind turbine when increasing the high number of wind turbines.

5.7 Aggregate Wind Farm Model Remarks

Simulation of large wind farms can be extremely expensive, depending on the size of the wind farm and on the extension of the power system network. Simulation of all wind turbines in a large extension of the power system is practically impossible. Therefore, there is a demand for equivalent models to analyse the power system interaction with the wind power.

The Aggregate Wind Farm model can replace the entire wind farm in power system simulation programs. It can be applied to replace large wind farms in order to simulate the impact on the power system characteristics, i.e. the power oscillations, power quality deviations and to analyse the control or to optimise the power system operation.

The AWF is time inexpensive and easy to implement in a conventional power system simulation tool used by the utilities. Using SIMPOW$^®$ installed in a Pentium III$^®$ - 750MHz (with 128Mb of ram memory), the simulation of the power produced from 6 wind turbines with the IWF took around 5 hours while using the AWF, in the same program installed in the same computer, the simulation time was reduced to 20 minutes.

The aggregate procedure focuses on the wind speed simulation. The wind speed model accounts to spatial coherence of turbulence on the entire wind farm representing the smooth effects on the power production in the wind farm.

The AWF has some limitations. The minimum power and standard deviation of the power in high wind speed and high turbulence intensity do not agree with the simulation of individual wind turbines.

However, the flicker agrees well. The flicker is mostly caused by the 3p effect from wind turbines, which region the AWF seems to reproduce well the IWF.

Finally, The AWF simulates reasonably the power produced from wind farms. The AWF makes possible power quality assessment of large number of wind turbines. Respecting the AWF limitations, the model supports the design and operation of the power system where the wind energy contributes to large part of the power production.

Chapter 6

6   Large Scale Integration – Case Analysis

The wind power impact on the power system quality and stability has been introduced and specific models have been presented. Here, three cases are investigated to illustrate interactions between wind power and power system in a large-scale integration. Figure 6.1 shows the cases studied here and the tools used to perform the analyses.
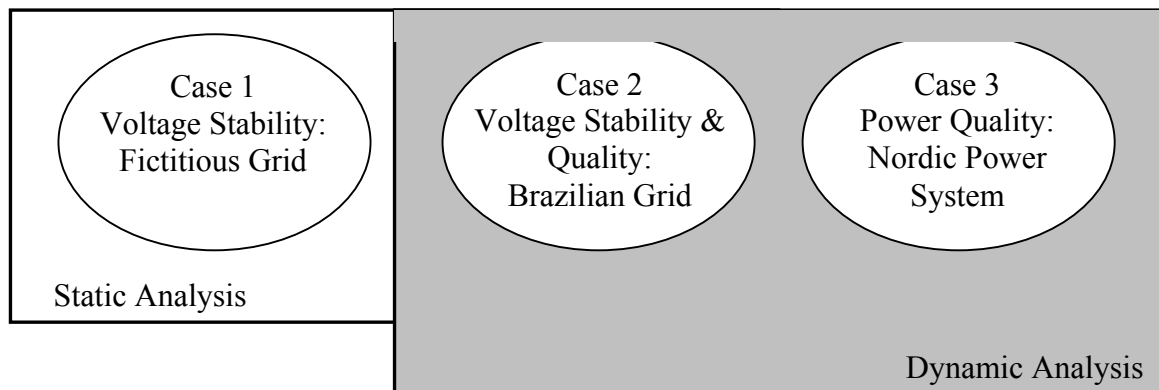
Figure 6.1 Case Studies.

6.1 Case Study 1: Voltage Stability in a Modern Power System

Large amount of wind energy can modify the voltage stability of a power system as introduced in the chapter 2. Here, the impacts of wind power to the voltage stability characteristics are illustrated.

A Load-flow program computes the loadability curves to the case analyse based on static models. The loadability curves are computed by increasing the load in specific buses of the power system (chapter 2). This way the power transfer capabilities is stressed until the voltage collapses.

6.1.1 Power System Characteristics

The power system studied is a small part of an existing power system. Figure 6.2 shows a single line diagram of the modelled power system where the rated voltage is 220kV. Figure 6.2 includes the total impedance of the lines and the loads installed on the network.

In Figure 6.2, the generators are installed on the buses 6 and 7. The bus 7 is the slack bus and bus 6 is a voltage-controlled bus (synchronous generator). Here, they have no restriction on reactive or active powers. The balance on bus 6 is an active power production of 110MW that explains why the loads are not expressed in the diagram. Bus 2 is supplying 20MVAr of reactive power to the network as indicated in the diagram and in addition, a capacitor bank with rated power of 50MVAr is installed on bus 3 to reduce the reactive power flux on the network.
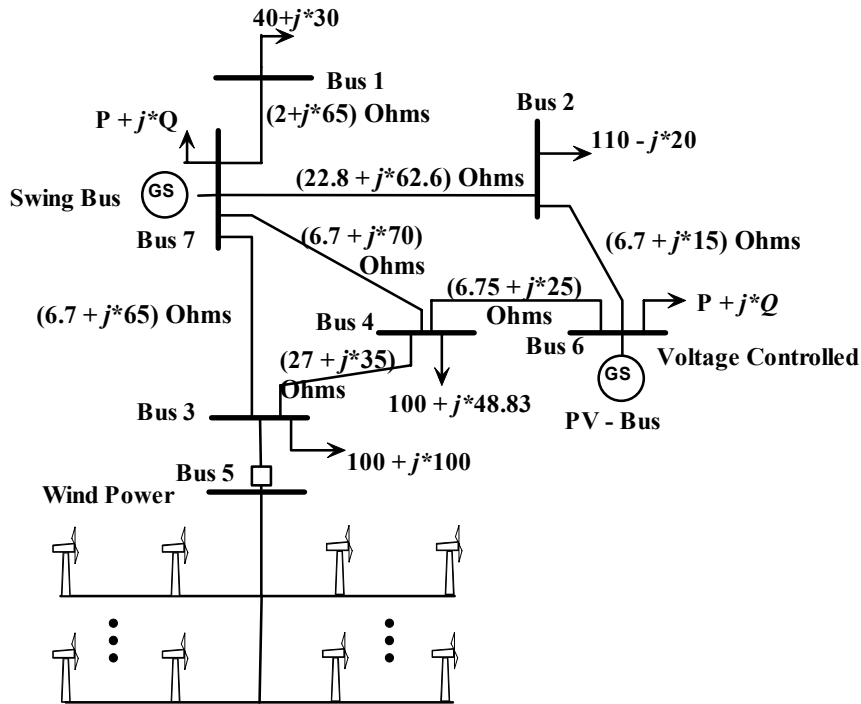
Figure 6.2 Diagram of the Power System used in analysis (loads in MW and MVAr).

Simulations show that bus 3 is the weakest node in the system due to long lines connecting to buses 7 and 4, in addition, bus 3 has a large reactive load installed that leads to a power factor of 0.7 largely compensated with shunt capacitor banks. Figure 6.3 shows the loadability curve to bus 3.
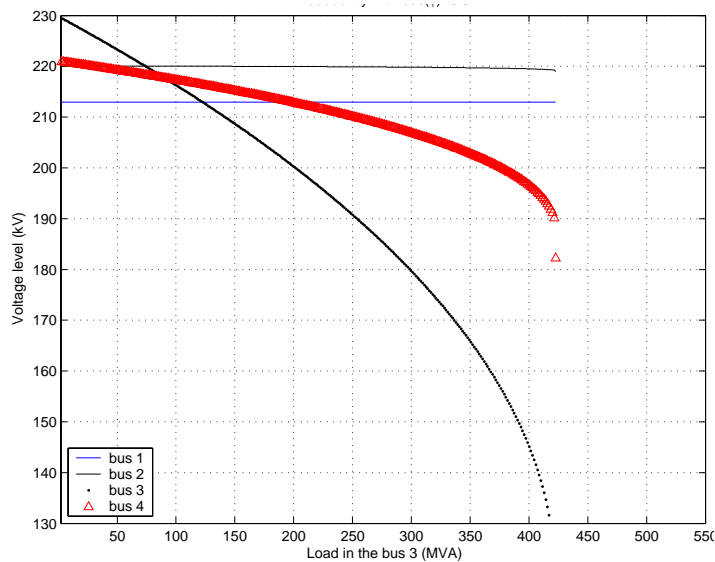
Figure 6.3 Loadability curve to bus 3 without wind turbines.

As expected, the lowest voltage is achieved on bus 3 because it has the highest load installed. The voltage on bus 2 is reduced due to high power flowing in the power system although it is located between two voltage-controlled buses. The voltage on bus 4 follows the behaviour on bus 3 because the power flow to bus 3 causes voltage drop in the network. Finally, the voltage on bus 1 remains constant because it is only connected to the bus 7 hence there is no change in the power flux in its transmission lines.

The voltage curves to bus 6 and 7 are not plotted because they are voltage fixed amplitude (synchronous generators without restrictions). The synchronous generator keeps the voltage constant on bus 6 by inserting or drawing reactive power. In this particular case, there is no reactive power limitation on the synchronous machine on bus 6 hence the voltage will always be constant. Bus 7 is the reference bus to the load flow calculations, which has constant voltage amplitude and the angle is the reference for the calculations on all other buses voltages. In addition, all active and reactive power balances are done on the reference bus, which has no restrictions. In reality, bus 1 would also suffer voltage variations once the voltage on bus (#7) starts to reduce because the power limits were reached on the synchronous generator on bus 7, similar behaviour will happen to bus 6.

In Figure 6.3, the active and reactive load to bus 3 were increased linearly, i.e. the active and reactive powers to bus 3 had fixed load factor, in this condition, the maximum load that can be installed is 424MVA, i.e. $300MW + j300MVAr$. The load flow problem is complex and the maximum active and reactive powers that can be delivered through the lines are different. Hence, the loadability procedure (load increase until the voltage collapses) is modified to two: in the first, the reactive power is kept constant then the active power increased linearly until the voltage collapses; in the second, the active power is kept constant then the reactive power increased linearly until the voltage collapses.

Using the new loadability procedure, the independent maximum loads to active and reactive powers are modified. In the first case, the maximum active power increased from 300MW to 540MW (the reactive power was kept constant 100MVAr). In the second case, the maximum reactive power increased from 300MVAr to 380MVAr (the active load was kept constant 100MW). The power system is weaker to transfer reactive power than active power, which is expected and related to the electrical characteristics of the transmission lines.

The maximum load that can be installed on bus 3 is basically limited to the network strength because there are no limitations on the synchronous generators and the loads are constant independent of the voltage. Inclusion of the reactive power limits on the synchronous generators is likely to reduce the maximum load supplied to bus 3 because when the synchronous machine reaches the maximum reactive power limit it loses the voltage control capability.

The loads dependency on the voltage is complex and constant power related to the voltage is a neutral assumption. An inverse dependency on the reactive, i.e. increase of power demanded as the voltage decrease, reduces the limit of maximum load that can be installed to bus 3, on the other hand, a direct power relation can increase the voltage stability limits because the loads (on the power system) reduce with the voltage reduction. In addition, the reactive power compensation with shunt capacitor banks is relevant to the voltage stability because of the high sensitivity to the voltage (i.e. reactive power proportional to V^2). In this power system, the loadability to bus 3 is influenced by shunt capacitors banks, which heavily compensate the reactive power (50MVAr). The voltage reduction leads to an increase in the flow of reactive power trough the lines that reduce further the voltage as introduced in chapter 2.

6.1.2 Wind Power Representation

In this section, a static model simulates the wind farm power production because the voltage stability problem is slow. The wind farm static model must simulate the reactive power demanded based on the active power and the voltage at the wind turbine bus.

In this thesis, the active (P) and the reactive (Q) powers are specified to the load flow program (that computes the loadability curves). The P component is the rated power of the wind farm to be installed on a specific site and Q is computed based on the voltage terminals with a polynomial function. Because the wind turbines have no active control on the voltage, this is a reasonable assumption that is very similar to the procedure suggested in [28].

The polynomial function used here was fitted based on three different sizes of induction machines as presented in Figure 6.4. Assuming the rated active power, the reactive power consumption depends on the voltage (as introduced in chapter 4). An increase in the voltage leads to an increase in the reactive power because the induction machine excitation (i.e. the reactive power consumption) is related to V^2 on the other hand the voltage decrease leads to an increase in the reactive losses that is related to V^{-2} increasing the total reactive power consumption.
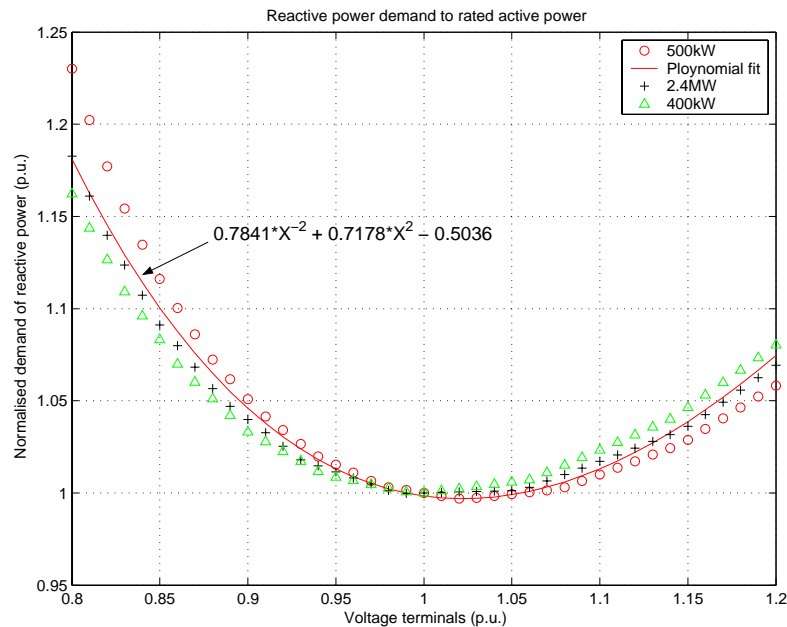
Figure 6.4 Loadability curve to bus 3 without wind turbines.

In Figure 6.4, the polynomial function to the reactive power for induction machines does not include the no-load capacitor bank installed at the wind turbines and the normalisation factor is the nominal reactive power at rated voltage. The reactive power compensation of the entire wind farm is modelled as shunt capacitor banks in the load flow program.

6.1.3 Wind Power Impacts on Voltage Stability

In order to investigate the wind power impacts on the voltage stability, bus 5 is connected to the power system. All the wind power in the power system is concentrated on

it. Bus 5 is connected to the weakest part of the network (bus 3) through a short radial line (Figure 6.2). Connecting large wind power to the weakest bus is expected to be the worst-case scenario to the voltage stability because this bus already faces limited power transfer capabilities. Figure 6.5 shows the behaviour of the voltage of the entire power system as a function of the wind power injected in bus 5.
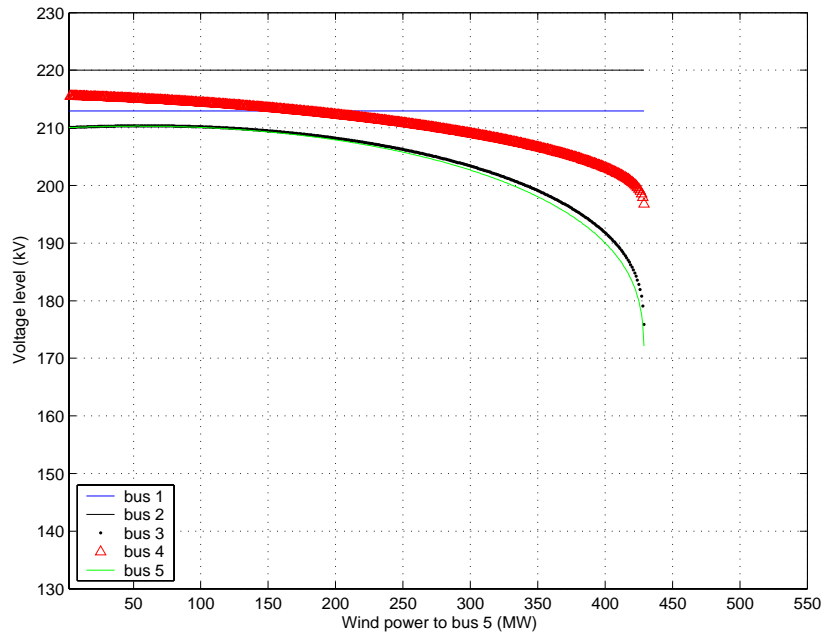
Figure 6.5 Maximum wind power integration concerning voltage stability.

Figure 6.5 is computed in a similar way to the loadability curve. The installed wind power in bus 5 is increased until the voltage collapses. The maximum wind power that can be installed before voltage collapses is 429MW being smaller than the maximum load that can be installed to bus 3 (537MW). The reactive power demanded by the wind power explains the small limit to wind power integration.

In order to investigate the wind power impacts on the voltage stability, a 100 MW wind farm is installed to bus 5 and new loadability curves to bus 3 are computed. This size of wind power represents 28% of power penetration in the power system.

Table 6.1 and Table 6.2 present the wind power impacts on the loadability curves concerning voltage stability. Table 6.1 presents the loadability limits increasing only the active load in bus 3. Two conditions are presented: in the first, the wind turbine reactive power is constant (i.e. the reactive power polynomial function is not used); in the second, the reactive power of the wind farm is represented with the polynomial function of the voltage.

Table 6.1 Bus 3 loadability limits keeping the reactive power constant.

Condition	P (MW)	P (MW)	Q (MVAr)
Without wind power	537	537	100
With wind power constant	580	---	100
With wind power reactive power polynomial representation	---	534	100
Difference	+43	−3	0

The row presenting the difference in Table 6.1 shows the impact of the wind power on the voltage stability. The wind power modifies the limits of voltage stability. At first sight, the wind power local production shall improve the loadability on bus 3 as the fist column presents an increase of 43MW. However, when the voltage dependency of reactive power demanded by the wind power is included, the loadability to bus 3 is reduced. Those results show that the reactive power from wind farms play an important role in the voltage stability.

Table 6.2 shows the loadability limits with the active load in bus 3 kept constant.

Table 6.2 Bus 3 loadability limits keeping the active power constant.

Condition	Q (MVAr)	Q (MVAr)	P (MW)
Without wind power	385	385	100
With wind power constant	350	---	100
With wind power reactive power polynomial representation	----	335	100
Difference	−35	−50	0

In this condition, the voltage stability limit is reduced because the reactive power to the wind farms flows through the same transmission lines that supply bus 3. Similar to the first case, the dependency on voltage of the reactive power from the wind farm strongly influences the voltage stability. Considering constant power the wind power reduces in 9% the loadability to bus 3 and including the voltage dependency, the reduction is 13%.

The demand of reactive power is the key factor on voltage stability from wind farms, hence wind turbines with power electronics, which can actively control the reactive power, can be used to regulate the voltage and improve the voltage stability. Following, Figure 6.8 illustrates the integration limits of wind power to bus 3 (concerning voltage stability) of wind turbines with power converters that can keep power factor unity independent of the voltage.
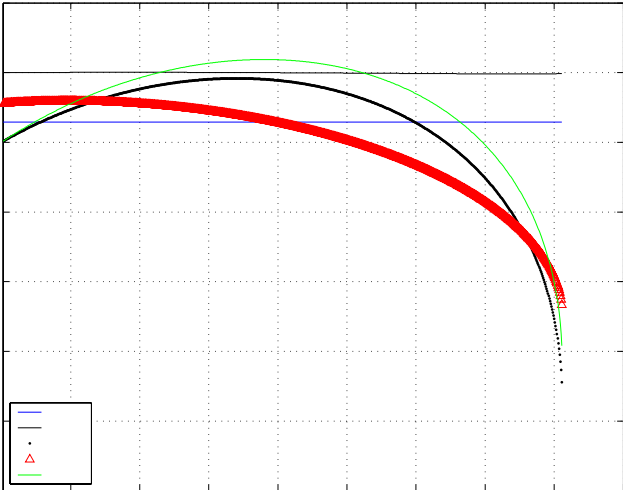
Figure 6.6 Maximum wind power integration concerning voltage stability (load factor unity).

In this case, the absence of reactive power flux to the wind farm improves the voltage stability. The voltage on bus 5 is higher than on bus 3 because it is injecting power, in this case the voltage tends to increase at first moment but as the power flux increases, the

associate losses increases leading to voltage reduction and finally to the voltage collapse. In this new condition, the maximum wind power to the power system is 811MW, which is much higher than the original case 429MW.

Another important feature using power electronics, as cited before, is that they can be used to regulate the voltage by injecting or draining reactive power. However, the maximum apparent power of the power converter must be respected. Figure 6.6 illustrates the loadability curve to the power system with 100MW wind farm installed in bus 5 using power electronics that can control the voltage (in this illustration, the voltage was set to 2% above the nominal).
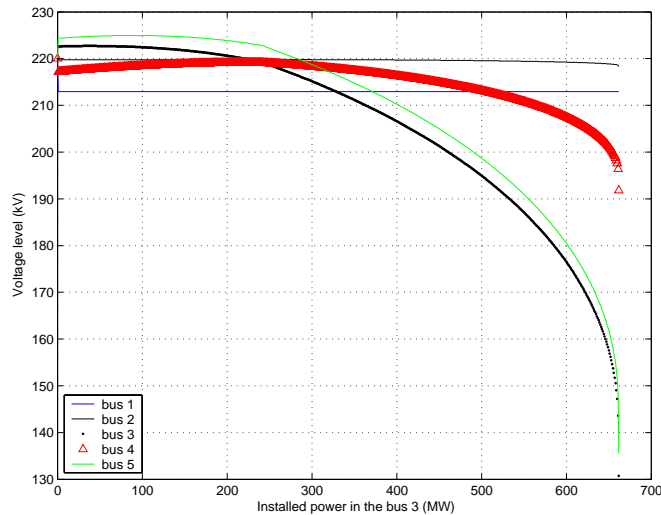
Figure 6.7. Loadability curve to bus 3 with wind turbines using power electronics.

As the maximum power from the power electronics must be respected, the wind farm is limited to 100MVA. The active power of the wind farm is 100MW that is reduced as the reactive power is injected in the power system. The power converter is limited to operate at minimum capacitive power factor of 0.8. When the wind farm reaches the maximum reactive power production, the wind turbines lose the voltage control capability hence they behave as fixed power production. Figure 6.8 illustrates the power production of the wind farm with the loadability of bus 3 as well as the power factor of the wind farm.
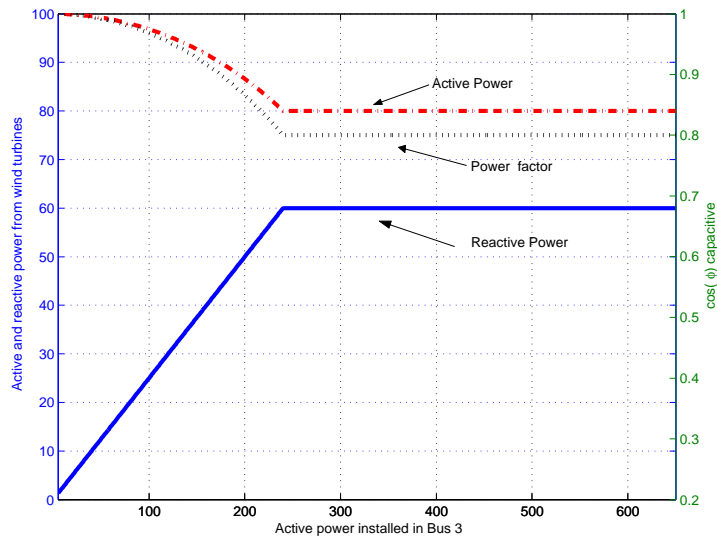
Figure 6.8 Evolution of the power production from the wind turbines (with electronic power converter).

The active power produced from the wind farm is reduced to respect the thermal limits of the power electronics. In particular example, the controllers were not implemented and the reactive power from the wind farm was increased linearly until it reaches the maximum of 60MVAr (corresponding to a power factor of 0.8 capacitive) and the active power is reduced to 80MW in order to respect the 100MVA limit.

6.2 Case Study 2: Voltage Stability and Quality in a Brazilian Power System

Large amount of wind power has been proposed to Brazil. The Brazilian power system is mainly composed by hydropower stations. However, in some regions, it is not possible to install more hydropower stations. In addition, during the last few years, a long dry season leaded the entire power system to a critical minimum water level on the reservoirs resulting in an national energy crisis [72].

The Brazilian government has introduced new regulations to diversify the power matrix. The wind power is one of them, which is expected to contribute to the energy in a large extend in years to come. The Northeast coast of Brazil presents good wind conditions and complementary wind characteristics to the main river flow along the year [73]. Therefore, to this region alone, more than 2000MW of wind power have been proposed. This section presents some investigations of the wind power integration to a part of the Northeast region.

6.2.1 Power System Characteristics

The interconnected Brazilian electrical power system is divided in four regional systems: North (N); Northeast (NE); Southeast (SE) and South (S). There are connections between all four regional systems. The connections between the NE system and the N are strong with a transfer capacity of few thousand Megawatts, however to the other regions there is a single link in 500kV with limited power transfer. Figure 6.9 illustrates the Brazilian interconnected system.
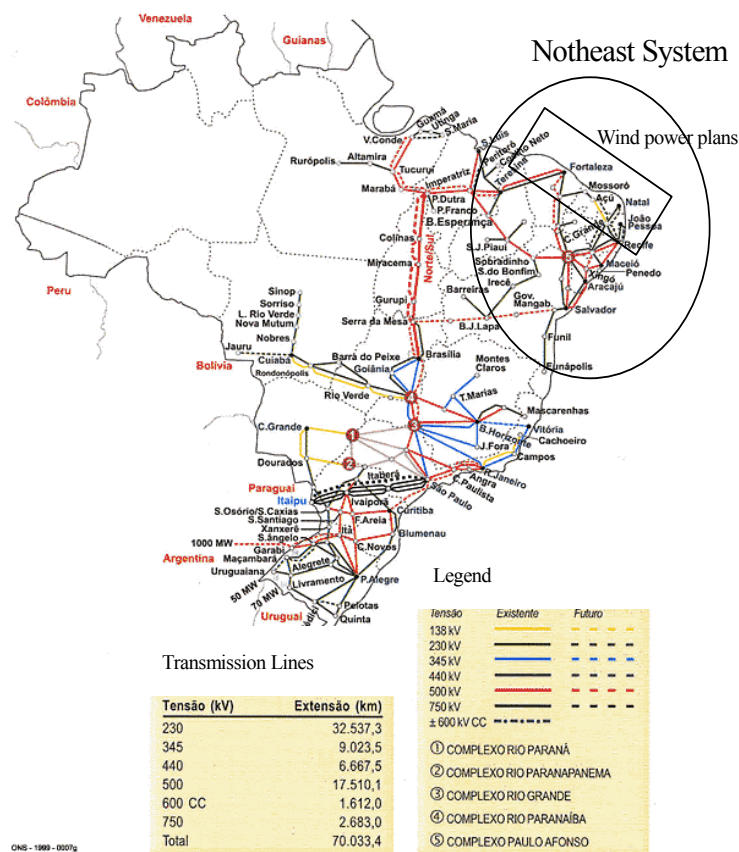
Figure 6.9 Brazilian interconnected system power system [72]

In Figure 6.9, the NE system is circled. The regional NE power system has approximately 10270MW of hydropower stations installed and 435MW of diesel power stations. The hydropower stations are concentrated in the middle of the region (marked as number 5 in Figure 6.9) far from the load consumption centres. All transmission lines in the region are AC lines with voltage levels from 500kV to long distances down to 138kV to short distances.

More than 2000 MW of wind power has been planned to the region [73]. The plans account to install large amount of wind turbines in the coast area from Natal to Fortaleza (North-Northeast coast marked in Figure 6.9).

The installation of 100MW to a part of the system is investigated with respect to the voltage stability and voltage quality during continuous operation. The 100MW is divided in 5 wind farms where all of them are installed to MOSSORO bus. Figure 6.10 presents a schematic representation of the network to which the wind farms are installed.
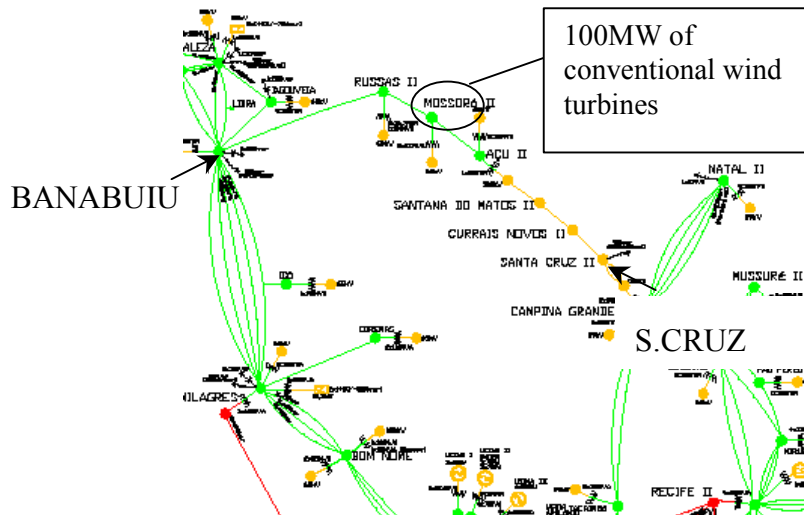
Figure 6.10 Brazilian network studied [72].

The case studied focus on the region between BANABUIU and S.CRUZ (Figure 6.10). In Figure 6.10, the rated voltage between BANABUIU and ACUII is 230kV and between ACUII and S.CRUZ is 138kV. The installation of the wind farm is planned to near future when reinforcement of the power system is planned. The simulations take into account the future power system condition [74]. In the future condition, between BANABUIU and MOSSORO will have a 230kV line and from ACUII to S.CRUZ will have an additional line in 230kV, where the link in 138kV will be open.

The load characteristics of the local network are presented in Table 6.3, which presents the load to relevant nodes in the study case to high and light conditions. BANABUIU and S.CRUZ are modelled as infinite nodes and all other buses are modelled as constant load, i.e. voltage independent.

Table 6.3 Relevant loads in the Brazilian power system studied.

Node	Heavy Load	Light Load
MOSSORO	93.66MW+j·20.72MVAr	58.73MW+j·12.99MVAr
RUSSAS	52.80MW+j·13.70MVAr	42.40MW+j·3.30MVAr
ACU	52.88MW+j·3.81MVAr	45.82MW+j·3.31MVAr

6.2.2 Wind Power Representation

The total wind power has 100MW of conventional wind turbines, i.e. directly connected to the network, that uses induction machines and partial reactive power compensation with shunt capacitor banks. The total wind power is divided in 5 wind farms with 30 identical wind turbines, all of them installed to MOSSORO bus on high voltage level (230kV).

The voltage stability analyses are similar to section 6.1 Case Study 1: Voltage Stability in a Modern Power System, where fixed active power and voltage dependent reactive power model the wind power. The reactive power dependency on the voltage is modelled with a polynomial function of voltage.

Here, the dynamic voltage quality is also assessed through the Aggregate Wind Farm (AWF) model (presented in chapter 5), which simulates the power produced from the entire wind farm. The aggregate wind farm represents identical 150 wind turbines (in five wind farms with 30 wind turbines each) of 680kW. Actually, the 680 kW wind turbine does not

exist, hence the wind turbine used in this section has the same normalised data from a similar wind turbine presented in chapter 5 (660kW).

The 100MW wind power is divided in 5 wind farms with identical layout and identical 30 wind turbines each. There is no wind correlation between the five wind farms and the aggregate wind speed model generates one time series to each wind farm.

Figure 6.11 presents the layout of each wind farm. The distance between wind turbines is 4 times the rotor diameter (i.e. 4x48m = 192m). With this wind speed direction, this is assumed the worst-case scenario because a large number of wind turbines are aligned in a row with the wind speed. The distance between the wind turbines is small that is acceptable because the wake effect is not simulated in the AWF.
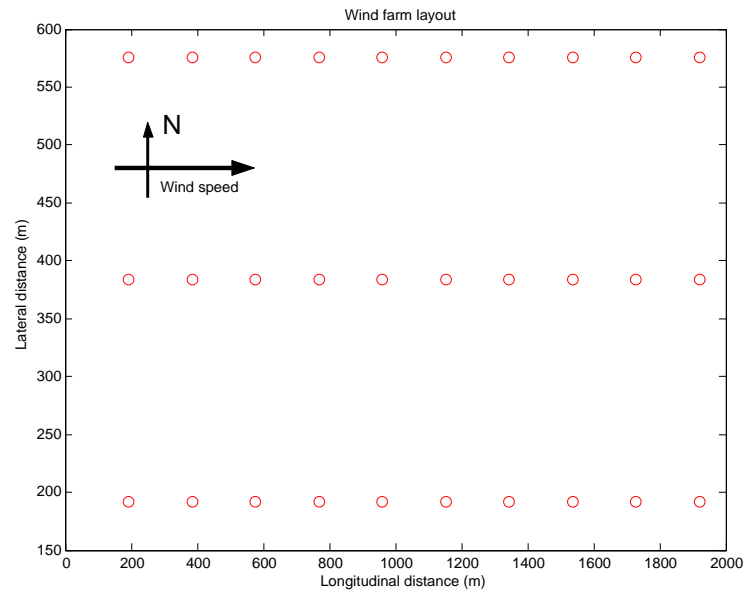
Figure 6.11 Layout of a single wind farm applied to the Brazilian power system studied.

6.2.3 Wind Power Impacts on the Voltage Stability

The loadability curves characterize the voltage stability in the study cases similar to the previous section. The power system in Figure 6.10 is implemented in the loadability computation tool (chapter 2) as presented in Figure 6.12.

In Figure 6.12, the arrows represent loads installed to the buses. The line between ACUII and S.CRUZ is modelled as 230KV according to the reinforcement plans. Similarly, the ring connection between BANABUIU and MOSSORO that is not present in Figure 6.10, here is included according to the reinforcement plans.
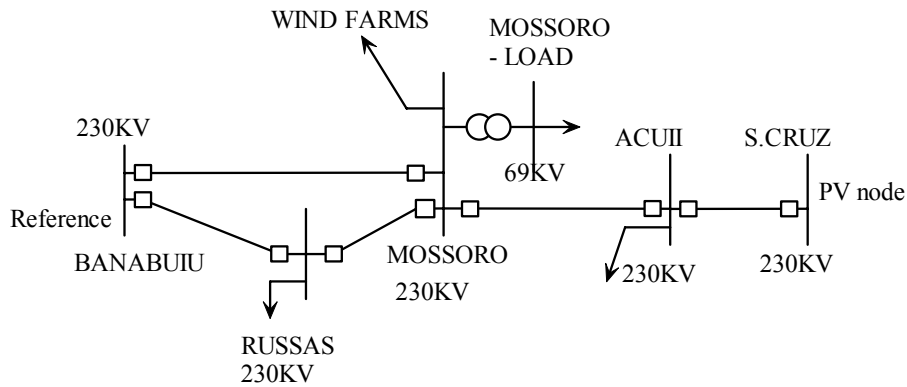
Figure 6.12 Network topology of Brazilian power system studied.

In order to characterize the original installation, loadability limits are computed to the MOSSORO bus. The loadability limits uses the same procedure presented in the previous section, which is to increase the active and reactive load individually until the voltage collapses. Table 6.4 presents the loadability limits to MOSSORO to different load conditions.

Table 6.4 Loadability limits to MOSSORO.

Load Conditions	Maximum Active load (MW)	Maximum Reactive load (MVAr)
Heavy Load	888	534
Light Load	733	460

The classification of the loadability limits to MOSSORO presented in Table 6.4 represents the maximum active and reactive loads that can be installed to MOSSORO before the voltage collapses independent of each other, as explained in the previous section.

The active load that can be installed to MOSSORO is higher than the reactive because of the electrical characteristics of the transmission lines in the local power system. In addition, the differences between heavy load and light load conditions happen because under heavy load, several shunt capacitors were switched on to compensate the reactive power, while under light load condition some shunt reactors were switched on to limit the voltage increase. However, the differences in terms of reactive power limits are smaller because the reactive power produced by the shunt capacitors is very sensitive to voltage variation.

The highest value (888MW, 364MVAr) characterizes the loadability limit to MOSSORO because with the load evolution all capacitors available in the power systems must be switched on to prevent high reactive power flow on the network.

Before analysing the impacts of wind power on the voltage stability, the limits to integration of wind power are drawn concerning the voltage stability. To this power system, the maximum wind power that can be installed to MOSSORO (respecting the voltage stability) are 780MW in heavy load and 727MW in light load. In both cases, the maximum wind power to the bus is small than the maximum load that can be installed because the wind turbines demand reactive power as explained in the previous section.

The difference between the heavy and light load conditions are related to the shunt capacitors installed in the system under heavy load condition similar to the loadability limits presented in Table 6.4.

Figure 6.13 presents the evolution of the voltage in the relevant buses along the wind power installed to MOSSORO (230kV) in light load condition.
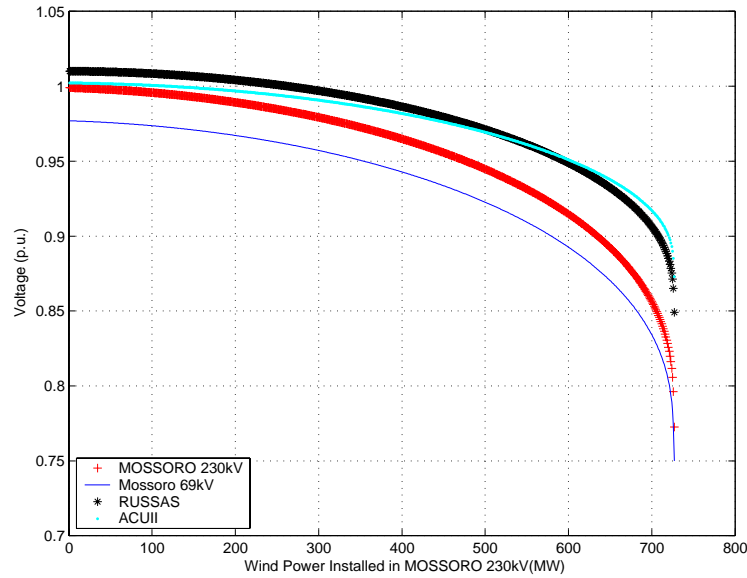
Figure 6.13 Maximum wind power to MOSSORO bus (light load condition).

The voltage on the power system reduces with the wind power inserted in MOSSORO. The closest buses present the high voltage variation while ACUII follow the general behaviour but with less severity. The MOSSORRO 69kV is included in Figure 6.13 just to present the voltage on the main load connected to the MOSSORO bus.

In order to assess the impacts of 100MW on the voltage stability, the wind power is installed to MOSSORO and new loadability curves are computed. Table 6.5 presents the loadability limits computed to different load conditions.

Table 6.5 Loadability limits to MOSSORO with wind power.

Conditions	Load condition	Maximum Active load (MW)	Maximum Reactive load (MVAr)
No wind power	Heavy Load	888	534
With wind power	Heavy Load	905	432 (+110MVAr to the wind farm)
No wind power	Light Load	733	460
With wind power	Light Load	758	380 (+114MVAr to the wind farm)

In Table 6.5, the loadability limits to MOSSORO in high and low load conditions are compared to cases with and without wind power installed (at rated power). In this power system, the wind power improves the voltage stability concerning the active. However, as expected, the net loadability limit concerning reactive power is reduced as the wind farms demand reactive power, but the total reactive power flowing to MOSSORO is slightly increased (7.4% in the light load and 1.5% in heavy load) because the wind farms have shunt capacitors that help to improve the voltage stability.

6.2.4 Wind Power Impact on the Voltage Quality

The impacts of 100MW wind farm on the voltage quality are analysed by means of dynamic simulations using the AWF presented in chapter 5. The AWF is applied to a

conventional fixed speed wind turbine connected to the transmission level at 230kV with dedicated lines and transformers.

The voltage is analysed under different wind speeds with two load conditions: heavy load and light load. The wind speeds are simulated (using the aggregate wind farm wind speed simulator from chapter 5) to 8, 10, 12 and 14 m/s all of them with 20% turbulence intensity. Those wind speeds represent the wind speed range with the most relevant power variations from wind turbines. Above 14 m/s the power conversion of the wind turbine limits the active power and the wind speed variations lead to relative small power variations and below 8 m/s the level of power is small and the power variations are also reduced.

Figure 6.14 shows the 10 minutes average values of the active power produced by the wind farms and its influences on the average voltages on MOSSORO under heavy and light load conditions. Figure 6.14 also includes the maximum and minimum values to each load condition as envelop curves.
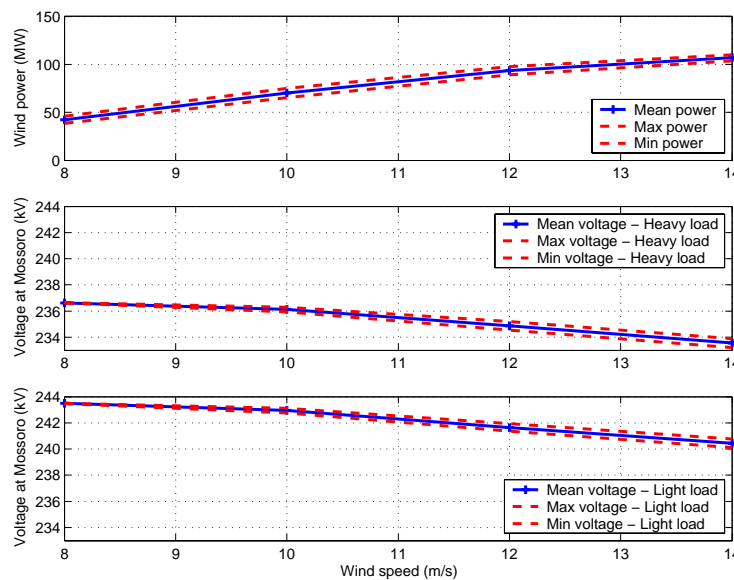
Figure 6.14 Wind power influences on the voltage to different wind speeds.

The power production by the wind power increases with the wind speed and the voltages on both load conditions reduce with the increased wind speed. As the mean wind speed increases, the wind power produced and the reactive power demands increase that causes voltage drops due to losses in the network. The main voltage differences between the heavy and light load are caused because of the reactive power compensation schemes to each load condition (i.e. large shunt capacitors installed under heavy load condition).

In Figure 6.14, the aggregation of 150 wind turbines leaded to a very smooth wind power production where the maximum and minimum powers are very close to the average. As an illustration, in the average wind speed of 10m/s, the difference between the maximum and minimum active powers is approximately 10MW while the mean power produced is approximately 70MW (next section presents the time series).

Another relevant characteristic, presented as follow, is the standard deviation of the power and voltage to different wind speeds as presented in Figure 6.15, where the reactive power is also plotted.
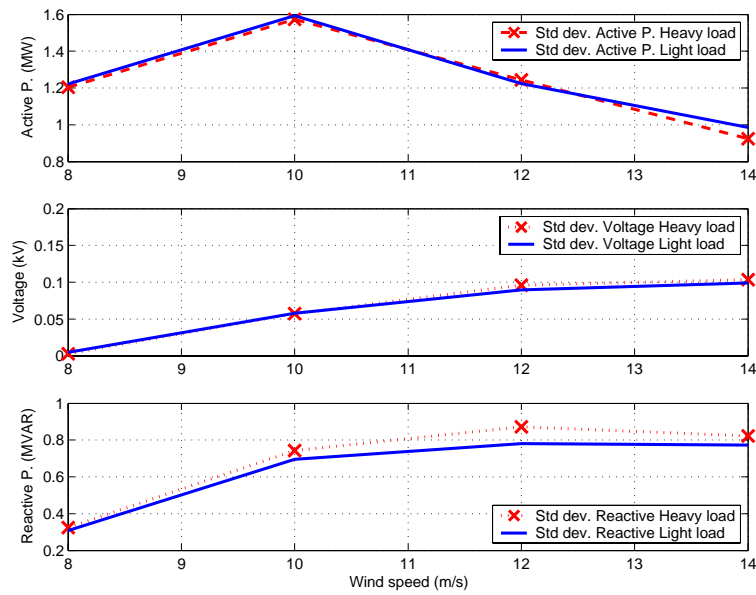
Figure 6.15 General wind power influences on MOSSORO bus.

The standard deviation (STD) gives an idea of the processes' fluctuations, from Figure 6.15, the SDT of the active power produced from the wind farm has a maximum on the mean wind speed of 10 m/s then reduces because of the non-linear characteristic of the power curve. The voltage and the reactive power are strongly related. Both STD of voltage and reactive power increases with the wind speed because on high wind speeds the high active power reduces the voltage that consequently reduces the reactive power produced by shunt capacitors leading to higher reactive power fluxes.

The main differences between the heavy and light load conditions are on high wind speeds where the voltage reduction influences the reactive power produced by the capacitors banks installed in the power system. Hence, the heavy load condition, which has more capacitors installed, presents the higher standard deviation of voltage and reactive power.

The curves above support that probabilistic load flow studies should be used for analysis in the future in order to assess the impact of the wind turbines in the whole operating range.

Following, the wind farm influences on the voltage quality to the wind speed of 10m/s are detailed to each load condition.

6.2.4.1 Light Load Condition

Figure 6.16 presents the time series of the wind power produced and the voltage on bus MOSSORO 230kV at mean wind speed 10 m/s and turbulence intensity of 20% in light load condition.
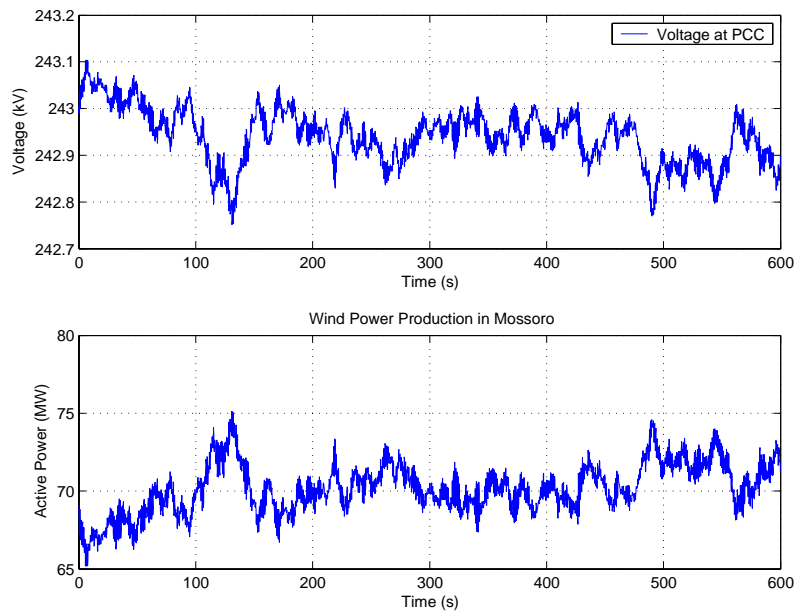
Figure 6.16. Voltage at MOSSORO and power flux from the wind farm in light load condition (mean wind speed 10m/s).

Most of the time, the voltage variations are within 0.3kV (0.125% of the mean voltage 240kV). The deepest voltage levels occur on the highest active power production because the total power flow in the network cause voltage drops as introduced in chapter 2. The voltage is 5.6% above the nominal value (230kV) because the system is designed to operate a little above the nominal in order to compensate the voltage drops in lower voltage levels. Following, Figure 6.17 presents the wind speed, active and reactive powers and voltage statistics in terms of histograms in light load condition.
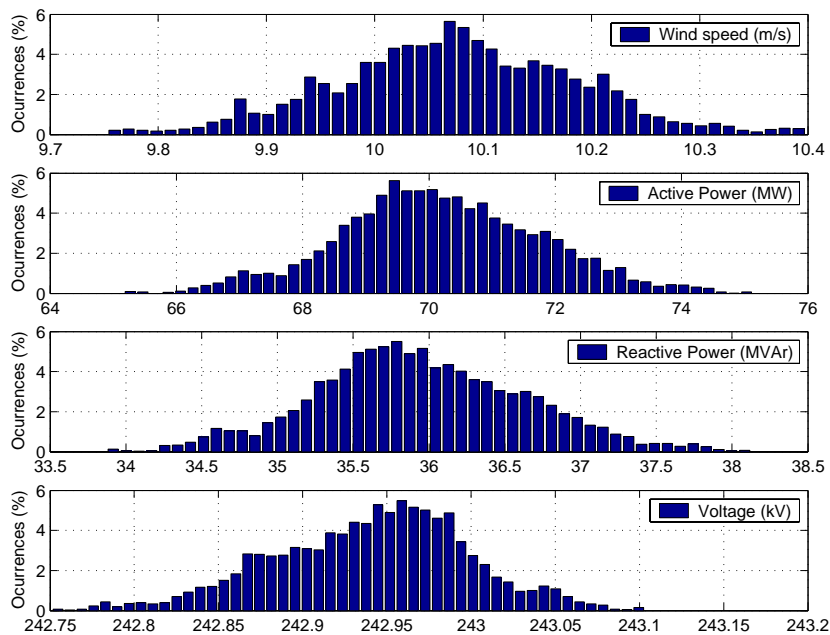
Figure 6.17 Statistics wind speed, active power, reactive power and voltage variations at MOSSORO (light load).

The voltage and reactive power variations are related to the active power production from the wind farm that depends on the aggregate wind speed. The reactive power demanded from the wind farm depends on the active power and on the voltage on MOSSORO. Higher wind speed leads to higher active power production that leads to higher reactive power demand that leads to lower voltages. The relation between the different parameters is not linear and it becomes more complex from the upper to the lower part of Figure 6.17, which explain the different statistical distribution of the voltage.

6.2.4.2 Heavy Load Condition

Following, Figure 6.18 presents the time series of the wind power produced and the voltage on bus MOSSORO 230kV at mean wind speed 10 m/s and turbulence intensity of 20% in heavy load condition.
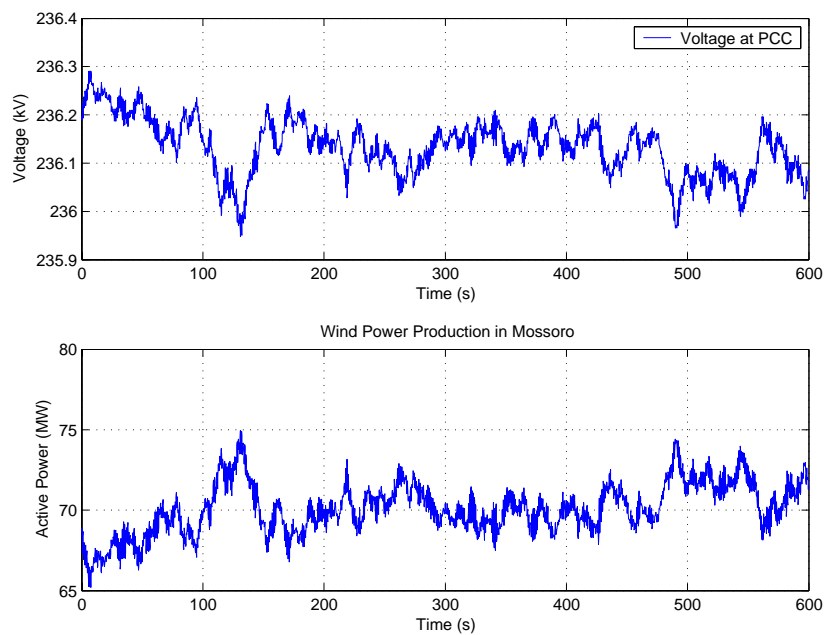
Figure 6.18 Voltage at MOSSORO and power flux from the wind farm in heavy load condition (mean wind speed 10m/s).

The time series to heavy load condition are very similar to the ones with light load condition. However, the mean value of voltage is different and the non-linear relation of the voltage and reactive power leads to a different statistical distribution of the voltage and reactive power as presented in Figure 6.17.
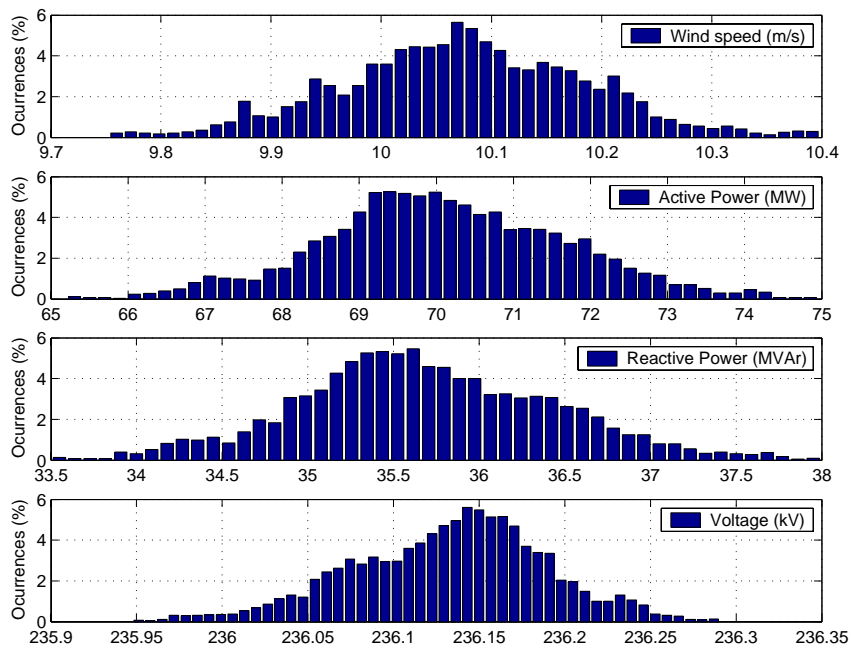
Figure 6.19 Statistics wind speed, active power, reactive power and voltage variations on MOSSORO (Heavy load).

The wind speed is exactly the same as the one applied to the light load condition, similarly the active power produced in heavy load condition is very similar to the light load condition. However due to the lower mean voltage, the distributions of the reactive power and voltage at this time are different. The voltage is more concentrated to the mean value and the reactive power more spread. Those differences can be related to the non-linear relation between the active power, reactive power and the voltage that in this case, in addition, the lower voltage level increases the losses.

The dynamic voltage variations in this power system are very small. This is related to two main conditions, first, the wind power is connected to transmission lines (high voltage), which are relatively strong and have lower losses that reduce the voltage drop. A second explanation resides on the power smoothing effects from the spatial distribution of the wind turbines. The low correlation between different wind speeds (acting on each wind turbine) smoothes the power produced by the wind farm that reduces the power flow variation hence lower voltage variation.

6.3 Case Study 3: Power System Interactions – NORDEL

The Nordic countries are expected to face large wind energy integration in the years to come. This section illustrates the impacts of large-scale integration of wind power to the frequency and voltage regulation of large power systems.

The Nordic power system has generators spread over large distances including Denmark, Finland, Iceland, Norway, and Sweden. This power system includes hydro, thermo (oil, coal fired and even geothermal) and nuclear power stations supplying in parallel electricity to more than 20 million inhabitants.

6.3.1 Power System Description

Finland, Sweden, Norway, and a part of the Denmark are synchronized in the Nordel system. The Nordel, hereby defined, permits power exchange between the Nordic countries (Denmark, Finland, Iceland, Norway and Sweden), whose primary aims are optimise and efficient electricity market.

Here, the objectives are the dynamic power quality and voltage assessment of the synchronized interconnected Nordel power system. Figure 6.20 illustrates the Nordic Power System [75].

Figure 6.20 High voltage Nordic power network [75].

The synchronous Nordel power system includes the eastern part of Denmark (Zealand), Finland, Norway, and Sweden. The western part of Denmark is not synchronized to the Nordel but to the European System. There are no interconnections between Iceland and the rest of the Nordel power system. There are HVDC links between the synchronized Nordel and Germany, Poland and the western part of Denmark.

In the synchronized Nordel, the frequency and voltage are regulated in order to remain within certain limits. The frequency regulation includes stability requirements and power exchange agreements. The frequency in normal conditions on the 400kV network must be within 49.9 and 50.1Hz [76]. Under exceptional conditions, the frequency can vary within 47.5 and 52Hz, however those conditions are related to transient and island problems. The voltage regulation in the Nordel includes optimised reactive power flux as well as stability requirements. In addition, the voltages in the Nordel during continuous operations can be within 90 and 105% of the nominal values [77].

The harmonious operation of the Nordic power system means that all machines contribute to the voltage and frequency control avoiding power oscillations and voltage deviations. The control characteristics are mainly based on agreements in power exchange and stability requirements. The size and characteristics of the Nordic power system makes it an interesting study case. In the Nordel, the primary frequency control automatically

keeps the balance of consumption and production and the secondary frequency control manually regulates the power production agreements in certain areas of the power system. The secondary frequency control is not studied here.

The combined primary frequency control, in order to keep the system frequency constant, shall react to the frequency variations with 6000MW/Hz. Table 6.6 presents the requirements of frequency regulation to Nordel.

Table 6.6. Requirements on frequency response in the Nordel power system.

Country	Frequency Response (MW/Hz)
Denmark	270
Finland	1050
Norway	2220
Sweden	2460
Nordel	6000

To maintain contractual voltage quality and avoid voltage collapse, the Nordel power system must be capable of keeping the voltage within permissible range. The voltage controllers are specified to keep the voltage within permissible level and to provide reactive power reserve to ensure reliable operation.

6.3.1.1 Reduced Nordel Model

In the following analysis, a reduced network simulates the dynamic electrical characteristics of the synchronized Nordel power system. The reduced Nordel power system model is explained in [38]. The reduced network represents the synchronized Nordel with 34 aggregate nodes. The aggregate nodes represent the loads and the generation units with the frequency and voltage controllers included. The power system representation is done as follow:

- Finnish system: 2 nodes in 400kV;

- Swedish system: 08 nodes in 400kV and 2 nodes in 300kV;

- Norwegian system: 11 nodes in 400kV and 11 nodes in 300kV;

- Danish system is included in the model as constant loads installed to the neighbours systems (these loads can be negative or positive).

The reduced model takes into account the electromechanical dynamic representation using aggregate models to the synchronous generators. The reduced model has 21 equivalent synchronous generators and includes equivalents controllers to the frequency and voltage. The HVDC links are modelled as constant PQ loads to the proper buses. Figure 6.21 presents the network topology of the reduced Nordel system.
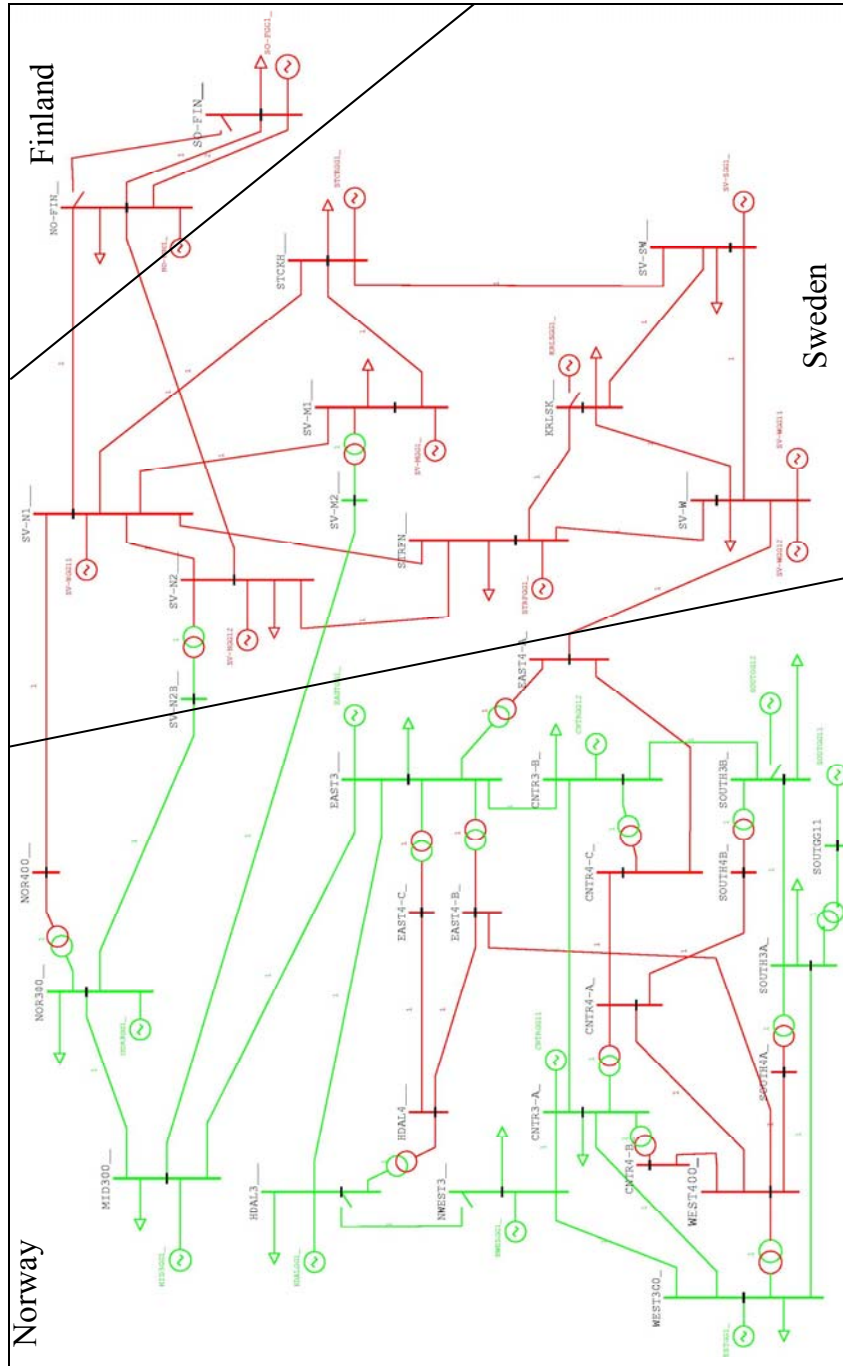
Figure 6.21 Reduced model to the Nordic power system [38].

In Figure 6.21, the network in red represents the 400kV grid and the network in green represents the 300kV grid. The aggregate synchronous generators and loads are also plotted in Figure 6.21. Table 6.7 presents the synchronous machines and the aggregate wind farms (AWF) connecting nodes.

Table 6.7 Nordel reduced machines connection nodes.

Machine #	Generators Name	Bus Name	AWF
1	Finland SO-FGG1_	SO-FIN	Yes
2	Finland NO-FGG1_	NO-FIN	Yes
3	Sweden: STCKGG1_	STCKH	Yes
4	Sweden: SV-SGG1_	SV-SW	Yes
5	Sweden: SV-WGG12	SV-W[2]	Yes[2]
6	Sweden: STRFGG1_	STRFN	No
7	Sweden: SV-NGG11	SV-N1	No
8	Sweden: SV-MGG1_	SV-M1	No
9	Sweden: SV-NGG12	SV-N2	No
10	Sweden: SV-WGG11	SV-W[2]	Yes[2]
--	No sync. Machine installed	KRLSK	Yes
11	Norway: EASTGG1_	EAST3	No
12	Norway: HDALGG1_	HDAL3	No
13	Norway: CNTRGG11	CNTR3-A	No
14	Norway: CNTRGG12	CNTR3-B	No
15	Norway: SOUTGG11	SOUTGG11	No
16	Norway: WESTGG1_	WEST300	No
17	Norway: NWESGG1_	NWEST3	No
18	Norway: MID3GG1_	MID300	Yes
19	Norway: NOR3GG1_	NOR300	Yes

6.3.1.2   Nordel Characteristics

Before connecting the large wind farms, the Nordel power system is characterized with modal analysis to indicate the main oscillation modes, the phase angle of the modes and the machines participating on those modes.

Using the dynamic simulation tool (SIMPOW), the relevant eigen-frenquencies to the Nordel are expressed in Figure 6.22 (without wind power installed).

In Figure 6.22, the x-axis presents the real part of the eigenvalue: smaller absolute values in the negative plane means close to instability. The y-axis presents the damped frequency (in Hz) of the mode (imaginary part of the eigenvalue). All eigenvalues are in the stable region of the plane.

---

[2] There is only one AWF installed to SV-W.
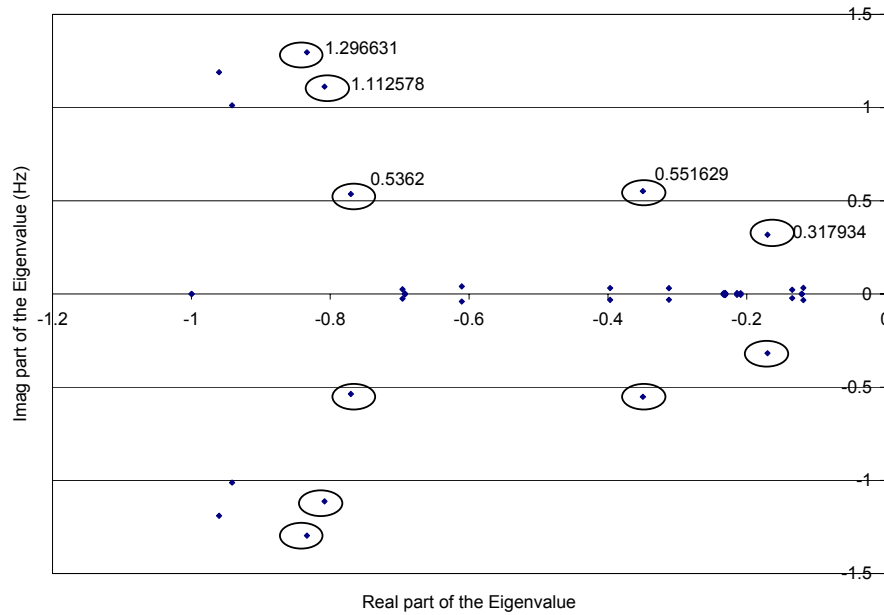
Figure 6.22 Relevant eigenvalues of the reduced model to the Nordel.

Considering that wind turbines produce relevant power variation up to few hertz, five modes (see marked modes in Figure 6.22) are characterized using modal analysis. The relevant characteristics of the selected modes are:

1. 0.318Hz – oscillation of the South Finnish system against to the entire power system;

2. 0.552Hz – general oscillation in the entire power system, see Figure 6.23.

3. 0.536Hz – oscillation of Stockholm node against the entire power system;

4. 1.113Hz – oscillation of the North Sweden against the power system;

5. 1.297Hz – oscillation of the East part of the system (Norway) system against West part of Sweden

Figure 6.23 presents the inter-area phase and amplitudes of participation from the synchronous machines in the second electromechanical mode selected (0.552Hz). In Figure 6.23, the vectors near to the generators represent the participation of the machines in the electromechanical mode. The modulus of the vector indicates the magnitude of the participation, i.e. to how extent this machine is involved in the electromechanical mode. The phase angle of the vectors indicates the tendency of rotor angle deviation of each machine, i.e. the power exchange between different machines (power system oscillation).
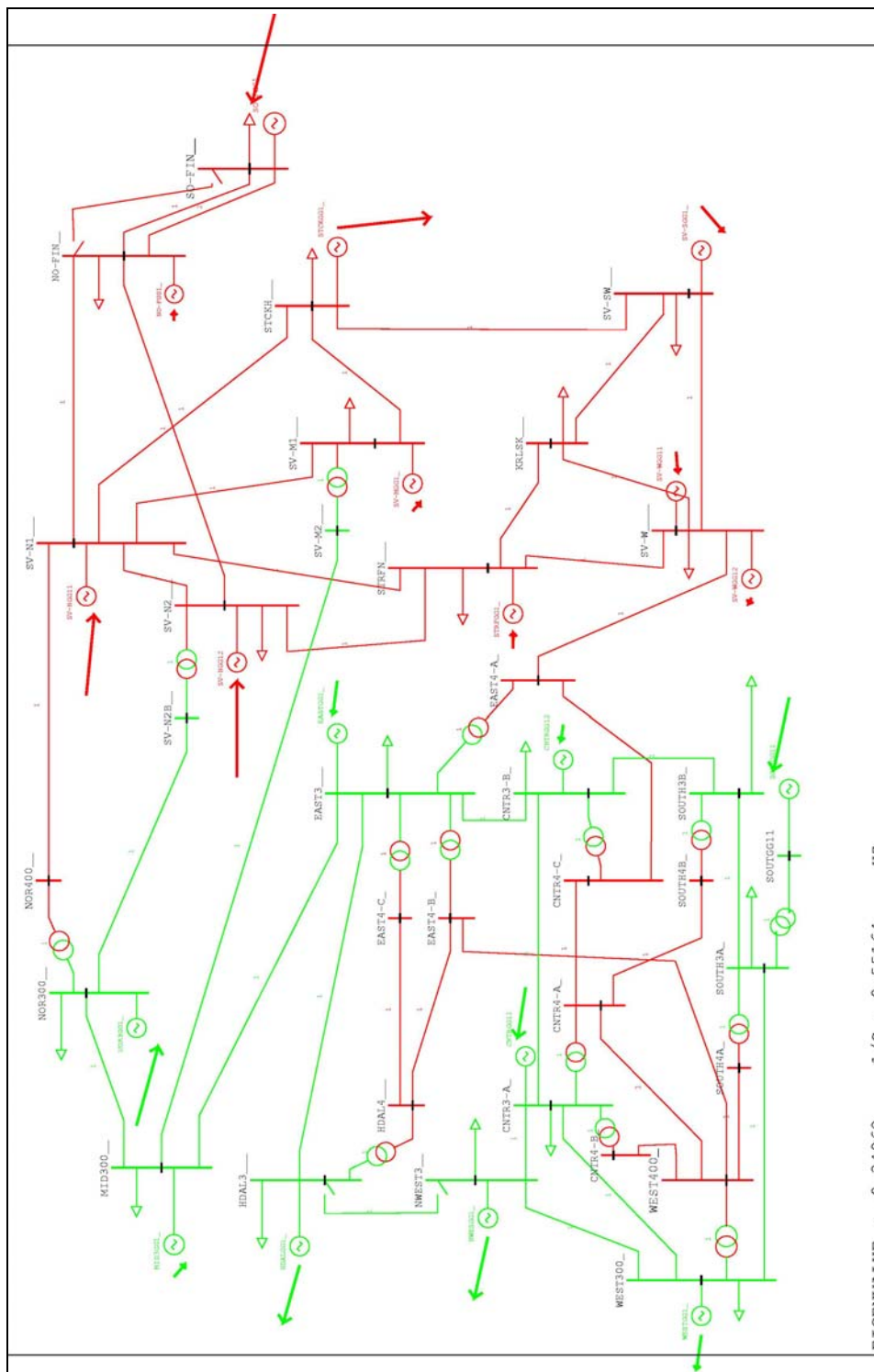
Figure 6.23 Modal analysis of the eigenvalue -0.34962 + 0.55164 Hz –Nordic Power System.

The entire power system can be excited in the frequency of 0.55Hz. At this particular electromechanical mode, the south Finnish system (machine installed to SO-FIN__), the Swedish system (machines installed to SV-N1__, SV-N2__ and STCKH__) and the Norwegian system (particularly the machines installed to NOR300__, SOUTH3B_, HDAL3_, NWEST3__) all have strong participation in this electromechanical mode. The phase angles from this graphical presentation shows that the South and Southwest of

Norway oscillates in phase with the SO-FIN__ and both of them oscillate against (i.e. almost opposite phase directions) the north of Norway and to some extent to the north of Sweden. Moreover, the Swedish machine installed in node STCKH oscillates in a different direction because of the complex power system operation.

All electromechanical modes are stable. Therefore, all the amplitudes of the power oscillations shall decay in time. The rotor angle stability in this power system representation from modal analysis does not present any unstable operation problem. The Finnish system is in most of the electromechanical modes, in addition, it has the less damped electromechanical mode. Hence, the Finnish system is expected to suffer severe oscillations compared to the other machines although the oscillations shall not increase in time.

6.3.2 Wind Power Projects and Representation

The wind power plants were chosen based on national wind power prognosis. A total of 4400MW of wind turbines are simulated to Finland, Norway, and Sweden. Eight sets of 550MW wind farms simulate the wind power integration to the Nordel. Table 6.8 presents the wind power plans simulated in this section.

Table 6.8 Wind power plans simulated (Figure 6.21 identifies the buses' name).

Country	Wind Power Installed
Finland	1100MW – installed 50% to NO-FIN and 50% to SO-FIN
Norway	1100MW – installed 50% to MID300 and 50% to NOR300
Sweden	2200MW – installed as four sets of 550MW to: SV-W, SV-SW, KRLSK, and STCK.

The dynamic AWF presented in chapter 5 models the wind power to the Nordel where sets of 550MW are installed to specific nodes on the Nordel (Table 6.8). The 550MW AWF represents 300 wind turbines of approximately 1.83MW. The wind turbines are a conventional type, i.e. directly connected to the network with induction generator and without power electronics.

The 550MW aggregate wind farm is composed of 10 wind farms with identical layout and identical 30 wind turbines each. There is no correlation between the 10 wind farms. The aggregate wind speed model generates time series to each wind farm and the 10 time series are averaged to produce a single aggregate wind speed.

The layout of each small wind farm is similar to Figure 6.11, where to this wind turbine, the distance between each wind turbine is approximately four times the rotor diameter (256m) where the rotor diameter is 64m. The wind speed angle is 90°, which means that 10 wind turbines will face strong correlated wind speed.

6.3.2.1 Aggregate Wind Farm Model

The aggregate wind farm is scale up of a 1.83MW wind turbine that formally does not exists, however the data is fitted based on similar size of wind turbines. Table 6.9 presents the main characteristics of the 1.83MW wind turbine used in the simulations.

Table 6.9 Basic characteristics of the 1.83MW wind turbine.

Nominal Power	1.83MW
Rotor diameter	64 m
Generator speed	1500 rpm
Rotor speed	21 rpm
Capacitor Bank	660kVAr
Electrical frequency	50Hz
Tower height	60 m
Gearbox ratio	71.43
First torsional frequency	1.0Hz
Estimated logarithmic damping to drive train	5%
Number of blades	3
3p frequency	1.05Hz

Eight different aggregate wind speeds are generated: two of 8m/s; two of 10m/s; two of 12m/s; and two of 16m/s all of them with turbulence intensity of 20% that is considered a strong turbulence intensity. The wind power produced from each aggregate wind farm is presented in Figure 6.24.
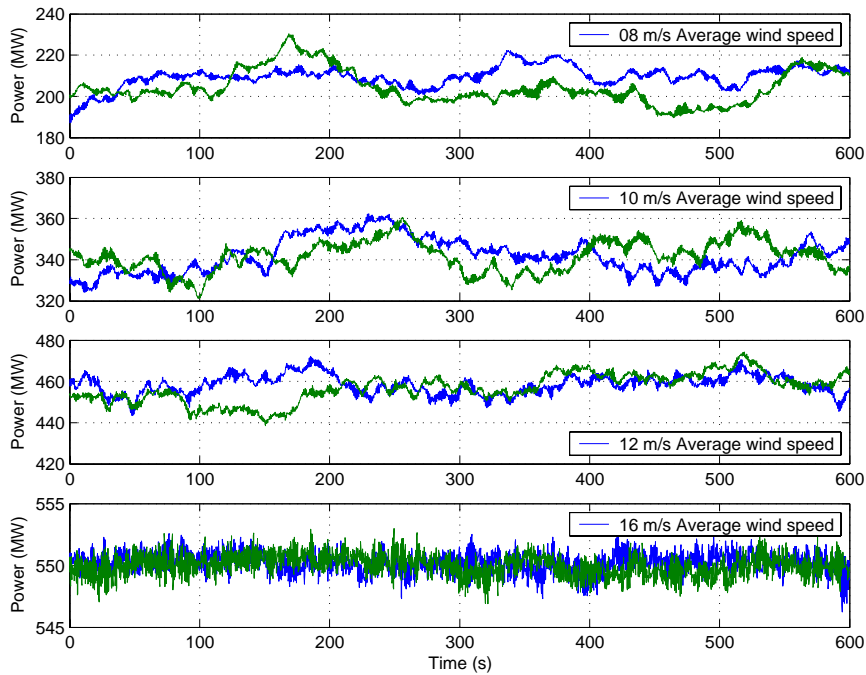
Figure 6.24 Aggregate wind farm power simulation.

In Figure 6.24, two time series of power produced from the AWF with mean wind speed at 8, 10 12 and 16m/s are presented. The larger standard deviation of the power occurs in the average wind speed of 10 m/s followed by the powers at 12m/s and 8m/s. At 16 m/s is the lowest standard deviation of power produced. Figure 6.25 presents the time series of the active power variations from different wind speeds.
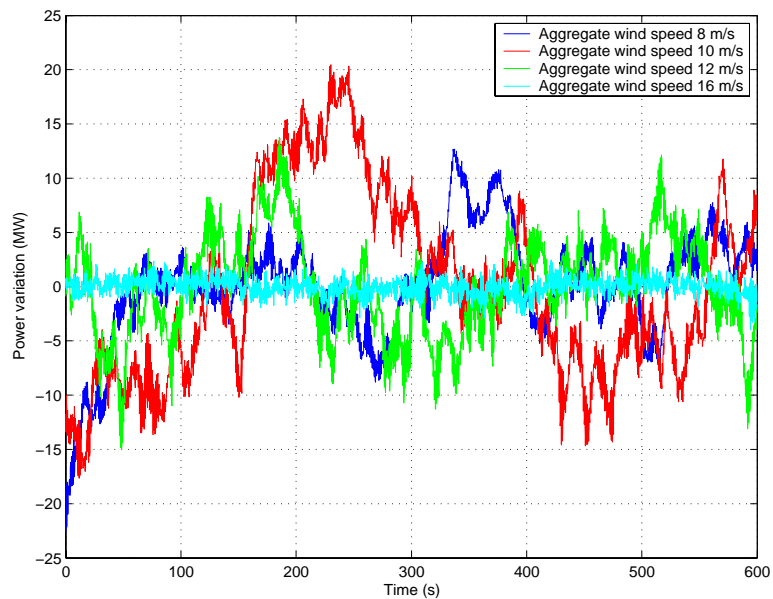
Figure 6.25 Aggregate wind farm power variation.

The power variation from the aggregate wind farm is very smooth compared to the power produced from a single wind turbine mainly because of the low wind correlation on large distances. The largest difference between maximum and minimum powers is at 10m/s (7% of the wind farm rated power) followed by the ones at 8m/s (6% of the rated power), at 12m/s (5.2%) and at 16m/s, which the difference is reduced to 1.6%.

The differences between the maximum and minimum powers (in less than 10 minutes) are relevant to the frequency controllers of the power system because they specify the maximum power range. However, the standard deviation can be even more relevant to express the power variation of the entire process than the range of power variation because the wind power does not vary instantaneously between the maximum and minimum. Figure 6.26 presents the power characteristics: mean, maximum, minimum and standard deviation produced by the AWF with the 8 time series of wind speed.
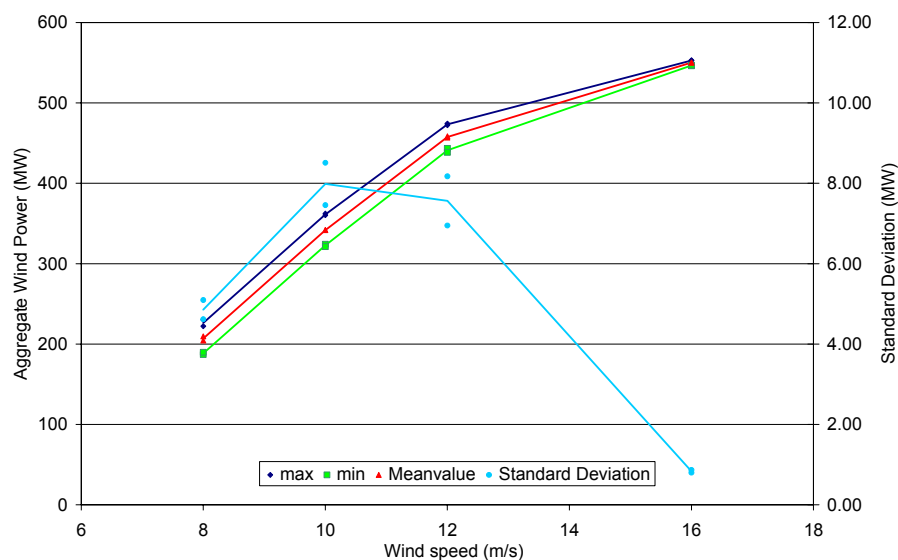
Figure 6.26 Aggregate wind farm power characteristics (at 20% turbulence intensity).

The power characteristics of the aggregate wind farms in different wind speeds are as expected. The standard deviation presented two quite different values because to each aggregate wind farm, new random seeds are used in order to avoid correlated time series of wind speeds and, as presented in chapter 5, the random seeds have influences on the standard deviation.

Each one of the 8 cases presented above, are installed to the Nordel where they simulate the large-scale integration of wind power. Different wind speeds are applied because it is not expected that the entire power system would have the same average wind speed.

6.3.3 Wind Power Impacts on the Power System Voltage and Frequency Regulation

The mean wind speed to each AWF has been assigned, to some extend, arbitrarily. However, because Finland has presented the less damped electromechanical modes of oscillations, to the two nodes, two cases are simulated: Case I which simulates large power variation from wind power (12m/s) and Case II which simulates small wind power variation (16m/s).

The average wind speed simulated to Norway is 10m/s, which have the largest power variation, was selected because from modal analysis, these nodes have a considerable participation on power oscillations. Table 6.10 presents the wind applied to the NORDEL where it is simulated large wind power variation to FINLAND.

Table 6.10 Aggregate wind farms average wind speeds.

AWF #	Country/ Near Generator	Bus Name	Wind speed (m/s)	
			Case I	Case II
1	Finland SO-FGG1_	SO-FIN	16	12
2	Finland NO-FGG1_	NO-FIN	16	12
3	Sweden: STCKGG1_	STCKH	8	8
4	Sweden: SV-SGG1_	SV-SW	8	8
5	Sweden: SV-WGG12	SV-W[3]	12	16
5	Sweden: SV-WGG11	SV-W[3]	12	16
6	Sweden: No sync. machine	KRLSK	12	16
7	Norway: MID3GG1_	MID300	10	10
8	Norway: NOR3GG1_	NOR300	10	10

6.3.3.1 Frequency controllers

The performance of the frequency controllers and of the power systems depends on several aspects. One of the relevant aspects here is the characteristic of the speed governors from all synchronous generators. The power oscillations are generated by the power unbalance and the properties of the speed regulators among other thinks. Figure 6.27 presents the simulated power balance of the entire Nordel as well as the total power variation from the wind turbines and from the synchronous generators.

---

[3] There is only one AWF installed to SV-W.
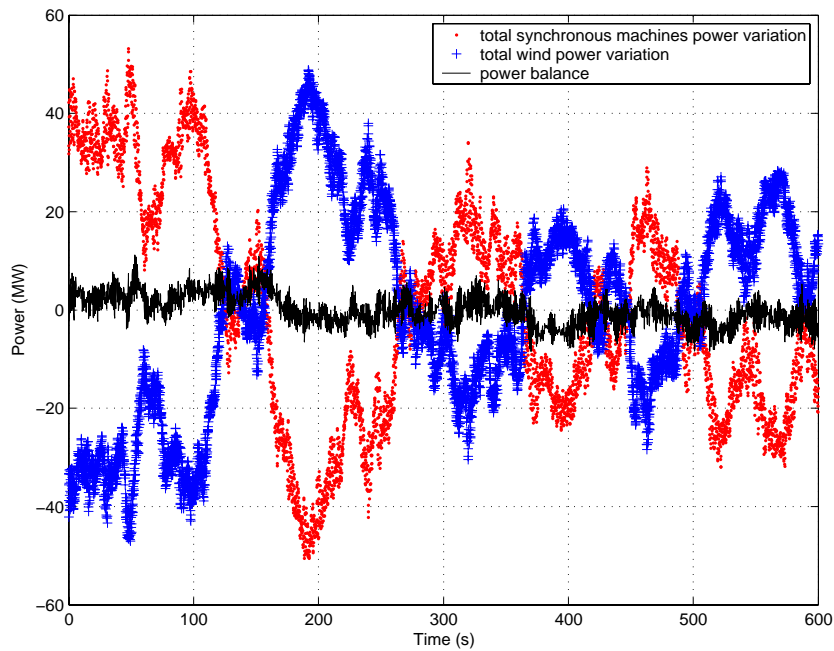
Figure 6.27 Power variations and power balance in the Nordel case studied.

In Figure 6.27, the total instantaneous variations of active power produced from all synchronous machines, from all AWF and the total instantaneous power balance are plotted. The total instantaneous variations are computed by adding the power from all machines at each time. The power balance is the difference between the power variation from the synchronous machines and the wind farms. The secondary frequency control is not modelled, so the set points of the synchronous generators were adjusted aiming to keep the regional power balances. In principle, the dynamic power balance presented in Figure 6.27 depends on the set points and characteristics of all generators and changing the average wind speed from different places did not significantly modify the total results presented in Figure 6.27.

In general, the power balance varies in a narrow range (within ±10MW) meaning a good combined response of the speed governors. However, the speed controllers are acting individually and independently in each machine, therefore some power oscillations between different machines cannot be presented in the total instantaneous power balance because they can be cancelled from those machines that the power oscillations are out of phase.

In order to verify the dynamic operation of the power system, Figure 6.28 presents the time series of the speed and the total standard deviation of the power from each machine in the Nordel, in addition, the total wind power production is included.
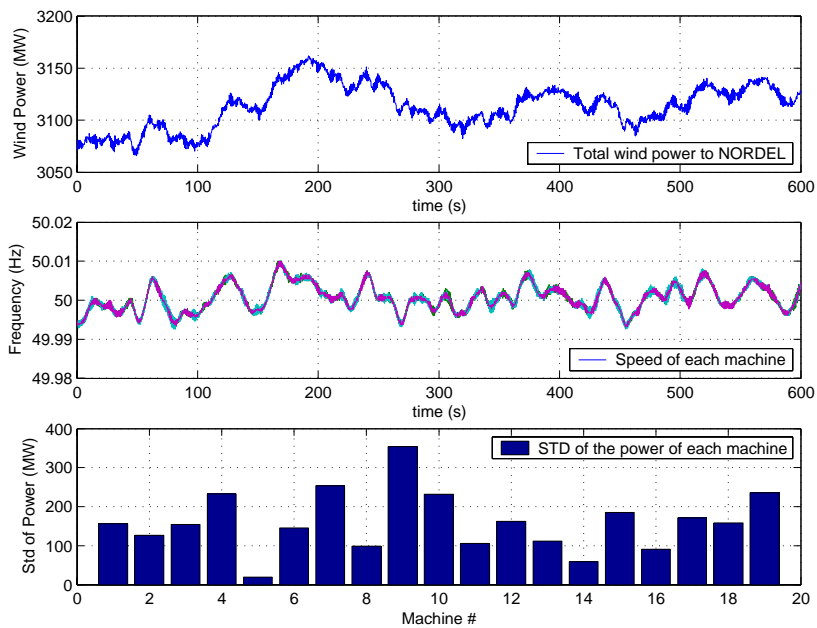
Figure 6.28 Wind power, frequency and standard deviation of power (mean wind speed at 12m/s to Finland).

The frequency in Figure 6.28 represents the speed in each machine that is well regulated and the variations are within 49.99 and 50.01Hz. An increase in the wind power leads to an increase on the frequency because the load on synchronous machines is reduced and the speed drop characteristics of the speed governors lead to an operational frequency slightly above the rated. Similarly, a reduction in the wind power leads to a decrease in the frequency.

The slow frequency variations are related to the total slow wind speed variation and the fast speed variations are related to the dynamic power variations from the wind turbines (e.g. 3p and torsional moments).

In the lower part of Figure 6.28, the standard deviation of the power from each synchronous machine is presented, where Table 6.7 presents the machine names. The higher power variation was presented by machine #9 that is connected to bus SV-N2__. This bus is connected to the Finnish system, to the Norwegian system and to the STCKH_ both of them with the higher wind power variations that explains the higher power variation.

In order to analyse in detail the dynamic behaviour of the power system with large wind power integration, the power spectral distribution of speed and power to the machines with high standard deviation (#9 and #7 from Figure 6.31) and the machine #1 (Finland that showed a strong electromechanical participation in the oscillation modes) are presented in Figure 6.29.
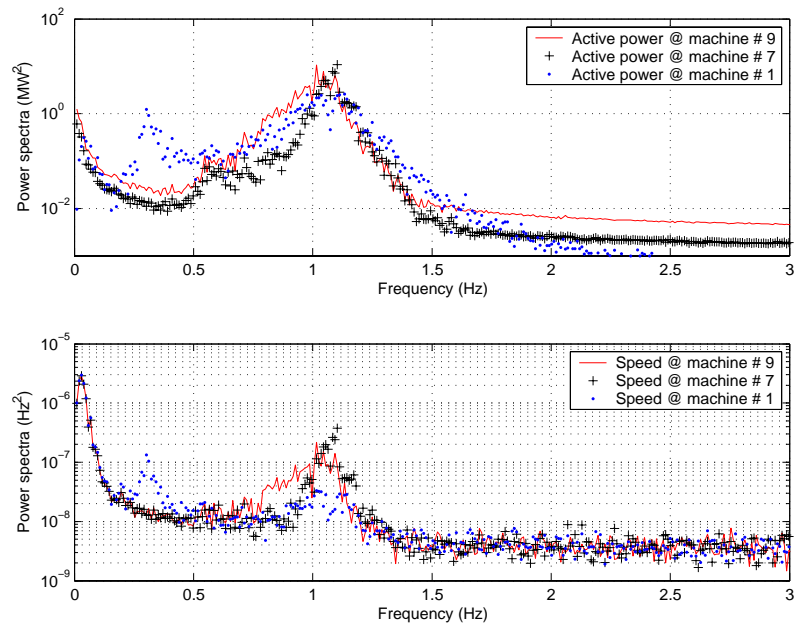
Figure 6.29 Power spectral distribution of the power and speed of selected machines (mean wind speed at 12m/s to Finland).

The wind power variations excite the power system in several modes. The electromechanical mode at 0.318Hz is excited in the Finish system (machine #1). The electromechanical mode around 0.55Hz is also excited. In this case, the wind power excites the power system with a frequency around 1Hz (3p) that influences several machines because at this frequency there are some electromechanical modes related to several machines as presented in the modal analysis.

The power spectral distributions of the speed variations in the machines are very small. The machine #1 presents a strong variation at 0.318Hz as expected because of its electromechanical mode of oscillation. All the other machines present higher power spectral speed variations at the 3p frequency because that is the frequency that the wind turbine excites the power system. The machine #7 presents a higher speed variation at 1.1Hz because that is the electromechanical mode associated to this machine.

As some important electromechanical modes are near to 0.5 Hz and taking into account that as the wind turbines grow in size there is a tend to reduce the speed of rotation, the rotational speed of the AWF is modified to 10 rpm. This slow speed of rotation leads to a 3p effect around 0.5Hz that will excite less damped modes of the entire power system. Figure 6.30 presents the power spectral distributions for the same machines similar to Figure 6.29 at this new condition, i.e. 3p from the wind turbines at low frequency 0.5Hz.
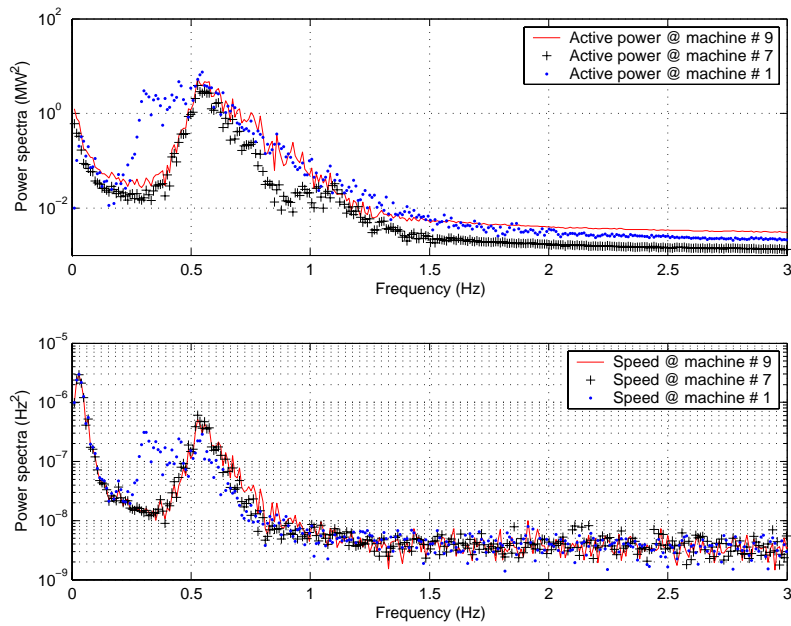
Figure 6.30 Power spectral distribution of power and speed to selected machines (AWF modified to lower rotational speed (3p~0.5Hz)).

In Figure 6.30, the wind power strongly excites the power system controllers. The power variations on the 3p effect are very similar to the ones presented in Figure 6.29, however at the frequency of 0.318Hz, the power variations by machine #1 are much higher than the previous case. In this case, it is possible to verify the isolated excitation of the machine #7 at 1.1Hz that is related to its electromechanical mode. The power spectral distributions of the speed variations on the selected machines are much higher particularly to machine #1 mostly because the proximity to the less damped electromechanical modes.

After having analysed the simulations to high wind power variation by the AWF in the Finish power system, here the mean wind speed applied to Finland is modified from 12 m/s to 16m/s in order to identify larger modifications on the results. Figure 6.31 presents the results of the dynamic simulation for case II (i.e. high wind speed to Finland).
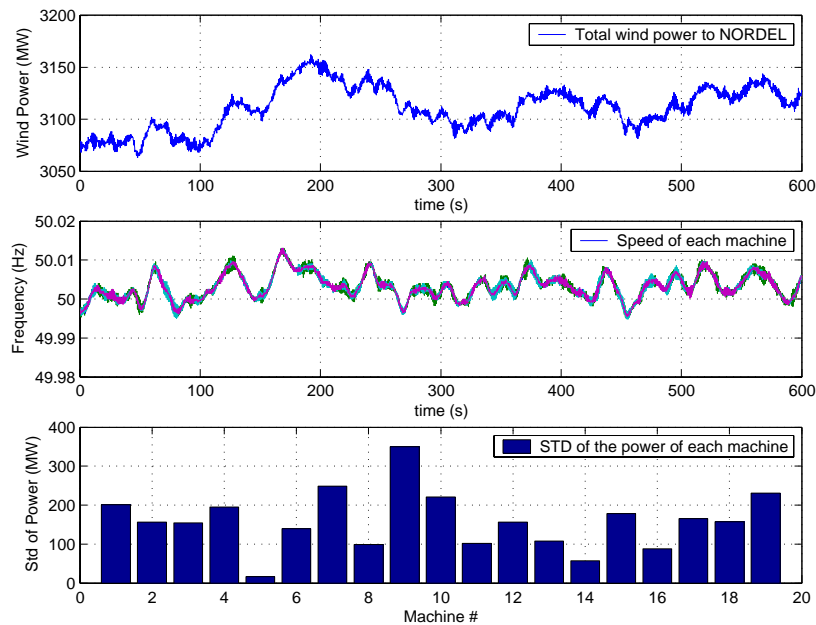
Figure 6.31 Wind power, frequency and standard deviation of power (average wind speed 16m/s to Finland).

There are no significant differences between Case I and II. The average frequency of the power system is slightly higher than the Case I meaning that it could be necessary an adjustment of the set points of the frequency controllers in order to keep the power production within the country areas. In the case II, the standard deviations of power to each synchronous machine have slightly changed. This is related to the fact that the speed governors of the synchronous machines shall react to the power variations from the nearest wind power avoiding the power flow between different areas of the power system.

6.3.3.2   Voltage Quality

Using the case I wind speed distribution and the original AWF (i.e. 3p frequency around 1Hz), the voltage on the Nordel network is analysed. Figure 6.32 presents the voltage simulated on all machines in the Nordel network. The voltages are in p.u. The differences in mean values come from the voltage set points specified to the machines in the power system.
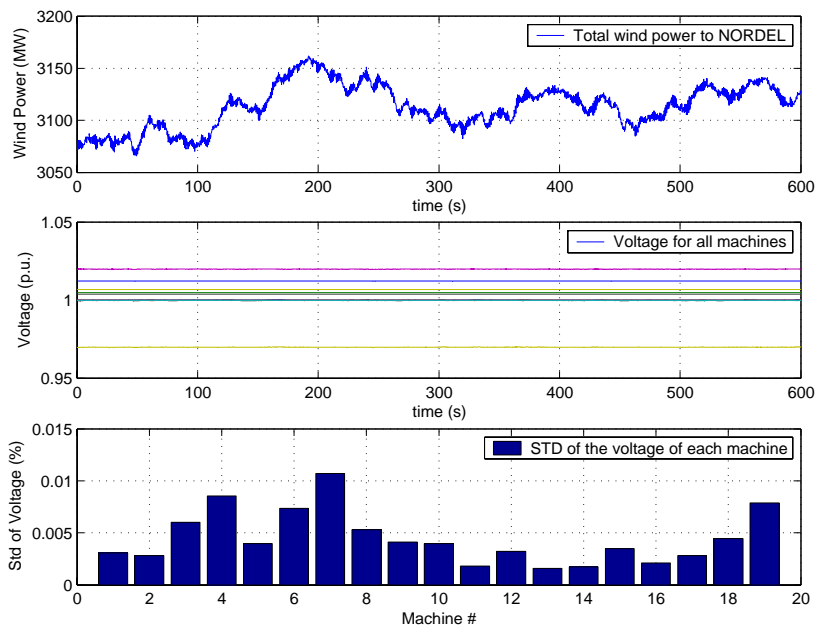
Figure 6.32 Wind power and voltage deviations simulated in Nordel system (mean wind speed 12m/s to Finland).

The total wind power installed to the power system is the same as presented in the previous cases. The voltage levels are not easy to identify in the graph, and the middle part of Figure 6.32 is only presented to show that the variations are very small meaning that the voltage regulators operate properly. The voltage quality does not seem to be an important issue here, anyway, similar to the frequency control analysis, the voltage variation to selected machines with high standard deviation of voltage are detailed as follow (Figure 6.33).
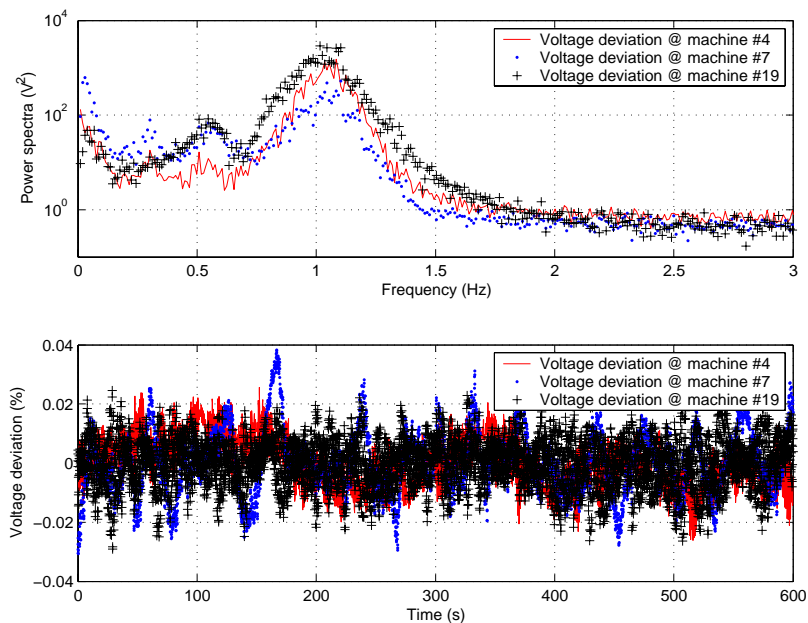
Figure 6.33 Power spectral distribution of voltage and voltage deviation to selected machines in the Nordel (Finland AWF at 12m/s).

In Figure 6.33, the power spectral distribution and time series of the voltage deviations to machines #4, 7 and 19 are presented. Those machines were selected because they presented higher standard deviation of voltage. The power spectral distributions of voltage show that the high variations occur at the 3p frequency from the wind turbine. It also shows that the electromechanical modes also influence the voltage controllers. The excitations of the synchronous machines are intrinsically related to the speed of the machine hence the presences of the modes were expected. The voltage deviations in time domain are within ±0.04% of the rated voltage that is very small.

Similarly to the frequency control analysis, the AWF was modified to rotate at 10rpm (3p=0.5Hz) in order to analyse the influences of the wind power on exciting the modes of the power system. Figure 6.34 presents the power spectral distribution of the voltage deviation as well as the time series of the voltage deviations on machines # 4, 7 and 19.
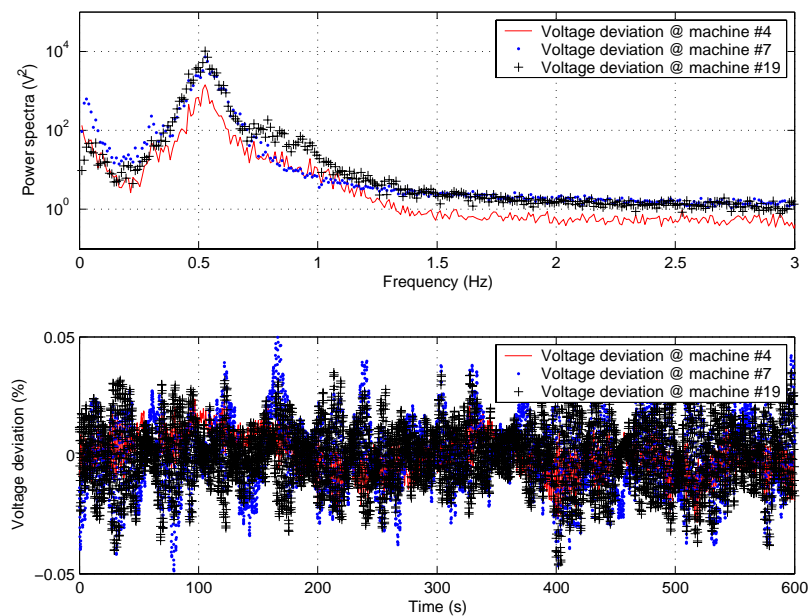
Figure 6.34 Power spectra distribution of voltage and voltage deviation simulated in Nordel System (mean wind speed 12m/s to Finland AWF low frequency (3p=0.5Hz)).

In this case, the power spectral distributions of the voltage are much higher at the 3p frequency. In the original AWF, the voltage power spectral at 1Hz were around 1000V², now that the 3p is around 0.5Hz, the corresponding power spectral peak is near to 10000V². This is explained because at the 0.5Hz an eigenfrequency of the power system is excited. The time series of the voltage deviations in this new condition agrees with the power spectral distribution, where the amplitudes now are limited to ±0.05%. However, it is important to note that the voltage variations simulated are very small (160V at 400kV) and it can be influenced by the precision of the simulations. Hence, the last three figures must be analysed with caution.

6.4 Case Analysis Remarks

Power quality and stability problems from large wind farms to the network have been investigated here. Three cases were analysed to illustrate the problems on the power quality and stability when integrating large amount of wind power, namely the voltage stability, voltage quality and the frequency control were investigated.

The voltage stability was illustrated by means of loadability curves drawn to the power system. The studied cases showed that the wind power can contribute to improve the voltage stability and that the reactive power is an important issue from large wind power concerning the voltage stability.

The voltage quality has been investigated by means of dynamic simulations using the Aggregate Wind Farm. The frequency control has been investigated by modal analysis and dynamic simulation using the AWF model. From the studied cases, the dispersion of the wind power over extensive areas smoothed the power variations from the wind turbines. The smoothed power variations caused small than expected voltage and frequency deviations in the high voltage network.

Following detailed remarks to each case are presented.

6.4.1   Remarks on Case 1

The first case presented only voltage stability analysis. The voltage stability was analysed with loadability curves to the power system with and without large amount of wind power.

The conventional wind turbines reduce the reactive power availability in the power system, fact that is deeply related to the voltage stability. In this power system studied, the voltage stability was in general reduced with wind power because of the reactive power demanded by the wind turbine generators. However, new wind turbine technologies using electronic power converters, which can regulate the reactive power from the wind turbine, improved the voltage stability and it can actively contribute to regulate the voltage.

The voltage stability depends also on the network characteristics. The case represents the integration to the transmission level (220kV) where the reactances inductive of the lines and the reactive power compensation schemes played an important role.

6.4.2   Remarks on Case 2

In the second case, the analysis of voltage stability and dynamic voltage quality of a Brazilian power system was presented. The voltage stability was studied with similar methodology as the one used in the case 1, however different load conditions were supplied improving the analysis.

The voltage stability was addressed in heavy and light load conditions, where the voltages on the network were modified in each condition due to the reactive power compensation schemes. The wind power had small impact on the voltage stability, where it increased the loadability limits of the local power system, fact that is different from the previous case. In this case, a relative low reactive power is flowing in the network when compared to case 1 that explains the improvements on the voltage stability.

The dynamic voltage variation has been studied using dynamic simulations with aggregate wind farm. The smoothing effects on the power fluctuation from the wind farm cased small voltage fluctuations on the power system. The worst-case scenario showed voltage variations within 0.3 kV at 230kV nominal voltage. The wind farms will be installed to the transmission level hence the voltage variations on the low voltage levels area can be influenced. When distribution grid data is available, the model must be extended to include the distribution grids and the voltage quality on the consumers must be assessed.

6.4.3 Remarks on Case 3

Case 3 analysed large-scale integration of wind power influence on the voltage and frequency controllers. The voltage control was related to the voltage quality and in this case, only the dynamic voltage variations were presented. The frequency control was related to dynamic stability and power quality.

The Nordic power system (here called Nordel) is very strong. Aggregate wind farms (AWF) represented the large-scale wind power in the Nordel based on the national plans of wind power.

Here some assumptions were taken:

- Two cases for each average wind speeds of 8, 10, 12 and 16 m/s were simulated with turbulence intensity of 20%. The cases covers a large extend of the power curve from wind turbines in addition, the 20% turbulence intensity is expected to be the worst scenario to normal operation of wind turbines.

- The wind farms were aggregate in similar blocks of 550MW. This assumption made ease to change the assigned average wind speeds to different AWFs, i.e. the time series of the aggregated wind speeds can be shifted to different AWF s without generating new time series. The application of the AWF to the real wind farms layout is straightforward when it is available.

- The layout of the wind farms, similar to case 2, assumed 90° wind direction leading to rows of 10 wind turbines with high correlated turbulence that might be considered one worst-case scenario.

- The connection points of the AWFs were assumed to buses in Sweden and Finland, where in Norway, EFI Sintef, from Norway, proposed specific buses to which the large scale wind power should be simulated.

- Except for the AWFs installed in Finland and Norway, the average wind speeds were assigned arbitrarily. The wind speeds in Finland and Norway were chose with high wind power variations because in some specific machines installed in these countries, which the wind power is planned, presented high participation on electromechanical modes at low frequency. The Finnish system presented the less damped mode so the high wind power variations were assigned to both buses in Finland (12m/s) and because of the same reason 10m/s was assigned to Norway. However, a sensitive analyse was carried, where the high wind power variation (12m/s) in Finland was replaced with the smallest at mean wind speed 16 m/s.

- The automatic secondary generation control unit was not implemented. Hence, the set points of the nearest synchronous machines were adjusted to maintain the areas (countries) balances.

The main conclusions from the simulations are classified on voltage and frequency control as following.

6.4.3.1 Frequency control

The frequency control was primarily analysed with modal techniques. Using modal techniques, some of the most significant electromechanical modes were identified and

characterized. The less damped modes were below 0.6Hz and all electromechanical modes were stable. With modal analysis was possible to characterize also the most important machines participating on each electromechanical mode and how was the direction of the relative rotor angle speed variation of the machines.

The AWF completes the analysis because it provided means of dynamic simulation to verify the behaviour of the frequency controllers (speed governors) under normal operation. From the dynamic simulations, the electromechanical modes were also identified. They are well damped (frequency controllers well designed) so the power oscillations caused from the wind power in the Nordel did not increase in time.

One of the machines that presented high participation on the electromechanical modes from the modal analysis was the machine #9 connected to bus SV-N2__ that was also identified on the dynamic simulation with higher speed and power variations during normal operation with wind power. This bus did not have wind turbines installed, but its specific location in addition to the electromechanical characteristics of the power system made this machine the most sensible in the simulations. This observation might indicate that the power variations from the wind power do not necessarily influence only locally but it can be transferred to remote parts of the power system.

In order to verify the extreme impacts of wind power in the less damped electromechanical modes of the power system, the aggregate wind turbine was modified to have the 3p effect at 0.5Hz. Under this new condition the power system still stable, however the wind turbines directly excite the less damped electromechanical modes hence higher power and speed variations at low frequencies were encountered, particularly on the machines with high participation on the electromechanical modes that was expected.

6.4.3.2 Voltage controllers

The voltage controller's performances were analysed by dynamic simulation using the AWF. The voltage controllers worked properly compensating the reactive power demanded from the AWF and keeping the voltage within 0.10% variations (±0.05%).

The wind power simulated did not represent a problem to the voltage quality. However, the dynamic simulation revealed that some modes that were excited from the wind power on the frequency analyses were also present on the voltages. Anyway, the voltage variations were small.

The dynamic analyses of large-scale wind power indicated that the voltage quality was not a concern on high voltage networks and it might be more relevant in lower voltage levels including the distribution networks. At those grids, the limited voltage regulation and the losses might lead to large voltage variations from wind power and become a problem so, when necessary, the grid must be detailed and the voltage analysed properly.

Chapter 7

7 Conclusions

A methodology to investigate the wind power influences on the power system was presented in this thesis. It includes analysis of the wind power influences on the voltage stability, power system stability and power quality characteristics.

The voltage stability was analysed with loadability curves to the power system. The voltage stability was influenced by the wind power integration, where the reactive power was the main factor. A loadability computation tool was developed in this thesis and a static model to the wind power on the voltage stability was presented. Modifications of the wind turbine characteristics, i.e. application of power electronics, were simulated improving the voltage stability.

The main conclusions for the voltage stability are that although the wind power alleviates the active power fluxes in the network, the reactive power flux to the wind farms will reduce the voltage stability limits. Wind turbine technologies with power converters that can actively control the reactive power consumption increased the voltage stability (i.e. extended the power limit of the voltage collapse) of the power system.

The power system stability and power quality were investigated with dynamic simulations. Dynamic models to large-scale wind power that can assess the power system stability and quality were presented. The dynamic models are based on aggregation procedures of wind turbines.

The aggregate wind farm model permits an easy assessment of the power system dynamic operation from large-scale integration of wind power. The assessment of power quality parameters such as voltage and frequency deviations due to the inclusion of large amount of wind power demands simulations of the wind farms power production and its interaction with the power systems. Dynamic simulations of a high number of wind turbines are unpractical for very large power systems. Therefore, the aggregate model is very suitable to identify the impact of large-scale wind power in the dynamic operation of the power system because it is time inexpensive and it includes the most relevant characteristics of the wind turbines power dynamics, particularly the turbulence and its spatial correlation. Using the aggregate models, the identification of voltage deviations and inadequate frequency regulation can be done in few minutes even for large power systems.

The aggregate wind speed that is applied to the aggregate wind turbine model was also developed and presented. It includes relevant characteristics of the turbulence and its spatial correlation effects on the power produced from wind farms. The power smoothing effect from the wind farms power production have been verified in the aggregate wind speed model to correctly represent the large wind farms power production.

In addition, the problems for the power systems stability that are mainly related to power oscillations were studied with modal analysis to identify the most relevant characteristics. The applications of the modal analysis with the dynamic simulations are recommended in order to assess possible power system stability problems.

Related to the power quality problems, the studied cases show that higher number of wind turbines smoothes the power variations consequently the flicker phenomena can be

considerably reduced. The simulated dynamic voltages were within limits and the flicker was not a concern however in the cases studied here, the network was strong and the wind power was connected to the high voltage network (transmission lines).

The frequency control was also investigated using a reduced model of the Nordel power system. The large-scale wind power integration interacts with the power system controllers. The power variation in broad frequency range excite some electromechanical modes of the power system however the frequencies variations were so low that it does not endanger the dynamic stability or cause serious power oscillations in the power system. Nevertheless, the dynamic simulations showed that the wind power do not impact only local machines but it can influence remote parts because of the power system electromechanical characteristics hence it is necessary to investigate the entire power system operation with large-scale integration of wind power.

Before introducing the aggregate wind farm, dynamic wind turbine models have been presented. The dynamic wind turbine model represents the most relevant wind speed and wind turbine characteristics to power quality characteristics. The frozen turbulence, rotational sampling turbulence and tower shadow effects are the most relevant to power quality hence included in the wind speed model. The wind turbine model described the most relevant aeroelastic components of wind turbines for simulation of power fluctuations. The aerodynamic power conversion including the dynamic stall is included in the aeroelastic model. In addition, the drive train dynamic operation is simplified to include the most relevant modes of oscillation of the power variations.

The aggregate wind farm presented some limitations that can be improved in future works. The inclusion of the wake effect phenomenon in the wind farm and the deterministic parts from the wind speed can be new tasks. Moreover, the extension of the model to variable speed wind turbines is also envisaged. In the near future, the variable wind turbines will account to large power production.

In addition, as future work, here the integration of wind speed forecasting in extensive areas with the aggregate wind speed model is proposed. The inclusion of this wind speed forecasting and geographical disposition of wind farms improves analyses of the dynamic integration of the large-scale wind power in the power systems. The forecast model can generate the mean wind speed (10 minutes) and turbulence intensity to specific locations that can be used as input to the aggregate wind speed model. The integration of different tools will improve the analysis of the power system characteristics with benefits to the analysis of the frequency secondary control in the power system and analysis of real conditions as well as storm fronts.

The inclusion of the loads characteristics and its time variation to the analysis of the dynamic power system operation it also proposed here as future work. The interaction of the loads in addition to the wind power variation on the power system dynamic operation can be relevant to characterize the power oscillations.

Finally, it is important to validate and improve the aggregate wind farm model by obtaining experimental measurements from large wind farms.

8 Reference List

[1] *IEC 61400-21 Measurement and assessment of power quality characteristics of grid connected wind turbines*. International Electrotechnical Commission, FDIS 2001.

[2] "Integration of Renewable Energy in the Electrical Network in 2010", draft final report, EU ALTENER PROJECT XVII/4.1030/Z/99-115, Brussels-Belgium, 2001.

[3] Y. Wan and B. K. Parsons, "Factors Relevant to Utility Integration of Intermittent Renewable Technologies", NREL Report NREL/TP-463-4953, Colorado, USA, August, 1993.

[4] J. E. Nielsen, S. Varming and C. Gaardesatrup, "Review of Technical Options and Constraints for Integration of Distributed Generation in Electricity Networks", Report SUSTELNET, (on-line: www.sustelnet.net/documents.html) Netherlands, December, 2002.

[5] J. Saxow, S. Skovgaard and P. Friis, "Power Plant Operation Correlated with wind energy production within the Elsam Utility Area – status 1995", Elsamprojekt A/S Power Station Engineering Report EP96/404a, Denmark, June, 1996.

[6] J. O. Tande, P. Nørgaard, P. Sørensen, L. Søndergaard, P. Jørgensen, A. Vikkelsø, J. D. Kledal and J. S. Christensen, "Power Quality and grid Connection of Wind Turbines"*, Summary report, Vol. 1, 2 and 3, Risø report Risø-R-853, Roskilde, Denmark, October, 1996.

[7] P. Sørensen, T. F. Pedersen, G. Gerdes, R. Klosse, N. Robertson, W. Davy, M. Koulouvari, E. Morfiadakis and Å. Larsson, "European Wind Turbine Testing Procedure Developments, Task 2: Power Quality", Risø report Risø R-1093(EN) (on-line: www.risoe.dk/rispubl/VEA/_veapdf/ris-r-1093.pdf), Roskilde, Denmark, May 2001.

[8] Å. Larsson, "The Power Quality of Wind Turbines", PhD dissertation (on-line: www.elkraft.chalmers.se/Publikationer/EMKE.publ/Abstracts/LarssonD.abstr.html), Department of Electrical Power Engineering, Chalmers University of Technology, Göteborg, Sweden, 2000.

[9] J. O. Tande, "Applying Power Quality Characteristics of Wind Turbines for Assessing Impact on Voltage Quality", In *Wind energy*, 5, 2002.

[10] V. Akhmatov, A. H. Nielsen and H. Knudsen, "Electromechanical interaction and stability of power grids with windmills", in *proceedings of the IASTED International Conference Power and Energy Systems*, Marbela , Spain, September, 2000.

[11]   M. Bruntt, J. Havsager and H. Knudsen, "Incorporation of Wind Power in the East Danish Power System", in *proceedings of IEEE Power Tech'99 conference*, Budapest, Hungary, September, 1999.

[12]   J. Wiik, J. O. Gjerde and T. Gjengedal, "Impacts from Large Scale Integration of Wind Farms into Weak Power Systems", in *Proceedings of PowerCon 2000*, Power System Technology, Australia, 2000.

[13]   L.L. Freris, "*Wind Energy Conversion Systems*". Prentice Hall, London, UK, 1990.

[14]   E. Hau, *Wind-Turbines Fundamentals, Techonlogies, Application, Economics*, Spring Verlag, Germany, 2000.

[15]   S. Heier, *Grid Integration of Wind Energy Conversion Systems*, John Willey and Sons, England, 1998.

[16]   J. Wilkie, W.E. Leithead and C. Anderson, "Modelling of Wind Turbines by Simple Models", *Wind engineering* vol. 14, No. 4, 1990.

[17]   A. I. Estanqueiro, "Dynamic Models of Wind Parks" (in Portuguese: Modelação Dinamica de Parques Eólicos), PhD dissertation, Instituto Superior Técnico, Universidade Técnica de Lisboa, Portugal, 1997.

[18]   T. Petru, "Modelling of Wind Turbines for Power System Studies", Licentiate technical report Nr. 391L (on-line: www.elkraft.chalmers.se/Publikationer/ EMKE.publ/Abstracts/Petru2001.abstr.html), Department of Electric Power Engineering, Chalmers University of Technology, Sweden, 2001.

[19]   P. Sørensen, A. Hansen, L. Janosi, J. Bech and B. Bak-Jensen, "Simulation of interaction between wind farm and power system". RISØ report R-1281(EN) (on-line: www.risoe.dk/rispubl/VEA/veapdf/ris-r-1281.pdf), Roskilde, Denmark, December 2001.

[20]   A. I. Estanqueiro, R. Aguiar, J. A. G. Saraiva, R. M G. Castro and J. M Ferreira de Jesus, "Development and Application of a model for power output fluctuations in a wind farm", in *proceedings of the European Wind Energy Conference*, Lübeck-Travemund, Germany, March, 1993.

[21]   G. Giebel, "On the Benefits of Distributed Generation of Wind Energy in Europe", PhD dissertation (on-line: gregie.hjem.wanadoo.dk/Ggiebel_Distributed WindEnergyInEurope.pdf), Reihe 6, report Nr. 444,VDI Verlag, Düsseldorf, Germany, 2001.

[22]   H.G. Beyer, J. Luther and R. Steinberger-Willms, "Fluctuations in the Combined Power Output from Geografically Distributed Grid Coupled Wind Energy Conversion Systems – An Analysis in the Frequency Domain", *Wind engineering* Vol 14, No. 3, 1990.

[23]   P. Kundur Ed, *"Power System Stability and Control"*, EPRI Power Engineering Series, McGraw Hill, 1993.

[24]   P. M. Anderson and A. A. Fouad, *"Power System Control and Stability"*, IEEE Power System Engineering Series, New York, 1993.

[25]   System dynamic performance subcommittee of the Power system engineering committee of the Power Engineering Society "Eigenanalysis and Frequency Domain Methods for Power Systems: Dynamic Performance", IEEE 90TH0292-3-PWR. IEEE, Piscataway, NJ, USA, 1989.

[26]   L. Wang, M. Klein, S. Yirga and P. Kundur, "Dynamic Reduction of Large Power System for Stability Studies", *IEEE transactions on Power System*, vol. 12 No. 2, May, 1997.

[27]   C. W. Taylor, *"Power System Voltage Stability"*, EPRI Power Engineering Series, McGraw Hill, 1994.

[28]   T. V. Custem and C. Vournas, *"Voltage Stability of Electric Power System"*, Kluvwer's Power Electronic and Power Systems Series. Series Editor: Thomas A Lipo and M.A. Pai, Brussels 1998.

[29]   System dynamic performance subcommittee of the Power system engineering committee of the Power Engineering Society, *"Voltage Stability of Power Systems: Concepts, Analytical tools, and industry experience"*, IEEE 90TH0358-2-PWR, Piscataway, NJ, USA, 1990.

[30]   C. Cañizares, *"Voltage Stability Assessment: Concepts, Practices and Tools"* Power System Stability Subcommittee Special Publication IEEE/PES, Final Document (thunderbox.uwaterloo.ca/~claudio/claudio.html#VSWG), August 2002.

[31]   S. Persaud, B. Fox and D. Flynn, Impact of remotely connected wind turbines on steady state operation of radial distribution networks, in *Proceedings of Generation Transmission and Distribution*, Vol. 147, N3, May, 2000.

[32]   *IEC 868-0 Flickermeter Functional and design specifications* CEI/IEC 868-0, 1986;

[33]   *IEC 868-0 Amendment 1 to Flickermeter Evaluation of flicker severity*. CEI/IEC 868-0, 1990;

[34]   *IEC 868-0 Flickermeter Evaluation of flicker severity*. CEI/IEC 868-0, 1991;

[35]   S. Johansson, "Long-term Voltage Stability in Power Systems - Alleviating the Impact of Generator Current Limiters". Technical Report No. 335, Chalmers University of Technology, Göteborg, Sweden. 1998.

[36]   D. Karlsson, "Voltage stability simulations using detailed models based on field measurements". Technical Report No. 230, Chalmers University of Technology, Göteborg, Sweden, 1992.

[37]   M. Larsson, "Coordinated Voltage Control in Electric Power Systems", Ph.D. thesis (www.iea.lth.se/publications/point/Theses/pdf_files/LTH-IEA-1025.pdf), Department of Industrial Electrical Engineering and Automation, Lund Institute of Technology, Lund, Sweden, 2001.

[38]   B. H. Bakken, "Technical and Economical Aspects of operation of thermal and hydro power systems", Ph.D. Dissertation, NTNU, report Nr. 16, Trondheim, Norway, 1997.

[39]   G. Rogers, "*Power System Oscillations*", Kluvwer's Power Electronic and Power Systems Series. Series Editor: M.A. Pai, Canada, 2000.

[40]   K. R. Padiyar, "*Analysis of Subsynchronous Resonance in Power System*", Kluvwer's Power Electronic and Power Systems Series. Series Editor: M.A. Pai, India, 1999.

[41]   O. Samuelsson. *"*Power System Damping - Structural Aspects of Controlling Active Power", Ph.D. dissertation (www.iea.lth.se/~ielolof/olof/PhDthesis.pdf), Department of Industrial Electrical Engineering and Automation, Lund Institute of Technology, Lund, Sweden, 1997.

[42]   B. Eliasson. *"*Damping of Power Oscillations in Large Power Systems", PhD dissertation, Department of Automatic Control, Lund Institute of Technology, Lund, Sweden, 1990.

[43]   R. M. Sundar and J. P. Sulivan, "Performance of Wind Turbines in a Turbulent Atmosphere". *Journal of Solar Energy,* Vol. 31, No. 6 pp. 567-575, 1983.

[44]   J. C. Kaimal, J. C. Wyngaard, Y. Izumi, and O. R. Cote, "Spectral Characteristics of Surface Layer Turbulence". *Quarterly Journal of the Royal Meteorological Society*, vol. 98, 1972.

[45]   J. T. Petersen and H. A. Madsen, "Local Inflow and Dynamics – measured and simulated on a rotating Wind Turbine Blade", Risø report, *DRAFT,* Risø-R-993 (EN), Roskilde, Denmark September 1997.

[46]   "*Voltage characteristics of electricity supplied by public systems*", European standard, CENELEC EN 50160, November, 1994.

[47]   D. Winkelaar, "Fast three-dimensional wind simulation of stochastic blade loads". *Paper presented at the 10th ASME Wind Energy Symposium,* Houston, 20-24 January 1991.

[48]   P. Madsen and F. Rasmussen, "Rotor loading on a three-bladed wind turbine", in proceedings of the *European Wind Energy Conference* EWEC'89*, Glasgow 1989.

[49]   P. Sørensen, *"Frequency Domain Modelling of Wind Turbine Structures"*. Risø publication Risø-R-749(EN), Roskilde, Denmark, April 1994.

[50]   W. Langreder, "Models for Variable Speed Wind Turbines", M.Sc. dissertation, CREST Loughborough University, UK, 1996.

[51]   P. H. Madsen, S. Fradsen, W. E. Holley and J. C. Hansen, "Dynamics and Fatigue Damage of Wind Turbine Rotors during Steady Operation". Risø report R-512, Risø National Laboratory, Roskilde, Denmark 1984.

[52]   H. A. Panofsky, "The atmospheric boundary layer below 150 metres". *Annual Review of Fluids Mechanics*, vol 6 pp.147-177, 1974.

[53]   Engineering Science Data Unit, *Characteristics of wind speed in the lower layers of the atmosphere near the ground: Strong wind (neutral atmosphere)*. Data Item 72026, ESDU London, 1972.

[54]   P. A. Rosas, P. Sørensen and H. Bindner, "Fast Wind Modelling", in *Proceedings of European Wind Energy Conference*, Kassel, Germany, 2000;

[55]   G. Solari, "Turbulence Modelling for Gust Loading". *ASCE Journal of Structural Engineering,* Vol. 113, No. 7, July 1987.

[56]   *"last og sikkerhed for vindmøllekonstruktioner"*) (in English: *Danish standard for loads and safety of wind turbines construction,* 1st edition May 1992, Danish Standard DS 472.

[57]   A. G. Davenport, "The spectrum of horizontal gustiness near the ground in high winds". *Quarterly Journal of Meteorology Society 87,* pgs 194 – 211, 1961.

[58]   W. Schlez and D. Infield, "Horizontal two points coherence for separations greater than the measurement height". *Boundary-Layer Meteorology 87,*Kluwer Academic Publishers Netherlands, 1998.

[59]   L. Kristensen and S. Frandsen, "Model for power spectra of the blade of a wind turbine measured from the moving frame of reference", *Journal of Wind Engineering and Industrial Aerodynamics*, 10 (1982) 249-262;

[60]   P. Sørensen, Methods for Calculation of the Flicker Contributions from Wind Turbines, Risø report Risø – I – 939 (EN), Roskilde, Denmark, December 1995.

[61]   G. C. Larsen, S. Frandsen, P. Sørensen and M. S. Courtney, "Design Basis for Horizontal Axis Turbines – Theoretical Background". Risø publication Risø-M-2836, Roskilde, Denmark, December 1989.

[62] S. Øye, "Dynamic Stall – simulated as time lag of separation" in *Proceedings of the 4th IEA Symposium on the aerodynamics of wind turbines*. Mc Anulty (Ed.), Rome Italy 1991.

[63] H. Bindner, "Active Control: Wind Turbine Model". Report number: R-920(EN) Risø National Laboratory, Denmark, 1999;

[64] H. Ganader and T. Thiringer, "An extended model of drive train dynamics". Report number 6R, Department of Electric Power Engineering, Chalmers University of Technology, Sweden, 1997.

[65] P. C. Krause, O. Wasynczuk and S. D. Sundhoff. *"Analysis of Electric Machinery and Drive Systems"*, IEEE Press, Willey-Interscience, second edition, 2002;

[66] T. J. Larsen, M. H. Hansen and F. Iov, "Generator dynamics in aeroelastic analysis and simulations", Risø report, Risø-R-1395(EN), Roskilde, Denmark, February, 2003.

[67] P. Sørensen, A. Hansen and P. A. Rosas, Wind models for prediction of power fluctuations from wind farms. *Journal of Wind Engineering*, n. 89 October 2001.

[68] A.I. Estanqueiro, R. F. Aguiar, J. A. G. Saraiva, R. M. G. Castro and J. M. F. D. Jesus. "On the effect of utility grid characteristics on wind park power output fluctuations", in *Proceedings of British Wind Energy Conference BWEA'15,* York 1993;

[69] T.Y.J Lem and R.T.H Alden, "Comparison of experimental and aggregate induction motor responses". *IEEE Transactions on Power Systems* Vol. 9, n. 4, November 1994, pgs:1895-1900;

[70] M. Akbaba and S. Q. Fakhro, "New model for single unit representation of induction motor loads, including skin effect, for power system transient stability studies". *IEE Proceedings* – B Vol. 139, n. 6, November 1992;

[71] D.C. Franklin and A. Morelato, "Improving dynamic aggregation of induction motor models". *IEEE Transactions on Power Systems* Vol. 9, n. 4, November 1994, pg: 1934-1941;

[72] DU_Rede Oper.N-NE.R20_26-12-02, North – Northeast Power System Diagram – from December 2002 (in Portuguese). Power System National Operator (*Operador Nacional do Sistema*) – on-line: www.ons.com.br/ons/sin/index.htm, Brasilia, Brazil, 2000.

[73] Approved wind projects to Brazil on line www.eolica.com.br/index_por.html, Recife, Brazil, 2002.

[74] Data base – Power system analysis in Portuguese (*Base de Dados - Estudos Elétricos*), reference case to the year 2004. National Operator of the Power System

ONS: 06/09/01 CICLO 02-04, on-line: www.ons.com.br/ons/sin/index.htm, Brasilia, Brazil, 2002.

[75] "Nordic High Voltage Network" (*"Det Nordiske Høyspentnette"*) on line diagram at www.nordel.org/Content/Default.asp?PageID=125, 2002.

[76] "Recommendations for frequency, time deviation, regulation and reserve" (*Rekommandasjon for frekvens, tidsavvik, reguérstyrke og reserve*) NORDEL available on-line at www.nordel.org/Content/Default.asp?PageID=130, 1996.

[77] "Operational Performance Specifications for Thermal Power Units larger than 100MW" NORDEL available on-line: www.nordel.org, 1995.

[78] T. Thiringer and J. Luomi, Comparison of reduced order dynamic models of induction machines, *IEEE Transactions on Power Systems*, vol 16, No 1, February, 2001.

[79] T. Thiringer, "*Measurements and Modelling of Low-Frequency Disturbances in Induction Machines*". Technical Report no.: 293, PhD dissertation, Department of Electric Power Engineering, Chalmers University of Technology, Sweden, 1996.

[80] Communication from ABB/SIMPOW Induction Machine Model – September 2002;

[81] P. A. Rosas, J. R. Hansen, P. Sørensen and H. Bindner, "Wind Power Influences on the Voltage Stability", *in Proceedings 2001 European Wind Energy Conference*, Copenhagen, 2001.

9 Annexes

9.1 Electrical Components Model in SIMPOW

The SIMPOW has been developed since 1977 in ABB. It is a dynamic simulation program dedicated to the power system problem. It is divided into 5 programs:

- OPTPOW – solves the network equations (static solution) using iterative method;

- STATPOW – solves the short circuit equations;

- DYNPOW – solves the differential equations to the power system in time;

- DSL – Dynamic Simulation Language;

- DYNPOST – plots the outputs;

To power quality assessment from wind turbines the OPTPOW, DYNPOW, DSL and DYNPOST are used. Any dynamic simulation demands at least the use of the upper four modules.

The OPTPOW computes the load flow in the power system. The wind turbine model in this program is an asynchronous machine, which the electrical characteristics of the machine and the active power produced are specified. The program automatically computes the voltage in all nodes, the power fluxes, and the mechanical speed and torque in the electrical machine.

The DYNPOW solves the differential equations to the power system in the dynamic simulation. In the DYNPOW module, the dynamic models of the electrical machinery and controllers of the machines are specified.

The DSL module is the dynamic simulation language. In the DSL, we implement the mechanical model of the wind turbine. The interface of the DSL and the DYNPOW modules is the mechanical torque. The wind turbine model is mostly done in the DSL module where the DYNPOW send the speed of the machine and the DSL return the torque on the main shaft of the electrical generator.

The DYNPOST module provides the graphical output of the simulation. Using DYPOST, it is possible to either analyse the electrical characteristics or export to an ASCII file that can be analyse in any other program.

The electrical components comprise the electrical generator, the reactive power compensation, control system, step-up transformer, transmission lines, and the entire power system. The transmission lines formally does not belong to the wind turbine unity but it is an important component in wind farm simulations therefore it is included here.

The electrical components are modelled using the standard library of SIMPOW/ABB. The SIMPOW library has verified models to most of the conventional electrical components in the power system including electrical machines, transmission lines, transformers and power electronics and controllers.

The electrical components in a conventional wind turbine are:

- Asynchronous generators,

- Step-up transformers,

- Lines (in a wind farm) and,

- Reactive power compensation

- Power system representation

Details of the electrical power system including the wind farm depend on the purpose of the simulation.

9.1.1   Electrical generator

The asynchronous generator is the most common type of electrical machine. It is mostly applied as motor. As generator, however, it has been used for many years in wind turbines.

The dynamic asynchronous generator model was implemented using the SIMPOW library. Figure 9.1 presents the main model parameters to the generator.

Electrical parameters: R, X

Air gap Torque (p.u.)

Speed (p.u.)

Electrical Generator Model

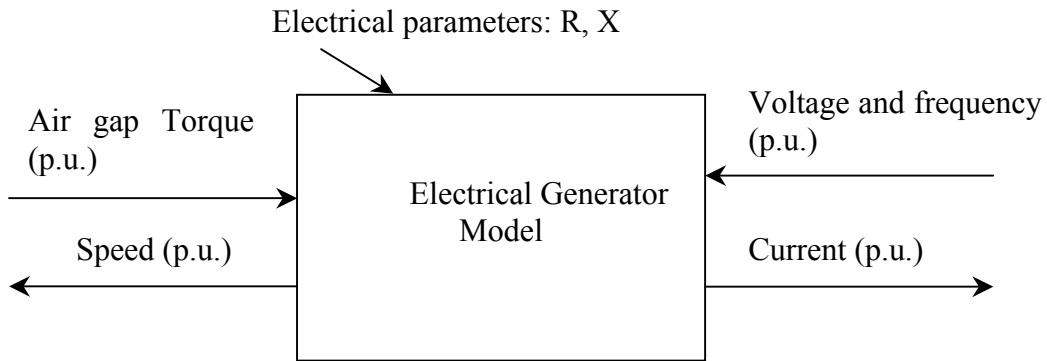Voltage and frequency (p.u.)

Current (p.u.)

Figure 9.1. Electrical generator model parameters.

The inputs to the model are the torque that is computed from the aeroelastic module (in DSL), the voltage and the frequency that comes from the next electrical component. The outputs are the mechanical speed (feed in the aeroelastic and wind model) and the current (feed in the next electrical component). The electrical parameters derive from the equivalent circuit presented in Figure 9.2.
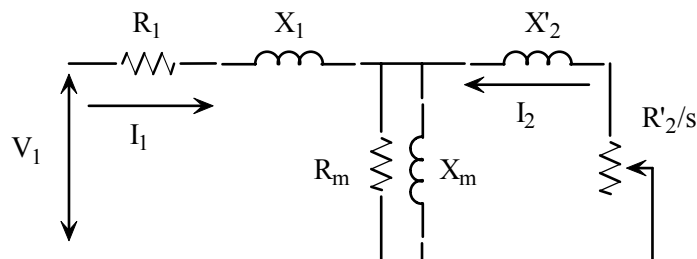
Figure 9.2. Electrical generator equivalent.

Where R_1 is the stator resistance the X_1 is the stator reactance inductive; X'_2 is the rotor equivalent reactance inductive referred to the stator, R'_2 is the rotor equivalent resistance referred to the stator; R_m is the resistance representing losses and X_m is the magnetization reactance. The rotor resistance is modelled as a function of the rotor speed in

order to model the skin effect in the rotor. The saturation can be also stated. All units are in per unit and the voltages and currents are vectors with an angle and amplitude.

The model itself is a so-called park model in d and q rotating reference frames where the transients of the stator are neglected. This model is also called as a third order model reduced from a fifth order. The third order model to induction machines represents reasonable the power quality characteristics [78] and [79].

The SIMPOW converts all parameters to a direct $– d –$ and a quadrature $– q –$ rotating axis so called park transformation. The dq reference frame is rotating at synchronous speed as determined by the electrical angular frequency of the impressed stator voltage, i.e. synchronously rotating axis [65] and [80].

9.1.2   Step-up Transformer

In these studies, a simple a symmetrical 3-phase without saturation transformer model is used. The configuration of the transformer depends on the installation. The characteristics and parameters of the model used are presented in Figure 9.3.
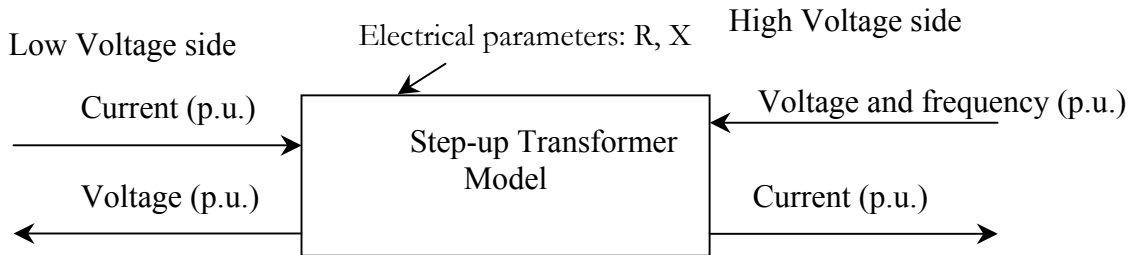

Figure 9.3 Structure of the transformer model.

The inputs to the model are the current from one side, the voltage from the other side and the reference frequency to the rotating dq-frame. Here, the wind turbine is connected to the low voltage side (step-up transformer), the current inputted comes from the wind turbine generator and from the reactive power compensation unity on the wind turbine terminals.

The model outputs the current in the high voltage side and the voltage on the low voltage side.

The transformer model uses the electrical parameters from a "T" electrical equivalent transformer model (see Figure 9.4).
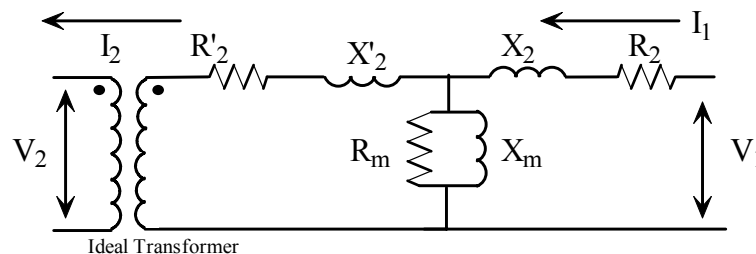

Figure 9.4 Electrical transformer model.

Where R_1 is the primary resistance the X_1 is the primary reactance inductive; X'_2 is the secondary equivalent reactance inductive referred to the primary side, R_2 is the secondary

side equivalent resistance referred to the primary side; R_m is the resistance representing losses and X_m is the magnetization reactance.

9.1.3   Reactive Power Compensation.

A switched capacitor bank usually supplies the reactive power in the wind turbines. A small capacitor bank supplies the no-load reactive power to the asynchronous generator and, during normal operation, small steps of capacitors can be connected to follow the reactive power demanded from the generator. Other technologies uses power electronics to compensate the reactive power, but here only the no-load capacitor bank supplies the reactive power during continuous operation.

9.1.4   Lines and Cables

Lines and cables can be modelled in different ways. Here, a concentrated π models the electrical behaviour of the lines and cables where depending on the distances and type of cables/lines it can be modified. Figure 9.5 presents the main structure of the basic cable/lines models.

Electrical parameters: R, X, B, d

Sending node

Receiving node

Voltage (p.u.)

Current (p.u.)
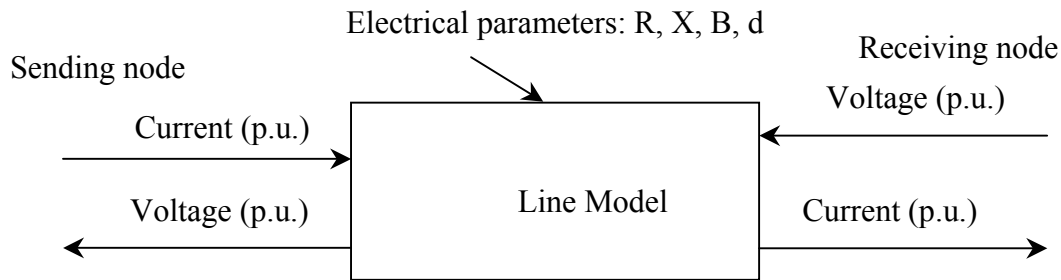
Line Model

Voltage (p.u.)

Current (p.u.)

Figure 9.5 Electrical Transmission structure model.

The model inputs are the one voltage and one current and it outputs the other voltage and current. The frequency reference is used to transform all variable to the dq-rotating frame and to compute the reactance in the lines. The electrical parameters come from the π electrical equivalent for the lines (see Figure 9.6)
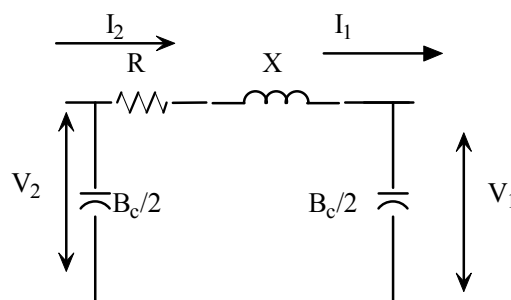
I_2 I_1

R   X

V_2 $B_c/2$ $B_c/2$ V_1

Figure 9.6 Electrical transmission model.

Where R is the equivalent resistance and the X is the equivalent reactance inductive of the line; B_C is the equivalent susceptance capacitive.

9.1.5   Slack bus

The slack bus is also reefed as reference node. It is modelled as a synchronous machine or by an infinite node connected through the short circuit impedance. Figure 9.8

presents the use of an infinite node to replace the power system with the short circuit impedance at the PCC.
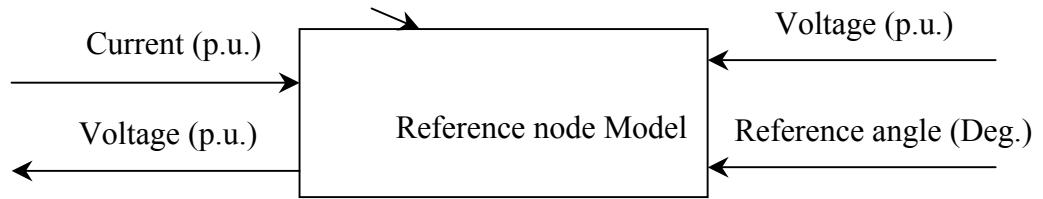
Electrical short circuit parameters: R, X

Figure 9.7 Slack bus structure.

The inputs to the model are: the voltage, the reference angle, and the currents computed from the other models. The electrical characteristics are the equivalent impedance at the PCC also called short circuit impedance. The model outputs the voltage at the PCC. A representation of the positive sequence of the slack bus is presented in Figure 9.8.
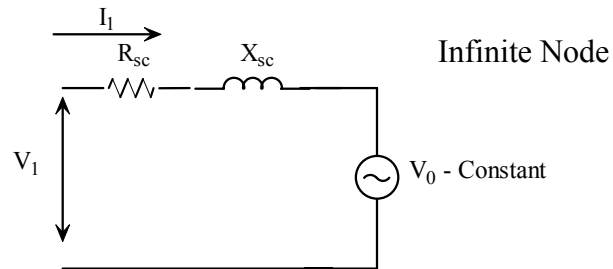

Figure 9.8 Slack bus model (positive sequence).

where R_{sc} is the short circuit resistance, the X_{sc} is the short circuit reactance inductive; V_0 is the voltage reference in the infinite node that is fixed.